POTENTIAL ANTI-THROMBOTIC NITRIC OXIDE GENERATING LAYER-BY-LAYER ASSEMBLY

By

Jun Yang

A dissertation submitted in partial fulfillment
of the requirements for the degree of
Doctor of Philosophy
(Chemistry)
in The University of Michigan
2010

Doctoral Committee:

Professor Mark E. Meyerhoff, Chair
Associate Professor Anna K. Mapp
Associate Professor Naír Rodríguez-Hornedo
Assistant Professor Stephen Maldonado

To my parents

Guirong Yang
Xiuzhen Ren

ACKNOWLEDGEMENTS

First and foremost, I would like to express my sincerest gratitude and respect to Dr. Mark Meyerhoff. Without his patient guidance, mentoring, and insightful idea, I could have never been able to achieve this point in my life. I am extremely grateful for his unfaltering support and words of encouragement. I would also like to extend my thanks to Drs. Anna Mapp, Naír Rodríguez-Hornedo, and Stephen Maldonado for serving on my dissertation committee. I also need to thank Dr. Marc Johnson for being a great teacher of me.

I am deeply indebted to my collaborators for their support and assistance, without whom this dissertation research would not have been completed. I wish to thank Dr. Jerome Lynch in Department of Civil and Environmental Engineering for generously providing me access to their automatic coating apparatus. I also thank Dr. Kenneth Loh, Dr. Andrew Zimmerman and Erik Jarva in Lynch's laboratory for their help in instrument training and scheduling. I want to thank Terry Major in the Extra-corporeal Membrane Oxygenation (ECMO) lab at the University of Michigan Medical School for preparing blood samples and performing animal experiments on the LbL coating. I also extend my thanks to Yang Wang in Dr. Prabir Roy-Chaudhury's laboratory at the University of Cincinnati for carrying out *in vivo* toxicity tests. In addition, I want to thank my undergraduate student, Saman

Mirkazemi, for his devotion in metal related application of NO generation LbL.

I need to give my heartful thanks to all the past and present members in the Meyerhoff group for the pleasant time we have spent together. In particular, I want to thank Dr. Wansik Cha and Dr. Sangyeul Hwang for their pioneering work in NO generation chemistry. I thank Dr. Melissa Reynolds and Dr. Yiduo Wu for their coaching in animal experiments. Special thanks go to Laura Zimmerman, Natalie Walker, Lin Wang, Kun Liu and Bo Peng for their proofreading and revision of this dissertation.

Finally and most importantly, I want to send my deepest appreciation to my family for their efforts and their faith in me. I owe many thanks to my parents, Guirong Yang and Xiuzhen Ren, for all that they have done and gone through to shape up my future and whatever I have achieved is a mere reflection of their affection. I also owe a big ‘thank you’ to my wonderful husband, Jinlin Xie, for being my best friend and mentor, and for always being there for me over the years.

TABLE OF CONTENTS

LIST OF FIGURES

FIGURE

LIST OF TABLES

TABLE

LIST OF SCHEMES

SCHEME

LIST OF ABBREVIATIONS

Alb-SNO	*S*-Sitrosoalbumin
Alg	Sodium Alginate
APS	3-Aminopropylsilane
AT-III	Anti-thrombin III
BSA	Bovine Albumin
cGMP	Cyclic Guanosine Monophosphate
CHES	2-(*N*-Cyclohexylamino)-Ethanesulfonic acid
Cu(II)-Cyclen	Cu(II)-1,4,7,10-Tetraazacyclododecane
Cu(II)-DTTCT	Cu(II)-Dibenzo-[e,k]-2,3,8,9-Tetraphenyl-1,4,7,10-Tetraaza-Cyclododeca-1,3,7,9-Tetraene
CysNO	*S*-Nitrosocysteine
DBHD	Dibutylhexyldiamine Diazeniumdiolate
DMF	Dimethylformamide
DTNB	5,5'-Dithiol-bis(2-Nitrobenzoic acid)
EC	Endothelial Cell
EDC	1-(3-Dimethylaminopropyl)-3-Ethylcarbodiimide
EDRF	Endothelium-Derived Relaxing Factor
EDTA	Ethylenediaminetetraacetic Acid
eNOS	Endothelium Nitric Oxide Synthase
EPR	Electron Paramagnetic Resonance
FA	Fluoroalcohol
FITC	Fluorescein Isothiocyanate
FSM	Fluorinated Surface Modifier
FTSC	Fluorescein-5-Thiosemicarbazide
FXa	Activated Factor X
GPx	Glutathione Peroxidase
GSH	Glutathione
GSNO	*S*-Nitrosoglutathione
H_2O_2	Hydrogen Peroxide
Hb	Hemoglobin
HbO_2	Oxyhemoglobin
Hep	Heparin Sodium Salt
HNO_3	Nitric Acid
ICP-MS	Inductively Coupled Plasma Mass Spectroscopy
LbL	Layer-by-Layer Assembly
LDI	Lysine Diisocyanate

MES	2-(*N*-Morpholino)-Ethanesulfonic Acid
metHb	Methemoglobin
MWCO	Molecular Weight Cut Off
$N_2O_3^-$	Dinitrogen Trioxide
$NaBH_4$	Sodium Borohydride
NHS	*N*-Hydroxysuccinimide
NiTi	Nitinol
NO	Nitric Oxide
NO_2^*	Excited State Nitrogen Dioxide
NOA	Nitric Oxide Analyzer
NOHb	Nitrosyl Hemoglobin
NONOate	Diazeniumdiolate
NOS	Nitric Oxide Synthase
O_3	Ozone
PA	Polyanion
PAA	Poly(acrylic acid)
PBS	Phosphate Buffered Saline
PDDA	Polydiallyldimethylammonium Choloride
PEI	Polyethyleneimine
PEO	Polyethylene Glycol
PPS	Pentosan Polysulfate
PSS	Poly(sodium 4-styrenesulfonate)
PTMO	Polytetramethyl Oxide
PU	Polyurethane
PVC	Poly(vinyl chloride)
PVS	Poly(vinyl sulfate)
RS^-	Thiolate Anion
RSe	Organoselenium Species
RSe^-	Organoselenolate Anion
RSeH	Organoselenol
RSeSeR	Diselenide
RSH	Thiols
RSNO	*S*-Nitrosothiols
RSSR	Disulfide
SeCA	Selenocystamine
SeDPA	3,3'-Diselenodipropionic acid
SEM	Scanning Electron Microscope
SePEI	Organoselenium Immobilized PEI
SMC	Smooth Muscle cell
SNAP	*S*-Nitroso-*N*-Acetylpenicillamine
SS	Stainless Steel 316L
Ti	Titanium
XPS	X-ray Photoelectron Spectroscopy

ABSTRACT

POTENTIAL ANTI-THROMBOTIC NITRIC OXIDE
GENERATING LAYER-BY-LAYER ASSEMBLY

By

Jun Yang

Chair: Mark E. Meyerhoff:

Nitric oxide (NO) is a potent platelet inhibitor released by healthy endothelial cells (EC) lining the human vasculature. Polymeric materials capable of releasing NO from synthetic NO donors have exhibited enhanced hemocompatibility *in vivo*. Alternatively, NO can be catalytically generated from endogenous *S*-nitrosothiols (RSNO) by some organodiselenide species (RSe). In this dissertation research, a Layer-by-Layer (LbL) assembly has been developed to immobilize RSe catalysts on diverse biomedical devices/materials to achieve surface NO generation. Because the preparation of such coatings is based on pure electrostatic interaction, universal application of this approach is expected.

The catalytic LbL was fabricated by manually depositing RSe linked to polyethyleneimine (SePEI) with sodium alginate (Alg) on quartz surfaces in an alternate

fashion. This $(SePEI/Alg)_n$ multilayer demonstrated potent catalytic activity to decompose RSNO, to NO in presence of free thiols. Under exaggerated reaction conditions, such an LbL exhibited good stability. The NO generated from given concentrations of *S*-nitrosoglutathione and glutathione is proportional to the number of (SePEI/Alg) bilayers deposited. The LbL was applied to silicone rubber and polyurethane substrates to demonstrate its applicability on commercial biomedical grade materials.

The fabrication of $(SePEI/Alg)_n$ LbL was ultimately automated using a commercial coating apparatus to achieve higher NO flux by increasing the number of (SePEI/Alg) bilayers. Under typical biological conditions, a $(SePEI/Alg)_{100}$ was discovered to generate an NO flux of 1.5×10^{-10} mol cm^{-2} min^{-1} using physiological RSNO levels, which is comparable with that of human EC layer. Even after prolonged contact with blood, the multilayer still showed significant NO generation activity. These automatically prepared LbLs were then successfully applied on exemplary metal surfaces (nitinol, titanium and stainless steel).

In addition, heparin was immobilized on the surface of $(SePEI/Alg)_n$ via either electrostatic interactions or covalently attaching the anti-coagulant on the aminated LbL surface. Both strategies lead to a surface with combined NO generation and anti-FXa activity. However, the covalent immobilization of heparin resulted in a decreased NO generation activity of the underlying catalytic LbL, due to decreased permeability of glutathione into the films.

CHAPTER 1

INTRODUCTION

Material induced thrombotic and thromboembolic complications remain a serious concern with cardiovascular devices despite the use of anti-platelet (e.g., clopidogrel (Plavix®)) and anti-coagulant (e.g., low-molecular-weight heparin (Fragmin®), warfarin (Coumadin®), etc.) therapies. Such thrombogenicity is believed to be inherently associated with the foreign character of materials and the only truly non-thrombogenic surface hitherto known is the human blood vessel lined with intact endothelial cells (EC). Consequently, various approaches have been pursued to decorate material surfaces with features mimicking the EC membrane.

Nitric oxide (NO), also known as the endothelium-derived relaxing factor (EDRF), has been recognized for its critical role in platelet inhibition,[1-3] vasodilatation,[4] and wound healing.[5-7] Compounds that can release NO under physiological condition have been incorporated within polymeric matrices and a significant reduction in thrombosis formation on such NO release surfaces has been observed by both *in vitro* and *in vivo* assessments.[8-11] However, this NO release concept is challenged by limited use-life due to the depletion of NO donors in the coatings. Recently, a novel strategy of catalytically

generating NO from endogenous NO donors, *S*-nitrosothiols (RSNO), using organoselenium (RSe) species has been pursued to create a long term supply of NO at surfaces.[12] The work described in this dissertation is closely related to this approach of catalytically generating NO from RSNO using RSe catalysts. Specifically, the feasibility of immobilizing RSe catalysts via Layer-by-Layer (LbL) assembly is investigated and subsequently proved to be universal on materials with diverse surface chemistry, owing to the pure physical driving force involved in the coating process. Biomedical polymers and metals were studied in detail to demonstrate that this NO generating LbL assembly is readily transferrable to commercial substrates. Heparin, which is a widely used anti-coagulant, was further immobilized on the NO generating LbLs for a potential synergic anti-thrombotic efficacy.

This introductory chapter will briefly survey current strategies used for improving biocompatibility of biomedical surfaces, with specific emphasis on using NO to inhibit platelet activity at the blood/device interface and hence to reduce thrombus formation. Then, the concept of LbL will be introduced with regard to the processing, the theory behind, as well as the uniqueness of this technique.

1.1. Material Induced Thrombosis and Enhancing Hemocompatibility of Biomedical Devices

Biocompatibility is defined as "the ability of a material to perform with an appropriate host response for a specific application".[13] Hemocompatibility, termed specifically as the biocompatibility of blood contacting devices, mostly relates to material induced thrombosis. Despite the use of anti-platelet and anti-coagulant therapies, such

inherent thrombogenicity occurs almost regardless of the physical/chemical properties of the material. Clinical manifestations of the thrombotic response of intravascular devices include: sudden and complete obstruction of stents within weeks;[14] acute and subacute thrombotic occlusion in medium sized vascular grafts;[15] embolic complications with artificial hearts,[16] catheters[17] and prosthetic valves;[18,19] and thrombotic complications during cardiopulmonary bypass[15] and angioplasty.[20] Even though the risk of thrombotic complication appears to be relatively low (varying between 2% and 10% depending on the device), the possible fatal outcomes as well as the cost associated with the follow-up interventions are not negligible.

Many years of intensive research suggests that thrombus forms via a rapid protein adsorption of plasma proteins on the device surface followed by two interrelated pathways involving platelet and coagulation factors, respectively. In the platelet pathway (see Figure 1.1), platelets deposit on the device surface through binding their membrane-bound glycoprotein IIb/IIIa integrin to the surface adsorbed proteins, predominantly fibrinogen. The adherent platelets then change in shape to irregular spheres with spiny pseudopods, accompanied by internal contraction and extrusion of their granule contents into the extracellular environment. These released agents include important mediators (e.g., ADP, fibrinogen, and Ca^{2+}, etc.) that can support platelet aggregation and recruit more platelets into the growing platelet aggregate. When platelets aggregate, their membranes provide a phospholipid surface that accelerates two critical steps of the blood coagulation sequence (see below). The platelet clusters are eventually interweaved by fibrin fibers into a massive clot, sometimes with red blood cells entrapped as well.

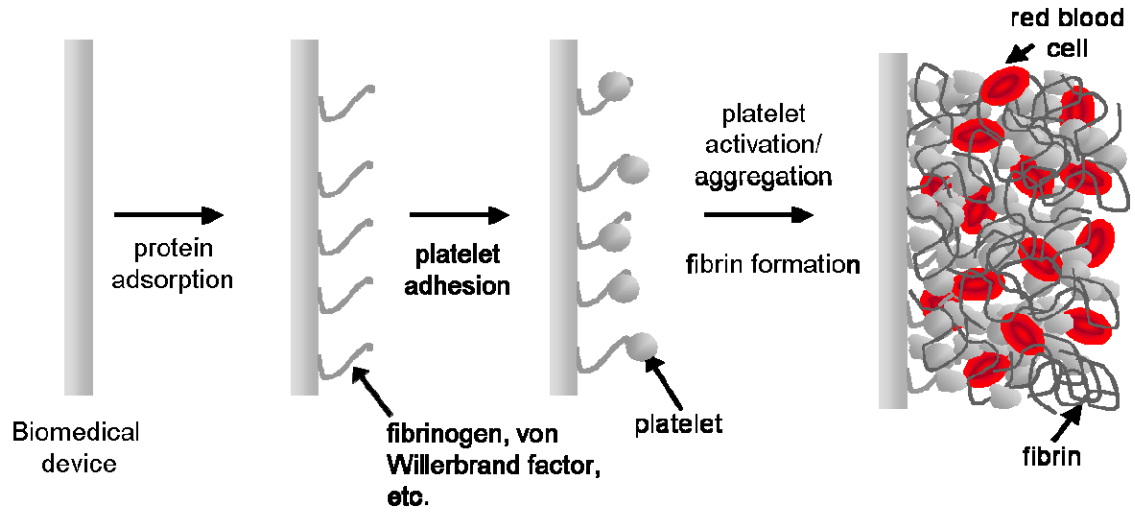

Figure 1.1. Thrombus formation involving platelets and fibrin on the surface of blood contacting biomedical devices.[21]

Blood responds to the artificial surface also through a cascade of self-amplifying reactions involving at least 12 plasma coagulation factors to form fibrin polymers (from fibrinogen) and generate agonists of platelet activation (see Figure 1.2). The cascade can be triggered intrinsically by surface mediated reactions, or extrinsically through factors derived from tissues. The two systems converge upon a final common pathway that leads to the formation of thrombin and an insoluble fibrin gel. At the implantation site, the proteins adsorbed on the device react with contact factors and thereby activate the intrinsic coagulation system. In the middle phase of intrinsic clotting, factor IX is activated and subsequently forms a complex with factor VIII on the phospholipid surface of activated platelets in the presence of calcium. The common pathway begins when factor X is activated by the factor IXa-VIIIa complex. The active form of factor X converts prothrombin (factor II) to thrombin in the presence of factor V, calcium and platelet phospholipids. Thrombin, in addition to its ability to modify factors V, VIII and platelet, acts on fibrinogen (factor I) to form polymerized fibrin gel which reinforces

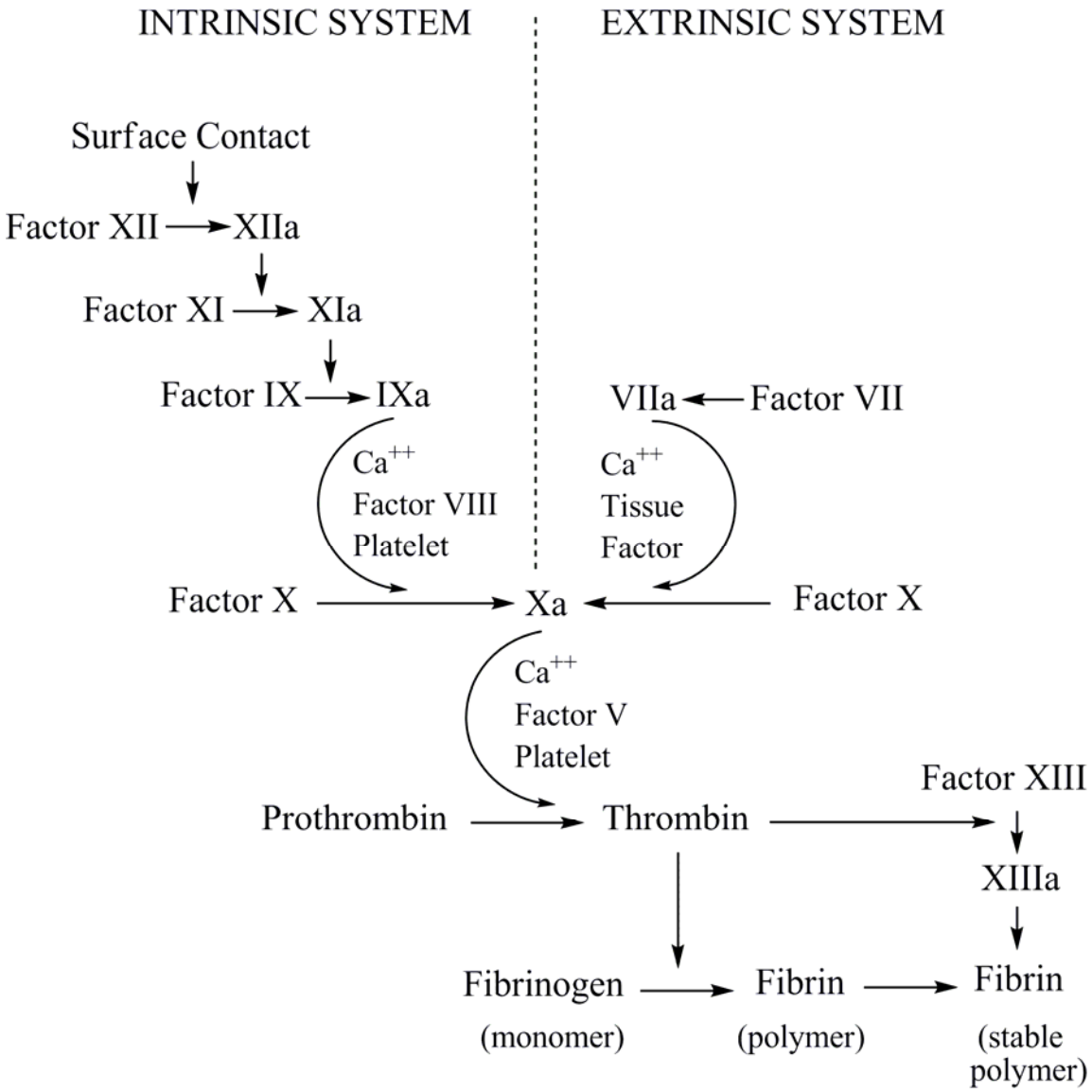

Figure 1.2. Simplified blood coagulation cascade as reviewed by biomaterial textbooks[13].

platelet aggregates.

Contrary to man-made materials, the endothelium layer lining the human vasculature remains thrombus-free through several control mechanisms acting in concert: a non-fouling phospholipids coating, membrane bound/released inhibitors of platelet and coagulation factors, as well as an efficient fibrinolytic system removing fibrin deposits. Consequently, surface modifications have been considered to render intravascular devices and similar interferential features to mimic the natural thromboresistancy of blood vessels. For instance, poly(ethylene glycol)[22] and zwitterionic amphiphiles[23] such as phospholipids[24] have been tethered on material surfaces to induce a hydration layer to help resist nonspecific protein adsorption. Surface immobilization of coagulation inhibitors have also been explored to prevent blood clotting by deactivating relevant coagulant factors. Examples are surface attachments of heparin[25-28] and thrombomodulin[28-31] leading to measurable inhibitory effect on thrombin and factor Xa, and factor Va and VIIIa, respectively. Alternatively, a surface capable of capturing plasminogen, the inactive form of the clot degrading enzyme plasmin, has been designed in attempt to decompose existing thrombus.[32] Although these methods demonstrate positive *in vitro* results, reports on the improvement of *in vivo* biocompatibility are limited and mixed.

1.2. Anti-thrombotic Surface with Nitric Oxide Release or Generation

1.2.1. Nitric oxide in biological systems

The biological importance of nitric oxide had not been appreciated until it was first identified as the EDRF in 1987.[33] Since then, there has been an explosion of activity

revealing this simple small molecule as an active player in critical physiological systems such as vascular tone, immunological response, and neurotransmission.[34] The major source of NO in biological systems is L-arginine which is enzymatically converted by nitric oxide synthase (NOS) to L-citrulline accompanied with the liberation of one equivalent of NO. Dependent on the site of formation, NO enters different metabolic pathways leading to its degradation or storage.

The most studied actions of NO are in the cardiovascular system, where it is continuously produced by endothelium nitric oxide synthase (eNOS). Here, NO can diffuse in three dimensions away from the cell of origin, passing through the cell membrane easily to bring about a range of physiological effects (see Figure 1.3). In vascular smooth muscle cells (SMC), NO activates soluble guanylate cyclase upon binding to its heme component to attenuate cyclic guanosine monophosphate (cGMP) levels which results in SMC relaxation. Nitric oxide also diffuses outward from the EC layer into the blood at an estimated rate of 1×10^{-10} mol cm^{-2} min^{-1}.[35] At the endothelium-blood interface, NO acts synergistically with prostacyclin to inhibit platelet aggregation and disaggregate platelets. Nitric oxide alone also inhibits platelet adhesion to the EC monolayer, further enhancing the thromboresistancy of blood vessels. Although the molecular level mechanisms of such anti-aggregation/adhesion activities have not yet been fully understood, it is believed that both processes are mediated by a cGMP pathway leading to a decrease in the intracellular Ca^{2+} level which eventually deactivates platelets.

The fate of NO released into the blood is affected by chemical reactions with blood constituents. Hemoglobin (Hb) and oxyhemoglobin (HbO_2) are the major scavengers

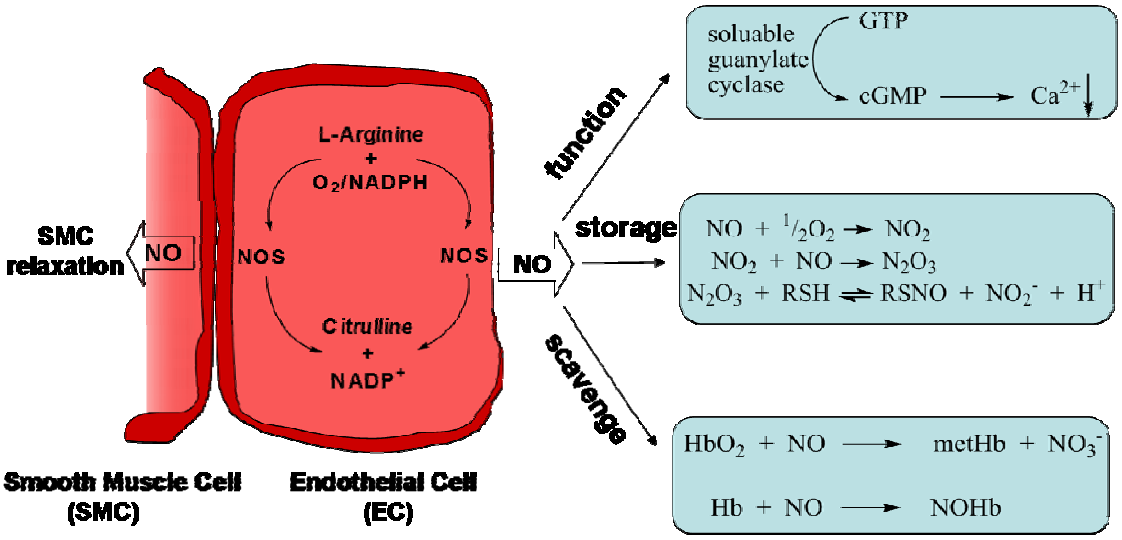

Figure 1.3. Metabolism of NO in human blood. NO is synthesized by NOS within the endothelium and diffuses into the blood stream to bring about its inhibitory effect on platelets, to react with RSH in the presence of O_2 to form RSNO, or to be scavenged by reactive species, e.g. hemoglobin derivatives.

that bind with NO to form nitrosyl hemoglobin (NOHb), or methemoglobin (metHb) and nitrate, respectively. This rapid scavenging accounts for an extremely short half-life of NO in whole blood which results in a highly localized inhibitory effect of NO on platelets. Oxidized NO (N_2O_3) also reacts with free thiols (RSH) which are the most abundant reductive species in plasma to form *S*-nitroso adducts. Indeed, human plasma contains low micromolar concentrations of *S*-nitrosothiols (RSNO), the majority of which is *S*-nitrosoalbumin (Alb-NO). These relatively long-lived adducts circulate in the blood stream and probably serve as carriers of short-lived NO to regulate vascular tone systematically.

1.2.2. Nitric oxide release from exogenous donors

The pharmacological implications of NO become increasingly noteworthy in light of its wide-ranging functions in the cardiovascular, nervous and immune systems. Indeed, NO adducts such as organic nitrates[36,37] and sodium nitroprusside[38] have long been used in the treatment of angina and hypertensive crises, respectively. Therefore, it is not surprising that NO has becomes a promising solution for reduction of thrombosis after its inhibitory effect on platelets was elucidated.[39] Distinct from the other anti-platelet or anti-coagulant reagents, NO is truly a local mediator that does not require complex metabolism for clearance due to its highly reactive nature. This has two important implications: first, once applied locally, NO can potentially reduce the risk of thrombosis without disturbing systemic hemostasis; and second, the exogenous NO source must be within close proximity of the implantation site so as to prevent unwanted scavenging of NO by a variety of reactive species (e.g., oxyhemoglobin) in the biological environment.

Initially, NO was supplied to the site-of-interest using reactive NO adducts capable of releasing NO under suitable biological condition (see Figure 1.4). Diazeniumdiolates (NONOates), prepared via exposing primary or secondary amines to NO gas, include a large array of compounds that have been investigated as potential NO donors for biomedical applications. These compounds undergo spontaneous proton-driven decomposition at physiological pH and temperature to generate two molar equivalents of NO. Applying these species on biomedical surfaces can be achieved by simply doping discrete NONOate small molecules into polymeric matrices, [11,25,28,40] or covalently attaching such species to the polymer backbone.[9,41-45] NO release is initiated upon water uptake by the polymer and the flux can reach several times that of the EC layer. *In vivo*

animal studies have demonstrated that biomedical devices such as extracorporeal circuits, vascular grafts and implanted oxygen-sensing catheters coated with this NO-releasing polymers exhibit dramatically enhanced blood compatibility.[11,46,47] However, this NO release surface is not good for long term implants because the released NO flux tends to decrease due to depletion of the NO donor reservoir. A decomposition byproduct, nitrosoamine, is also of concern for its potential carcinogenicity, if leached out from the coating. An alternative class of NO donors is *S*-nitrosothiols (RSNO), which have been shown to release NO using heat or photo stimuli. Synthetic RSNOs with a broad range of release rates have been achieved by tailoring the parent thiol species. However, such compounds can decompose via more complex catalytic mechanisms via metal ions, thiols, superoxide and some enzymes, requiring that they be carefully handled.[48]

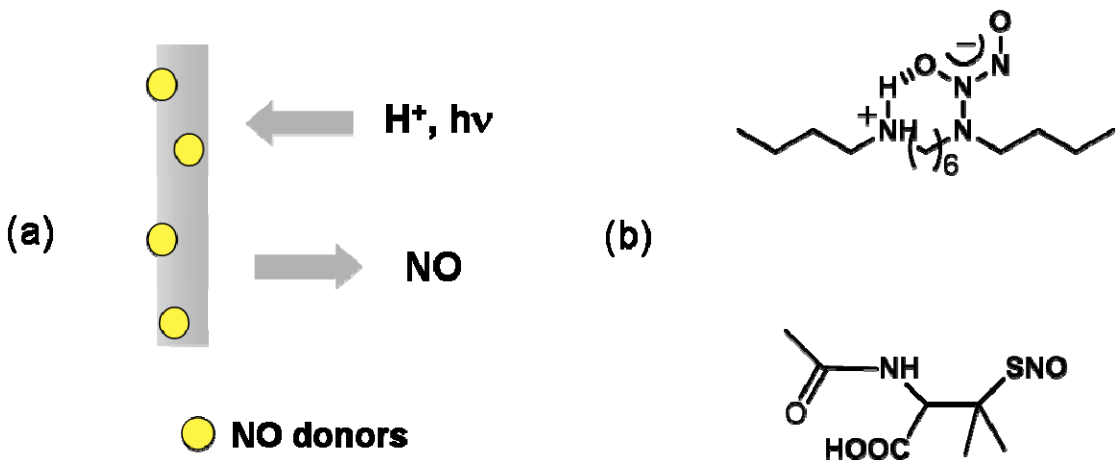

Figure 1.4. (a) Schematic representation of NO releasing materials and (b) exemplary compounds of two common NO donors: dibutylhexyldiamine diazeniumdiolate (DBHD, top) and *S*-nitroso-*N*-acetylpenicillamine (SNAP, bottom).

1.2.3. Nitric oxide generation from endougenous *S*-nitrosothiols

As mentioned in 1.2.1, there is a class of compounds with the generic structure R-S-N=O known as *S*-nitrosothiols (RSNO) that exist in animal and human blood. These compounds are believed to store and carry transient NO to bring about its systemic biological function after being generated by NOS. The representative endogenous RSNOs in plasma include *S*-nitrosoglutathione (GSNO), *S*-nitrosocysteine (CysNO) and *S*-nitrosoalbumin (Alb-SNO) (see Figure 1.5). Although often viewed as an NO adduct, RSNO can not be formed by direct reaction between NO and a thiol. Several possible routes have been hypothesized to account for *in vivo* RSNO formation; however, a consensus has not been reached.[49] In the laboratory, small molecule (e.g., GSNO and CysNO) can be prepared via reacting the corresponding thiol with nitrous acid in extremely acidic condition (eq. 1.1a), whereas *S*-nitroso-proteins can only be approached tactfully via a transnitrosation reaction between their cysteinyl residue and small molecule RSNOs (eq. 1.1b).

$$HNO_2 + RSH \longrightarrow RSNO + H_2O \qquad (1.1a)$$

$$RSNO + R'SH \rightleftharpoons RSH + R'SNO \qquad (1.1b)$$

The stability of RSNOs is subject to several factors, such as heat, direct radiation and reactive species such as superoxide.[48] Particularly, RSNOs can be decomposed by certain catalysts to produce NO. Therefore, the current study of interest focuses on rendering the device surface catalytically active to generate NO *in situ* at the blood/device interface. The potential advantage of this NO generation concept is that a sustained NO flux can be achieved because the endogenous RSNO levels at the implantation site is constantly

replenished by blood circulation.

It is well established that metal ions, particularly Cu(II), can mediate RSNO decomposition.[48] In fact，the active species was further recognized as Cu(I) which forms from reduction of Cu(II) by a reductive equivalent (i.e., free thiol and ascorbic acid).[50] The Cu(I) then reacts with RSNO to liberate NO by transferring one electron, thus forming a disulfide and regenerating Cu(II) (see Figure 1.6). Such a reaction can be partially hindered or completely inhibited in the presence of strong Cu(II) chelating reagents (e.g., ethylenediaminetetraacetic acid (EDTA), disulfide, and neocuproine).[50,51] Nevertheless, some Cu(II) complexes still show significant activity to catalyze RSNO decomposition (see Figure 1.6), which has lead to design of a series of NO generation materials. For example, a lipophilic Cu complex (e.g., Cu(II)-DTTCT) was blended in poly(vinyl chloride) and polyurethane.[52,53] Another copper complex, Cu(II)-cyclen, was

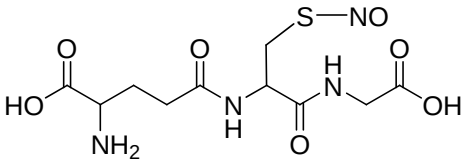

S-nitrosoglutathione (GSNO)

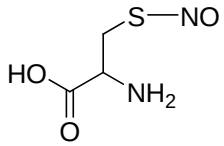

S-nitrosocysteine (CysNO)

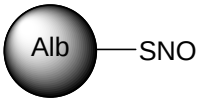

S-nitrosoalbumin (Alb-SNO)

Figure 1.5. Structures of common endogenous RSNO species in plasma: GSNO, CysNO and Alb-SNO.

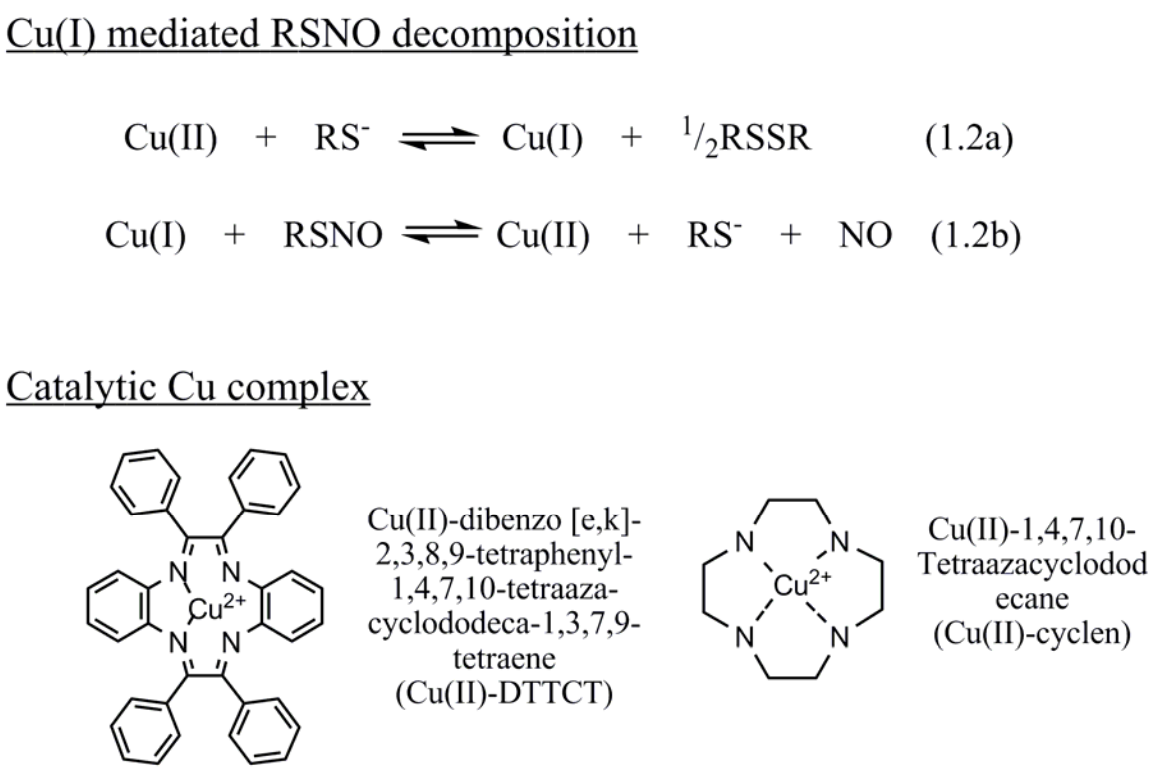

Figure 1.6. Cu(I) mediated RSNO decomposition: mechanism and exemplary Cu(II) complex catalysts.

covalently tethered to polymethacrylate[54] and high-water-uptake polyurethane.[55] Further, Cu^0 particles in micro/nanometer size were embedded in a polymer phase and this material was shown to convert RSNO to NO.[56] In this case, the Cu^0 particles are corroded by the biological fluid (or PBS instead) to release free Cu^{2+} ion into the peripheral region where they are reduced into reactive Cu(I). These Cu-based NO generation surfaces have been reported to be able to generate NO fluxes up to 8×10^{-10} mol cm^{-2} min^{-1} from biological concentrations of GSNO and GSH. In an *in vivo* study, coatings containing

Cu^0 micro/nano particles were applied on the surface of catheter type oxygen sensors and significant thrombosis reduction was observed using a swine model for intravascular measurements of oxygen.[56]

In addition to metal ions, RSNO decomposition can also be mediated by organoselenium (RSe) species. This phenomenon was first noted using glutathione peroxidase (GPx) to potentiate inhibition of platelets by RSNOs.[57] The enzyme has a selenocysteine active center which normally converts peroxides into water or alcohols by consuming GSH as the reducing equivalent. The inhibition of platelet was suggested tp occur via NO production from the GPx catalyzed RSNO decomposition. In a later mechanistic study, experimental evidence proved that not only GPx, but also some simple organoselenium compounds can catalyze RSNO decomposition to NO.[58] Recently, the reaction was revisited to demonstrate the catalytic mechanism and explore the feasibility of producing NO from RSNOs using surface immobilized RSe species.[12] Figure 1.7 shows the proposed mechanism that comprises a fast denitrosation of RSNOs by diselenide (eq. 1.3d), and a slower catalytic cycle involving an active selenol species (RSeH) (eq. 1.3a-c). The catalytic intermediate, RSeH, is generated by an interchange reaction of diselenide or selenosulfide with the thiol to yield a disulfide. The RSeH subsequently reduces RSNO to form NO and the corresponding selenosulfide forms from which RSeH can be regenerated. The NO production rate is dependent on temperature, pH, as well as concentration of thiol species, indicating the regeneration of RSeH is the rate limiting step. Indeed, selenol is an efficient catalyst for disulfide reduction to thiols, owing to its strong nucleophilicity, good leaving group properties and low pKa value.[59] Sulfhydryl compounds (e.g., GSH) can completely reduce diselenide to selenol when

RSe mediated RSNO decomposition

$$RSe\text{-}SeR + GSH \rightleftharpoons RSe\text{-}SG + RSe^- + H^+ \quad (1.3a)$$
$$RSe\text{-}SG + GSH \rightleftharpoons RSe^- + H^+ + GS\text{-}SG \quad (1.3b)$$
$$RSe^- + H^+ + R'S\text{-}NO \rightleftharpoons {}^1/_2 RSe\text{-}SeR + R'SH + NO \quad (1.3c)$$
$$RSe\text{-}SeR + 2R'S\text{-}NO \rightleftharpoons 2RSe\text{-}SR' + 2NO \quad (1.3d)$$

Catalytic RSe species

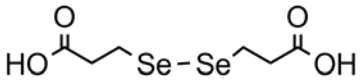

3,3'-diselenodipropionic acid
(SeDPA)

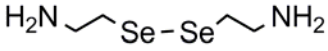

selenocystamine
(SeCA)

Figure 1.7. Organodiselenide mediated RSNO decomposition: mechanism and exemplary RSe catalysts: 3,3'-diselenodipropionic acid and selenocystamine.

they are in considerable excess.[60] *In vivo*, the abundant GSH reservoir provides the necessary reducing equivalents to maintain the redox activity of proteins containing selenol active centers, for example, enzymatic degradation of H_2O_2 by GPx.[61]

Organoselenium based NO generation catalysts are advantageous over Cu based species due to the availability of large pool of organoselenium species with reactive functionalities, e.g., selenodipropionic acid (SeDPA) and selenocystamine (SeCA). These molecules are readily linkable to different surfaces through diverse reaction methods. For instance, SeCA has been covalently immobilized on oxidized cellulose

filter paper and ion exchange resin particles.[12] Polyethyleneimine was coupled with SeDPA via amide bond and the resulting derivative was crosslinked within the pores of dialysis membrane.[12] Preliminary studies demonstrate these RSe immobilized surfaces can catalytically generate NO from RSNO solution effectively in the presence of thiols.[12]

1.2.4. Nitric oxide detection with chemiluminescence

Despite the availability of diverse NO detection methods, the majority of methods described to detect NO rely on probing the relatively stable NO metabolites including nitrite, nitrate and metal-nitrosyls. This can often lead to misleading results, owing to the presence of these metabolites in the samples from which NO is to be detected. Hence, more complex but direct methods are preferred. These include chemiluminescence, electron paramagnetic resonance (EPR), mass spectrometry, and amperometric/voltammetric analysis. Chemiluminescence is of particular advantage due to its very low detection limit, selectivity toward NO without separation steps to eliminate interferences, good temporal resolution, simple experimental setup as well as easy instrumental accessibility. These features allow direct and continuous monitoring of NO flux generated from heterogeneous phases and therefore is utilized as the primary tool for NO detection in this thesis work.

The chemiluminescence NO analyzer (NOA) detects NO via a reaction with ozone (O_3) to form a nitrogen dioxide in the excited state (NO_2^*) which releases a photon as it spontaneously relaxes back to the ground state.[62] The emission falls in the red and infrared region (~640 – 3000 nm) with the peak intensity at ~1100 nm. Typically, commercial instruments are equipped to detect the emitted light in the range between

640-900 nm.[63] To measure the NO flux, a substrate with catalyst immobilized on its surface is immersed in a sealed reaction chamber in which phosphate buffered saline containing given concentrations of GSNO and GSH is injected (see Figure 1.8). A given amount of EDTA is also added to chelate any free Cu^{2+} in the buffer so that only the NO generation at the catalytic substrate surface is observed. The solution is constantly purged with N_2 to drive NO from the solution phase so as to be carried by the N_2 stream into the NOA.

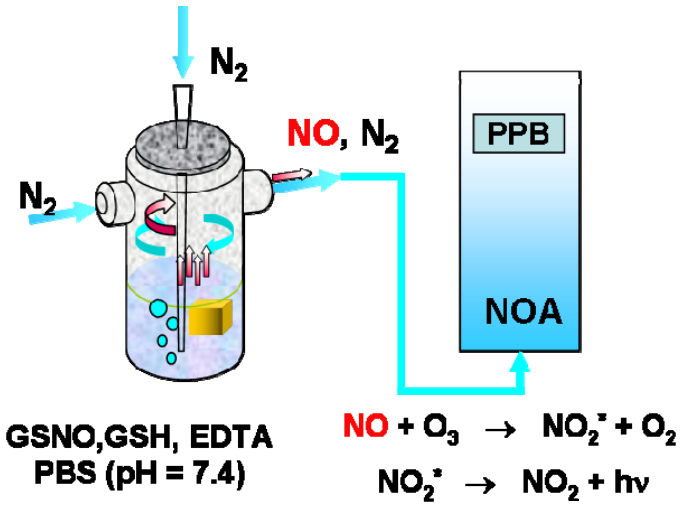

Figure 1.8. Schematic presentation of experimental set-up for detection of NO generated from GSNO/GSH solution using chemiluminescence NO analyzer.

1.3. Surface Modification via Layer-by-Layer Self-Assembly (LbL)

1.3.1. Layer-by-Layer deposition and the theory behind the technique

In 1966, Iler first presented a technique for building films of controlled uniform thickness by the alternate adsorption of positively and negatively charged colloidal particles.[64] Although some singular attempts of similar experiments have been reported,

the method was systemically extended to charged amphiphiles and polyelectrolytes by the Decher group in 1990s.[65] The name "Layer-by-Layer" was given to the method as a description of its stepwise coating procedure. Later, the method has been adopted to prepare multilayer assemblies using interactions other than electrostatic ones, such as hydrogen bonding, electron transfer, and specific interactions between biological molecules.[66] It needs to be stressed that the term "LbL" in the context of this thesis is limited to the films constructed based on electrostatic attraction of polyelectrolytes.

The practical set-up of LbL may be extremely simple, e.g., just dipping the support into beakers filled with the polyelectrolyte solutions (see Figure 1.9). The dipping can be done manually, although automatic dipping devices may provide better control and enhanced reproducibility. The amount of adsorbed material is self-limiting and surplus

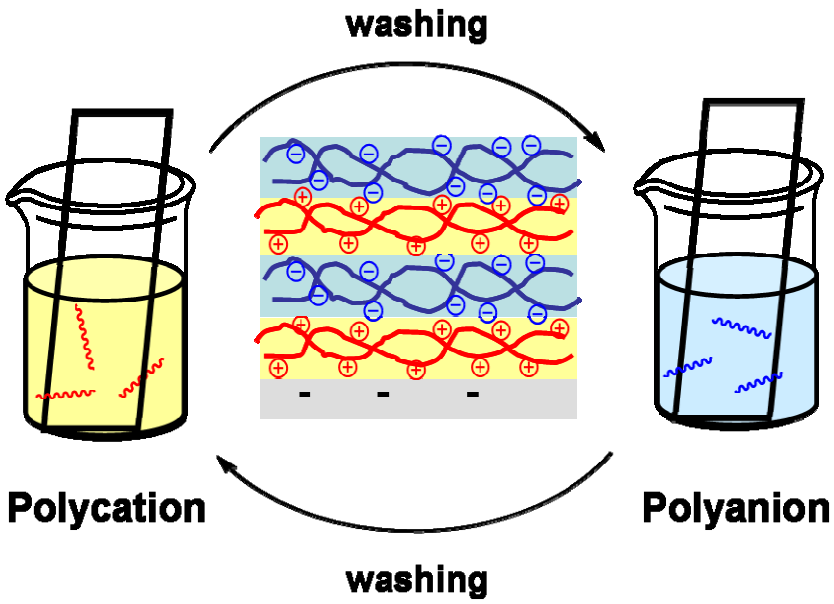

Figure 1.9. Schematic representation of method to construct an LbL. A substrate is arbitrarily presumed to bear negative charges on its surface and is immersed in beakers containing polycation and polyanion, alternately. The sample is washed when the coating solution is switched. To coat a positively charged surface, the substrate is simply placed in polyanion solution first, then switch to polycation solution.

polymer solution adhering to the support is removed by simple washing with buffer. Under proper conditions, a polyelectrolyte with larger than the stoichiometric number of charges (relative to the substrate) is adsorbed, so that the sign of the surface charge is reversed (i.e., charge overcompensation). Consequently, when the substrate is exposed to a second solution containing a polyion of opposite charge, an additional polyion layer is adsorbed. But this reverses the sign of the surface charge again. Consecutive cycles with alternating adsorption of polycations and polyanions result in the stepwise growth of polymer films.

The simplest adsorption theory of polyelectrolytes on an oppositely charged surface is based on an ion-exchange model: the polyelectrolyte competes with the counterions to ion-pair with the charged sites on the surface. The primary driving force is entropy, not enthalpy. The polyelectrolyte loses entropy upon adsorption, but more entropy is gained by the liberated low molar mass counterions. An additional entropic gain may derive from the liberation of solvent molecules from the solvation shell of the polymer-bound ionic groups. In contrast, the number of electrostatic bonds in the overall system is not changed upon polyion adsorption. Inherently associated with its simplicity, this theory is far from satisfactory in explaining the diverse behavior of LbL deposition by neglecting the role of secondary interactions such as specific ion-ion interaction, hydrophobic interaction, electron transfer, hydrogen bonding etc.[67] A detailed discussion can be found elsewhere.[68]

A factor that dominates LbL deposition is the charge reversal, which is dictated by a kinetic controlled process. The adsorption of polyion is often viewed to proceed in two steps: 1) a rapid anchoring of polyions on the surface within minutes; and 2) a slow

reconformation of the adsorbed layer via chain rearrangement of the polyelectrolyte.[68] If conformation change is slower than adsorption, charge overcompensation is expected. During the fast adsorption, polyelectrolyte chains anchor by only some of their charged groups to the surface, and, before they have time to reconform in order to occupy the neighboring charged sites on the surface, these latter sites are occupied by other polyelectrolyte chains. The attached polymer molecules progressively create a surplus of charge that eventually leads to an electrostatic barrier which repels other polyelectrolyte chains from attaching to the substrate. In other words, the phenomenon is self-regulating. The polyelectrolyte adsorption is not fully reversible so that the built-up film does not represent an equilibrium structure. This adds to the complexity of the LbL method by emphasizing careful adjustment of the various coating parameters in order to control film growth.

LbL gains its remarkable popularity largely because stable films with precisely controlled thickness can be prepared using this method without expensive instruments. The adsorption cycle comprising consecutive dipping-and-lifting actions has barely any limitation on the physical form of the substrates. Since water is usually used as the solvent, this technique is environment friendly. What most distinguishes the LbL method from the conventional surface modification approaches is its generic nature: the method can be employed on a wide range of substrates using varied polyions, probably due to the pure physical driving force and entropic dominance of the adsorption process. Over the past decades, films have been prepared from not only synthetic polymers but also proteins,[69] dyes,[70] inorganic platelets,[71] latex particles,[72] dendrimers[73] and even viruses.[74] The lack of sensitivity to chemical nature also renders the method useful on

almost any substrate materials carrying net charge by choosing proper coating condition. Even the sign of the charge is not a problem. This privilege is superior to traditional surface modification methods which require suitable functional groups on both the substrates and the immobilized species.

1.3.2. Properties of Layer-by-Layer assembly

In complete contrast to the simplified theory, LbL formation, as well as the properties of the resulting films, are highly sensitive to a large number of experimental parameters: polyelectrolyte pairs (molar mass, polydispersity, chain stiffness etc.), adsorption time, adsorption concentration, ionic strength, pH, low molar mass counterions, solvent, rinsing step, and the drying procedure applied between dipping cycles. The influence of these parameters has been reviewed elsewhere.[75] Combinations of these variables lead to countless possible LbL structures presenting diverse composition, physical properties and mechanical performance. An in depth discussion on this topic is out of the scope of this thesis and only several common characteristics of LbL will be stressed below.

The term “Layer-by-Layer”, although it describes well the coating process, always causes misunderstanding with respect to the actual structure of the LbL. This misconception is further enhanced by the alternating surface properties displayed by the LbL films, such as contact angle,[76] chemical composition[77] and ζ-potential, etc.[78] However, a well defined multilayer structure was not detected using X-ray reflectivity[79] or small angle neutron reflectivity.[80] This indicates that the LbL is not a hierarchy structure with layers of polycation and polyanion superimposed on each other. Rather, the polymers are interpenetrated and the film is stratified. Since the build-up of such an

interdigitated structure does not proceed under thermodynamic equilibrium conditions but under control of deposition and wash kinetics, the intuitive stoichiometric composition (i.e., polyanion and polycation interacting in a 1:1 ratio) is not obligatory. Indeed, both stoichiometic and unstoichiometic films have been reported, although the stoichiometric cases seem to dominate.[78] Nevertheless, low molar mass ions are found in the outmost layers due to the charge overcompensation.[81] It is also conceivable that some buried charges of the outer layer may not be accessible for polyelectrolyte complexation in the next deposition step and hence has to be balanced by small counterions.

Once formed, the complexation of weaved polyions is not very reversible. This can be attributed to the high number of ion pairs present, which lock the polyions within the LbL film and therefore freeze the multilayer structure. In many cases, this strong ionic bonding also renders the films prepared with outstanding solvent resistance,[82] even at high ionic strength[83] and under strong acidic/basic condition.[82] However, such an immobilized configuration of polymer in the LbL films does not exclude local chain rearrangement. Actually, a continuous rearrangement of molecular fragments even within lower lying layers during film growth is strongly suggested by a number of dye labeled systems according to the spectra shifts observed.[84,85] An obvious chain rearrangement that significantly changes the film appearance has also been observed during a so-called annealing event.[86] For LbLs made from weak polyelectrolytes, the structure may be partially or fully deconstructed upon prolonged exposure in extremely high ionic strengths or strongly acidic/basic conditions,[87] but the extent is absolutely determined by the polyion pair on a case-by-case basis.

A distinctive character of LbL is the independency of film growth on the substrate

after a certain number of deposition cycles. This is not surprising considering that the charge overcompensation due to the adsorption of the top layer determines the amount of adsorbed polyion in the next step. Observations have been made with many systems demonstrating that the thickness of the layers in LbL depends on the chosen polycation-polyanion pair.[78,88] Accordingly, a linear growth of film thickness and the amount of polymer deposited versus the number of dipping cycles is expected for a well-behaved polyion pair. However, nonlinear growth has been often observed in the initial stage, i.e. less than 5 bilayers, which is probably attributed to a lack of affinity between the polyelectrolyte and the substrate.[89] For certain polyion pairs, an exponential growth trend or a combination of both regimes can also occur due to the diffusion of one polyionic species into the underlying multilayers.[90]

1.3.3. Useful substrates for Lay-by-Layer assembly

As described above, the build-up of a LbL assembly is initiated by adhesion of charged species onto a solid support bearing charge of opposite sign. Apparently, this is easy to realize on materials prone to have net surface charge, e.g., glass, quartz, and silicon wafer of which the silanol groups on the surface can be easily deprotonated by base. Some metals, e.g., stainless steel,[91] have a naturally occurring surface oxide layer that can facilitate anchoring of the polyions without extra surface treatment.

However, for practical applications, neutral substrate materials are also desirable, mostly organic polymers. At first glance, these hydrophobic surfaces are thought to be not very suitable to apply LbLs. However, in this circumstance, the surface can be primed so as to create a minimal surface charge. One relatively general method is

treating the substrate with an ammonia or oxygen plasma to graft amine or carboxylate groups to the substrate.[92] Other than chemical modification, pre-adsorption of adherent polyions, e.g., polyethylene imine[84] or poly(allylamine hydrochloride),[93] on the surface through nonspecific interactions has also proved to be a viable route to initiate LbL deposition. Besides, specific reactions can be utilized to introduce ionic or ionizable functionality. For instance, commercial poly(ethylene terephthalate), a polyester, was briefly treated with hot base to hydrolyze the ester bonds to carboxylate groups.[94] All these facts illustrate that the natural surface charge is not a strict precondition for selecting substrates suitable for the LbL technique.

1.4. Statement of Dissertation Research

The purpose of this dissertation is to investigate the feasibility of immobilizing RSe catalysts via an LbL method to develop a NO generating surface based on the catalytic decomposition of endogenous RSNOs. The LbL was characterized for bulk/surface physicochemical properties as well as its activity towards NO generation. Substrates with a diverse nature have been selected to apply this novel NO generation coating to demonstrate that the LbL technique is truly generic, with application to a broad range of surfaces. The LbL possessing RSe sites can be used as a strategy to endow biomedical devices with an EC-like function and hence potentially can improve their hemocompatibility.

Chapter 2 develops the general concept of building up an RSe immobilized LbL to generate NO from RSNOs. The RSe catalyst was first coupled to a polycation and then the resulting conjugate was manually coated on the substrate with a polyanion. The

properties of the resulting LbL were characterized using combined analytical means and more importantly, the NO generation behavior of the RSe immobilized in the LbL was confirmed. For characterization convenience, the LbL was primarily applied on quartz; however, polymeric substrate surfaces were also examined to prove the genericity of the LbL technique. Aimed at an ultimate biomedical application, the coating was preliminarily examined for potential systemic toxicity in concert with local adverse effects on the tissue in contact with the RSe contained LbL. This chapter lays the foundation of the entire thesis by demonstrating that the LbL is a feasible route to immobilize RSe sites on various solid supports to create NO generating surfaces.

Chapter 3 further discusses the benefit of using an automated coating apparatus to construct LbLs with up to 100 coating cycles. This thicker film with more RSe sites is shown to be capable of generating an NO flux comparable to that of an EC layer under biological conditions.

In Chapter 4, three kinds of metals, all of which are widely used to make vascular stents, were chosen as representatives of commercial biomedical surfaces to apply the automatic coated LbL. The LbLs were characterized and compared in parallel. The major purpose of this chapter is to show the ease of transferring this NO generation LbL from a bench-top idea to real commercial products.

Combining the NO generation capacity with a surface immobilized heparin on the same LbL coating for a synergic anti-thrombotic potency was explored in Chapter 5. Heparin was immobilized through different strategies, i.e. electrostatic adsorption or covalent attachment, and the resulting heparinized surfaces were assayed for their inhibitory activity on FXa. The impact of the surface anchored heparin on the LbL

stability and RSe site accessibility were also studied.

Chapter 6 provides conclusions and future directions for this dissertation work. Unresolved technical challenges on this RSe immobilized LbL are discussed. Potential development of novel RSe catalysts as well as LbL with improved performance to suit the *in vivo* animal test is addressed.

Finally, it should be noted that all of the chapters except Chapter 1 and 6 were converted from manuscripts published or submitted for publication. The work described in Chapter 2, which is the most significant achievement of this dissertation, has been published as a full paper in *Langmuir* (2008).[95] Chapters 3 and 5 will be combined into a full paper. Chapter 4 is under preparation for a communication type manuscript.

1.5. References

1. Samama, C. M.; Diaby, M.; Fellahi, J. L.; Mdhafar, A.; Eyraud, D.; Arock, M.; Guillosson, J. J.; Coriat, P.; Rouby, J. J. *Anesthesiology* **1995**, *83*, 56-65.

2. Krejcy, K.; Schmetterer, L.; Kastner, J.; Nieszpaurlos, M.; Monitzer, B.; Schutz, W.; Eichler, H. G.; Kyrle, P. A. *Arterioscler. Thromb. Vasc. Biol.* **1995**, *15*, 2063-2067.

3. Salvemini, D.; Masini, E.; Anggard, E.; Mannaioni, P. F.; Vane, J. *Biochem. Biophys. Res. Comm.* **1990**, *169*, 596-601.

4. Moncada, S.; Higgs, E. A.; Hodson, H. F.; Knowles, R. G.; Lopezjaramillo, P.; McCall, T.; Palmer, R. M. J.; Radomski, M. W.; Rees, D. D.; Schulz, R. *J. Cardiovasc. Pharmacol.* **1991**, *17*, S1-S9.

5. Rizk, M.; Witte, M. B.; Barbul, A. *World J. Surg.* **2004**, *28*, 301-306.

6. Witte, M. B.; Barbul, A. *Am. J. Surg.* **2002**, *183*, 406-412.

7. Broughton, G.; Janis, J. E.; Attinger, C. E. *Plast. Reconstr. Surg.* **2006**, *117*, 12S-34S.

8. Wu, Y. D.; Meyerhoff, M. E. *Talanta* **2008**, *75*, 642-650.

9. Frost, M. C.; Reynolds, M. M.; Meyerhoff, M. E. *Biomaterials* **2005**, *26*, 1685-1693.

10. Fleser, P. S.; Nuthakki, V. K.; Malinzak, L. E.; Callahan, R. E.; Seymour, M. L.; Reynolds, M. M.; Merz, S. I.; Meyerhoff, M. E.; Bendick, P. J.; Zelenock, G. B.; Shanley, C. J. *J. Vasc. Surg.* **2004**, *40*, 803-811.

11. Batchelor, M. M.; Reoma, S. L.; Fleser, P. S.; Nuthakki, V. K.; Callahan, R. E.; Shanley, C. J.; Politis, J. K.; Elmore, J.; Merz, S. I.; Meyerhoff, M. E. *J. Med. Chem.* **2003**, *46*, 5153-5161.

12. Cha, W.; Meyerhoff, M. E. *Biomaterials* **2007**, *28*, 19-27.

13. *Biomaterials science: an Introduction to materials in medicine.*; 2 ed.; Ratner, B. D. H., A. S.; Schoen, F. J.; Lemons, J. E., Ed.; Elsevier Academic Press: London, 2004.

14. Bittl, J. A. *J. Am. Coll. Cardiol.* **1996**, *28*, 368-370.

15. Clagett, G. P. E., R.C. In *Hemostasis and thrombosis: basic principles and clinical practice.*; Colman, R. W. H., J.; Marder, V.J.; Salzman, E.W., Ed.; Lippicott: Philadelphia, 1994, p 1486-1505.

16. Bick, R. L. In *Disorders of hemostasis and thrombosis.*; Bick, R. L., Ed.; American Society of Clinical Pathologist Press: Chicago, 1992.

17. Eberhart, R. C.; Clagett, C. P. *Semin. Hematol.* **1991**, *28*, 42-48.

18. Geiser, T.; Sturzenegger, M.; Genewein, U.; Haeberli, A.; Beer, J. H. *Stroke* **1998**, *29*, 1770-1777.

19. Edmunds, L. H. *Tex. Heart Inst. J.* **1996**, *23*, 24-27.

20. Mickelson, J. K.; Lakkis, N. M.; VillarrealLevy, G.; Hughes, B. J.; Smith, C. W. *J. Am. Coll. Cardiol.* **1996**, *28*, 345-353.

21. Meyerhoff, M. E. *Trac-Trends in Analytical Chemistry* **1993**, *12*, 257-266.

22. Tan, J.; Brash, J. L. *J. Biomed. Mater. Res.* **2009**, *90A*, 196-204.

23. Ladd, J.; Zhang, Z.; Chen, S.; Hower, J. C.; Jiang, S. *Biomacromolecules* **2008**, *9*, 1357-1361.

24. Chapman, D. *Langmuir* **1993**, *9*, 39-45.

25. Zhou, Z. R.; Meyerhoff, M. E. *Biomaterials* **2005**, *26*, 6506-6517.

26. Nojiri, C.; Kido, T.; Sugiyama, T.; Horiuchi, K.; Kijima, T.; Hagiwara, K.; Kuribayashi, E.; Nogawa, A.; Ogiwara, K.; Akutsu, T. *ASAIO J.* **1996**, *42*, M468-M475.

27. Elgue, G.; Blomback, M.; Olsson, P.; Riesenfeld, J. *Thromb. Haemostasis* **1993**, *70*, 289-293.

28. Wu, B.; Gerlitz, B.; Grinnell, B. W.; Meyerhoff, M. E. *Biomaterials* **2007**, *28*, 4047-4055.

29. Yeh, H. Y.; Lin, J. C. *J. Biomater. Sci. Polymer Ed.* **2009**, *20*, 807-819.

30. Sperling, C.; Salchert, K.; Streller, U.; Werner, C. *Biomaterials* **2004**, *25*, 5101-5113.

31. Kishida, A.; Akatsuka, Y.; Yanagi, M.; Aikou, T.; Maruyama, I.; Akashi, M. In *41st Annual Conference of ASAIO* Chicago, Il, 1995, p M369-M374.

32. Fowers, K. D.; Kopecek, J. *Colloids and Surfaces B-Biointerfaces* **1997**, *9*, 315-330.

33. Ignarro, L. J.; Buga, G. M.; Wood, K. S.; Byrns, R. E.; Chaudhuri, G. *Proc. Natl. Acad. Sci. U. S. A.* **1987**, *84*, 9265-9269.

34. Butler, A. R.; Williams, D. L. H. *Chem. Soc. Rev.* **1993**, *22*, 233-241.

35. Vaughn, M. W.; Kuo, L.; Liao, J. C. *Am. J. Physiol. Heart Circ. Physiol.* **1998**, *274*, H2163-H2176.

36. Ahlner, J.; Andersson, R. G. G.; Torfgard, K.; Axelsson, K. L. *Pharmacol. Rev.* **1991**, *43*, 351-423.

37. Parker, J. D.; Parker, J. O. *N. Engl. J. Med.* **1998**, *338*, 520-531.

38. Butler, A. R.; Glidewell, C. *Chem. Soc. Rev.* **1987**, *16*, 361-380.

39. Degraaf, J. C.; Banga, J. D.; Moncada, S.; Palmer, R. M. J.; Degroot, P. G.; Sixma, J. J. *Circulation* **1992**, *85*, 2284-2290.

40. Mowery, K. A.; Schoenfisch, M. H.; Saavedra, J. E.; Keefer, L. K.; Meyerhoff, M. E. *Biomaterials* **2000**, *21*, 9-21.

41. Reynolds, M. M.; Frost, M. C.; Meyerhoff, M. E. *Free Radic. Biol. Med.* **2004**, *37*, 926-936.

42. Zhou, Z. R.; Annich, G. M.; Wu, Y. D.; Meyerhoff, M. E. *Biomacromolecules* **2006**, *7*, 2565-2574.

43. Taite, L. J.; Yang, P.; Jun, H. W.; West, J. L. *J. Biomed. Mater. Res., Part B* **2008**, *84B*, 108-116.

44. DeRosa, F.; Kibbe, M. R.; Najjar, S. F.; Citro, M. L.; Keefer, L. K.; Hrabie, J. A. *J. Am. Chem. Soc.* **2007**, *129*, 3786-3787.

45. Reynolds, M. M.; Hrabie, J. A.; Oh, B. K.; Politis, J. K.; Citro, M. L.; Keefer, L. K.; Meyerhoff, M. E. *Biomacromolecules* **2006**, *7*, 987-994.

46. Frost, M. C.; Rudich, S. M.; Zhang, H. P.; Maraschio, M. A.; Meyerhoff, M. E. *Anal. Chem.* **2002**, *74*, 5942-5947.

47. Annich, G. M.; Meinhardt, J. P.; Mowery, K. A.; Ashton, B. A.; Merz, S. I.; Hirschl, R. B.; Meyerhoff, M. E.; Bartlett, R. H. *Crit. Care Med.* **2000**, *28*, 915-920.

48. Williams, D. L. H. *Acc. Chem. Res.* **1999**, *32*, 869-876.

49. Giustarini, D.; Milzani, A.; Dalle-Donne, I.; Rossi, R. *J. Chromatogr. B Analyt. Technol. Biomed. Life Sci.* **2007**, *851*, 124-139.

50. Dicks, A. P.; Swift, H. R.; Williams, D. L. H.; Butler, A. R.; AlSadoni, H. H.; Cox, B. G. *J. Chem. Soc.- Perkin Trans. 2* **1996**, 481-487.

51. Noble, D. R.; Swift, H. R.; Williams, D. L. H. *Chem. Comm.* **1999**, 2317-2318.

52. Oh, B. K.; Meyerhoff, M. E. *Biomaterials* **2004**, *25*, 283-293.

53. Oh, B. K.; Meyerhoff, M. E. *J. Am. Chem. Soc.* **2003**, *125*, 9552-9553.

54. Hwang, S. Y.; Meyerhoff, M. E. In *228th National Meeting of the American-Chemical-Society* Philadelphia, PA, 2004, p 292-POLY.

55. Hwang, S.; Meyerhoff, M. E. *Biomaterials* **2008**, *29*, 2443-2452.

56. Wu, Y. D.; Rojas, A. P.; Griffith, G. W.; Skrzypchak, A. M.; Lafayette, N.; Bartlett, R. H.; Meyerhoff, M. E. *Sensor Actuator B Chem.* **2007**, *121*, 36-46.

57. Freedman, J. E.; Frei, B.; Welch, G. N.; Loscalzo, J. *J. Clin. Invest.* **1995**, *96*, 394-400.

58. Hou, Y. C.; Guo, Z. M.; Li, J.; Wang, P. G. *Biochem. Biophys. Res. Comm.* **1996**, *228*, 88-93.

59. Singh, R.; Kats, L. *Anal. Biochem.* **1995**, *232*, 86-91.

60. Dickson, R. C.; Tappel, A. L. *Arch. Biochem. Biophys.* **1969**, *130*, 547-&.

61. Jacob, C.; Giles, G. L.; Giles, N. M.; Sies, H. *Angew. Chem. Int. Ed.* **2003**, *42*, 4742-4758.

62. Clyne, M. A. A.; Wayne, R. P.; Thrush, B. A. *Trans. Farad. Soc.* **1964**, *60*, 359-&.

63. Hampl, V. V.; Walters, C. L.; Archer, S. L. In *Methods in nitrc oxide research*; Feelisch, M., Stamler, J. S., Eds.; John Wiley & Sons Ltd: Chichester, England, 1996, p 309-318.

64. Iler, R. K. *J. Colloid Interface Sci.* **1966**, *21*, 569-&.

65. Decher, G. *Science* **1997**, *277*, 1232-1237.

66. Zhang, X.; Chen, H.; Zhang, H. Y. *Chem. Comm.* **2007**, 1395-1405.

67. Kotov, N. A. In *4th International Conference on Nanostructured Materials (NANO 98)* Stockholm, Sweden, 1998, p 789-796.

68. Arys, X.; Jonas, A. M.; Laschewsky, A.; Legras, R. In *Supramolecular polymers*; Ciferri, A., Ed.; Marcel Dekker: New York, 2000, p 505-564.

69. Cai, K. Y.; Rechtenbach, A.; Hao, J. Y.; Bossert, J.; Jandt, K. D. *Biomaterials* **2005**, *26*, 5960-5971.

70. Ariga, K.; Onda, M.; Lvov, Y.; Kunitake, T. *Chem. Lett.* **1997**, 25-26.

71. Podsiadlo, P.; Tang, Z. Y.; Kotov, N. A. In *229th National Meeting of the American-Chemical-Society* San Diego, CA, 2005, p 548-COLL.

72. Donath, E.; Walther, D.; Shilov, V. N.; Knippel, E.; Budde, A.; Lowack, K.; Helm, C. A.; Mohwald, H. *Langmuir* **1997**, *13*, 5294-5305.

73. Li, C.; Mitamura, K.; Imae, T. *Macromolecules* **2003**, *36*, 9957-9965.

74. Li, N.; Deng, Z. Q.; Lin, Y. A.; Zhang, X. J.; Geng, Y. H.; Ma, D. G.; Su, Z. H. *J. Appl. Phys.* **2009**, *105*.

75. Bertrand, P.; Jonas, A.; Laschewsky, A.; Legras, R. *Macromol. Rapid Comm.* **2000**, *21*, 319-348.

76. Levasalmi, J. M.; McCarthy, T. J. *Macromolecules* **1997**, *30*, 1752-1757.

77. Laschewsky, A.; Mayer, B.; Wischerhoff, E.; Arys, X.; Bertrand, P.; Delcorte, A.; Jonas, A. In *7th International Conference on Organized Molecular Films (LB7)* Numana, Italy, 1995, p 334-337.

78. Hoogeveen, N. G.; Stuart, M. A. C.; Fleer, G. J.; Bohmer, M. R. *Langmuir* **1996**, *12*, 3675-3681.

79. Lvov, Y.; Decher, G.; Mohwald, H. *Langmuir* **1993**, *9*, 481-486.

80. Lvov, Y. M.; Decher, G. *Kristallografiya* **1994**, *39*, 696-716.

81. Schlenoff, J. B.; Ly, H.; Li, M. *J. Am. Chem. Soc.* **1998**, *120*, 7626-7634.

82. Caruso, F.; Caruso, R. A.; Mohwald, H. *Chem. Mater.* **1999**, *11*, 3309-3314.

83. Sukhorukov, G. B.; Schmitt, J.; Decher, G. In *1st International Symposium on Polyelectrolytes/Discussion Meeting of Deutsche-Bunsen-Gesellschaft-fur-Physikalische-Chemie on Polyelectrolytes in Solution and at Interfaces* Potsdam, Germany, 1995, p 948-953.

84. Delcorte, A.; Bertrand, P.; Wischerhoff, E.; Laschewsky, A. *Langmuir* **1997**, *13*, 5125-5136.

85. Kaneko, F.; Baba, A.; Advincula, R.; Fells, E.; Jones, N.; Guzman, J. *Abstracts of Papers of the American Chemical Society* **1999**, *217*, 181-POLY.

86. Yang, S. G.; Zhang, Y. J.; Zhang, X. Y.; Guan, Y.; Xu, J.; Zhang, X. L. *Chemphyschem* **2007**, *8*, 418-424.

87. Li, B. Y.; Rozas, J.; Haynie, D. T. In *10th Annual Conference of the Institute-of-Biological-Engineering* Athens, GA, 2005, p 111-117.

88. Fischer, P.; Laschewsky, A.; Wischerhoff, E.; Arys, X.; Jonas, A.; Legras, R. *Macromol. Symp.* **1999**, *137*, 1-24.

89. Dejeu, J.; Buisson, L.; Guth, M. C.; Roidor, C.; Membrey, F.; Charraut, D.; Foissy, A. In *Conference Formula IV - Frontiers in Formulation Science* London, ENGLAND, 2005, p 26-35.

90. Picart, C.; Mutterer, J.; Richert, L.; Luo, Y.; Prestwich, G. D.; Schaaf, P.; Voegel, J. C.; Lavalle, P. *Proc. Natl. Acad. Sci. U. S. A.* **2002**, *99*, 12531-12535.

91. Tan, Q. G.; Ji, J.; Barbosa, M. A.; Fonseca, C.; Shen, J. C. *Biomaterials* **2003**, *24*, 4699-4705.

92. Lappan, U.; Buchhammer, H. M.; Lunkwitz, K. *Polymer* **1999**, *40*, 4087-4091.

93. Park, J.; Hammond, P. T. *Macromolecules* **2005**, *38*, 10542-10550.

94. Chen, W.; McCarthy, T. J. *Macromolecules* **1997**, *30*, 78-86.

95. Yang, J.; Welby, J. L.; Meyerhoff, M. E. *Langmuir* **2008**, *24*, 10265-10272.

CHAPTER 2

NITRIC OXIDE GENERATION FROM S-NITROSOTHIOLS BY ORGANOSELENIUM IMMOBILIZED LAYER-BY-LAYER ASSEMBLY

2.1. Introduction

As discussed in Chapter 1, NO generation has emerged as a new anti-thrombotic strategy by circumventing the depletion of NO donors during long term application. The concept is based on utilizing endogenous *S*-nitrosothiols (RSNO) as the NO source instead of synthetic diazeniumdialote species, and catalytically breaking down RSNOs to produce NO at the device surface. A sustained NO flux is within expectation because the endogenous RSNO levels at the implantation site are constantly maintained by blood circulation.

Organoselenium (RSe) small molecules have been shown to potently catalyze RSNO decomposition to produce NO.[1] The proposed mechanism comprises a fast denitrosation of RSNO by diselenide, and a slower catalytic cycle involving a selenolate intermediate which is regenerated by the reducing agent (see Section 1.2.3.). These RSe catalysts have been chemically immobilized on model substrates, and the immobilized RSe sites display remarkable catalytic activity. Although various RSe derivatives are available

for direct coupling, complicated processing is usually required on the device to provide the surface functionality needed for covalent bonding, especially when the devices are made of chemically inert materials. For example, cellulose filter paper was first oxidized by periodate to generate dialdehyde groups so that selenocystamine could be subsequently immobilized.[1] Recently, a carboxylic acid terminated RSe species was covalently linked to polyethyleneimine (PEI) which was then crosslinked into a hydrogel film within the pore structure of a cellulose dialysis membrane to prepare an amperometric *S*-nitrosothiol sensor.[2] Unfortunately, most modern biomedical devices in use do not possess the necessary surface functionality, porosity, or geometric form to enable convenient covalent attachment of the RSe species. Hence, a simple and universal immobilization method that is applicable to various types of surfaces is needed.

As mentioned in Chapter 1, Layer-by-Layer assembly (LbL) is a coating technique relying on the electrostatic adsorption of polyions onto a charged substrate and the subsequent surface charge reversal. The distinctive nonspecific driving force allows this method to be applied onto substrates with net surface charge regardless of their nature and topology. The properties of an LbL assembly are widely believed to be determined primarily by the nature of the polyelectrolytes employed, making this method a truly "generic" surface modification approach. Furthermore, the straightforward dip-wash processing in aqueous solution is more economical, environmentally benign and suitable for automation.

Herein, the feasibility of depositing an LbL film using RSe immobilized

polyelectrolyte is investigated (Figure 2.1). The resulting LbL on quartz substrate was characterized using combined analytical techniques. The catalytic potency of such immobilized RSe coatings was studied using GSNO as a model RSNO and GSH as the source of reducing equivalent. Further, the LbL was also applied on polymeric substrates to demonstrate its universal application on various surfaces.

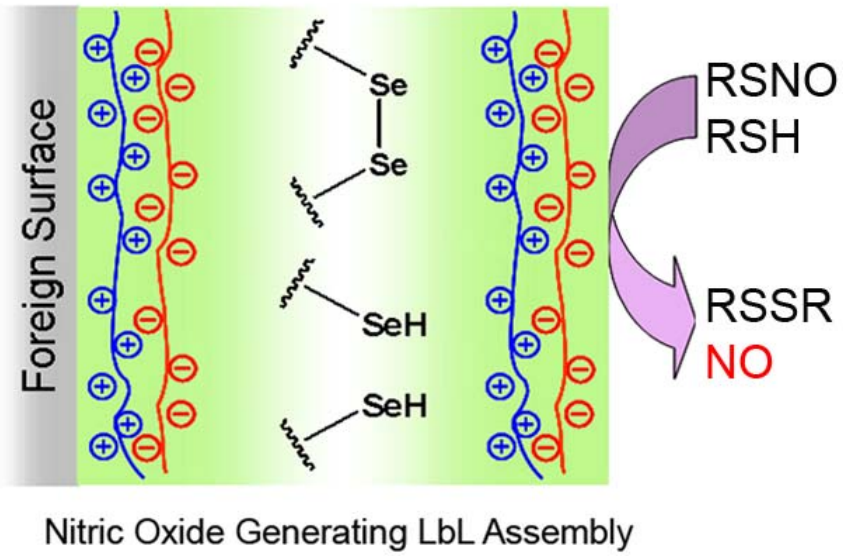

Figure 2.1. Nitric oxide generation from endogenous RSNOs by an LbL constructed using RSe immobilized polyelectrolyte.

2.2. Experimental

2.2.1. Materials

Polyethyleneimine (PEI, M_w 25 kD), polydiallyldimethylammonium chloride (PDDA, M_w 100-200 kD), poly(vinyl sulfate) (potassium salt; PVS, M_w 170 kD), poly(sodium 4-styrenesulfonate) (PSS, M_w 70 kD), heparin sodium salt (17-19 kD), pentosan polysulfate (PPS), poly(acrylic acid) 35 wt.% solution in water (PAA, M_w 100 kD), sodium alginate (Alg, M_w 12-80 kD), fluorescein-5-isothiocyanate (FITC), glutathione (GSH), 1-(3-dimethylaminopropyl)-3-ethylcarbodiimide (EDC), sodium borohydride ($NaBH_4$), *N*-hydroxysuccinimide (NHS), 2-(*N*-morpholino)ethanesulfonic acid (MES), and 2-(*N*-cyclohexylamino)-ethanesulfonic acid (CHES) were obtained from Sigma-Aldrich (St. Louis, MO) and used as received. The 3140 RTV silicone rubber was purchased from Dow Corning Corporation (Midland, MI). 3,3'-Diselenidedipropionic acid (SeDPA) and *S*-nitrosoglutathione (GSNO) were synthesized as described previously.[1] All solutions were prepared with 18 MΩ cm^{-1} deionized distilled water obtained from a Milli-Q system (Millipore Corp., Billerica, MA).

2.2.2. Preparation of organoselenium immobilized polyelectrolyte

RSe derivatized PEI (SePEI) was synthesized following a procedure slightly modified from the one reported earlier.[1] Briefly, SeDPA (76 mg, 0.25 mmol) was activated with EDC (285 mg, 1.5 mmol) and NHS (115 mg, 1 mmol) and then was allowed to react with

given amounts of PEI in MES buffer (pH = 6.0) for 2 h. The reaction mixture was then centrifuged in an Amicon® centrifugal filter unit (MWCO = 3 kD, Millipore Corp., Billerica, MA) at 4,000 rpm for 40 min to remove the coupling reagents and any unreacted SeDPA. The resulting yellow SePEI solution was reduced with $NaBH_4$ to break any diselenide crosslinks into selenols and then exhaustively dialyzed (Spectra/Por® 7, MWCO = 3.5 kD, Spectrum Laboratories Inc., Rancho Dominguez, CA) in 50 mM NaCl for 3 d to liberate any unreacted -SeC_2H_4COOH halves. The dialyzed solution was concentrated into a yellow viscous solution and stored at 4 °C until use. The Se loading was determined by digesting SePEI dry polymer with known mass using fuming nitric acid and measuring the Se quantity in the digestion solution using ICP-MS.

2.2.3. Labeling of SePEI with fluorescein chromophore

Despite its characteristic absorbance in near UV region, the diselenides present in the LbL coating are not easily observed due to their low quantity and low molar extinction coefficient (ε_{300} = 240 M^{-1} cm^{-1}).[3] Therefore, the SePEI polymer was labeled with FITC chromophore (ε_{495} = 76,000 M^{-1} cm^{-1})[4] to render the polymer spectroscopically visible. SePEI in CHES (2 mg mL^{-1}, 10 mL) was mixed with FITC/DMF solution (1 mg mL^{-1}, 0.8 mL) under constant stirring for 1 h. The resulting orange adduct was washed, concentrated and redissolved in PBS for subsequent use. The labeling degree was calculated to be 0.53 following protocol provided by Sigma Aldrich. This labeled SePEI was exclusively employed for UV-Vis study to observe stepwise deposition of SePEI

during the LbL process.

2.2.4. Fabrication of organoselenium immobilized Layer-by-Layer films on quartz

All polyelectrolytes were made into 1 mg mL^{-1} PBS solution (pH = 7.4), except for PDDA (Figure 2.2a) which was dissolved in CHES buffer (pH = 9.3). The quartz slide was cleaned using piranha solution (3:7 v/v H_2SO_4/H_2O_2 mixture) for 30 min before use to fully remove surface impurities. *(Caution: this solution is extremely corrosive.)* The LbL multilayer was prepared by manually immersing a quartz slide alternately into the polycation (SePEI or PDDA) and polyanion (Figure 2.2b-g) solutions for 10 min. The slide was dip-washed using PBS buffer after each adsorption step to remove any residual polymer solution on the surface (see Scheme 2.1). For UV-Vis characterization, the LbL was deposited on the inner wall of a quartz cuvette by filling the cuvette with polyelectrolyte solutions or washing buffers in the same sequence as described above. Notably, FITC labeled SePEI was used exclusively for UV-Vis characterization, whereas plain SePEI was used for all other experiments.

2.2.5. Characterization of NO generation LbL

UV-Vis. The stepwise growth of the LbL film was monitored using a UV-Vis spectrophotometer (Lambda 35, Perkin Elmer, MA). The cuvette was scanned from 550 nm to 450 nm with a data interval of 1 nm after every (SePEI/Alg) bilayer was deposited. The FITC labeled SePEI species was employed exclusively in this study.

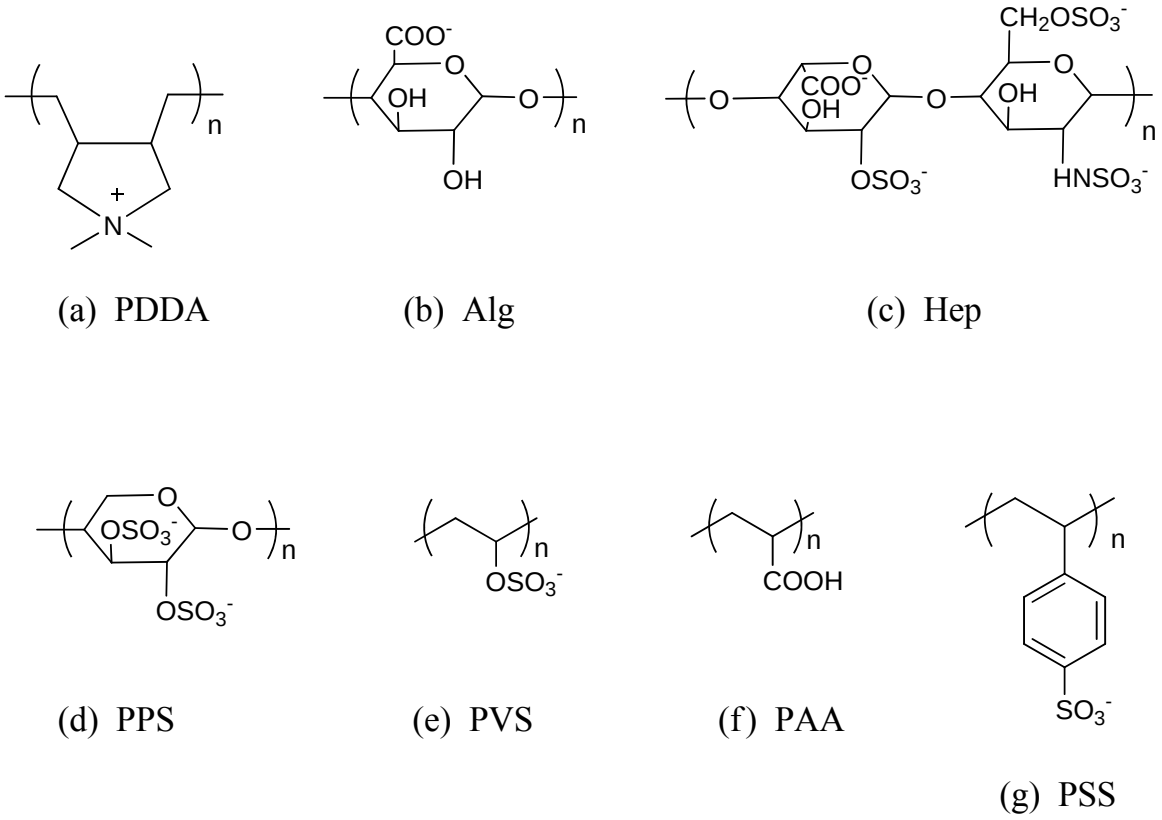

(a) PDDA (b) Alg (c) Hep

(d) PPS (e) PVS (f) PAA (g) PSS

Figure 2.2. Polyelectrolytes used: (a) poly(diallyldimethylammonium chloride) (PDDA); (b) sodium alginate (Alg); (c) heparin (Hep); (d) pentosan polysulfate (PPS); (e) poly(vinyl sulfate, potassium salt) (PVS); (f) poly(acrylic acid) (PAA); (g) poly(sodium 4-styrenesulfonate) (PSS).

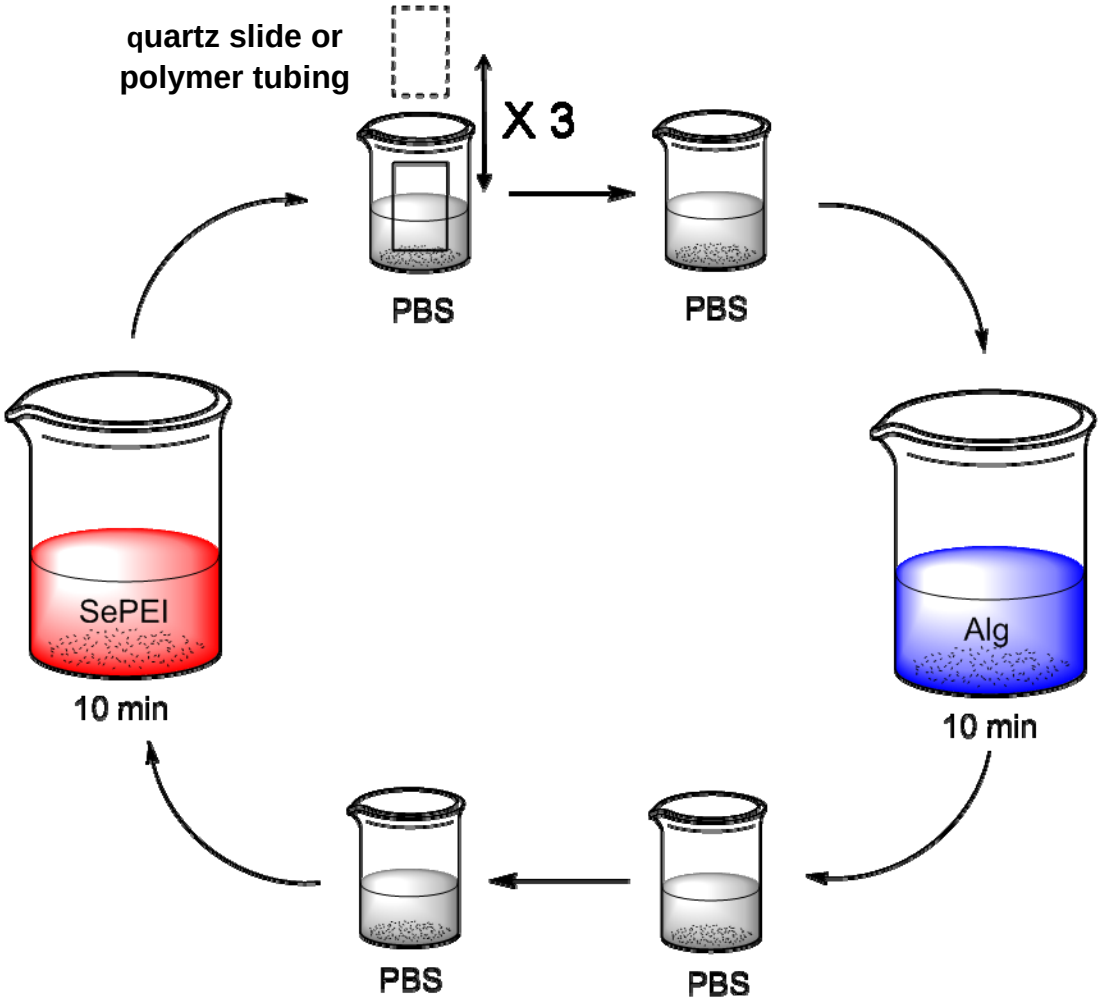

Scheme 2.1. Schematic representation of the procedure to manually assemble an LbL structure. The substrate is allowed to adsorb polyelectrolyte molecules for 10 min in each polyion solution. After the adsorption, the substrate is washed in two PBS bathes by quickly dipping the substrate into the buffer three times.

XPS. X-ray photoelectron spectroscopy was performed on a Kratos Axis Ultra XPS (Kratos Analytical, England). The X-ray source employed was a monochromatized Mg Kα operated at 10 kV/ 80 W with pass energy of 80 eV. Charge neutralization was used to compensate the charge accumulation on the sample. The coating was scanned at step sizes of 1 eV and 0.1 eV (0.1 s each step) for survey and core scans, respectively. Prior to the measurement, the sample was out-gassed overnight in the sample transfer chamber under high vacuum. The spectrum was processed using CasaXPS version 2.3.12.

SEM. Surface morphology of the polyelectrolyte multilayers was examined on a FEI Nova Nanolab Scanning Electron Microscope via the detection of secondary electrons. The specimens were dried in a N_2 atmosphere overnight and then gold coated using a SPI Sputter Coater at 18 mA for 60 s for better imaging.

Contact Angle. Static air–water contact angles were measured by a sessile drop method using a Cam-100 Optical Contact Angle Goniometer (KSV Instruments Ltd., Monroe, CT) at ambient humidity and temperature. The annealed LbL coated quartz slides were dried with N_2 flow for 2 days. For each polymer surface, 4 drops were examined to obtain the average contact angle values.

Quantification of Se in $(SePEI/Alg)_{10}$. A slide (1 × 2 cm) coated with 10 (SePEI/Alg) bilayers was placed in a vial containing 4 mL 100% fuming nitric acid. The polyelectrolyte film immediately peeled off from the slide upon acidification and floated freely in the acid. The vial was capped and kept at room temperature for 24 h during which the LbL broke down into a number of small pieces. Then, the acid was heated to

60°C until all these small pieces were completely digested. The digesting solution was brought to a volume of 25 mL using a volumetric flask and sent for ICP-MS to determine the Se concentration. Another vial containing same amount of nitric acid but without the multilayer digest was also prepared following the same protocol and was used as a control.

Se Leaching Test. $(SePEI/Alg)_{10}$ was coated on glass shell vials (1.5 cm ID, 3.5 cm, Fisherbrand®, Fisher Scientific Inc., Pittsburgh, PA) with a coating area calculated to be 12.4 cm^2. Four mL of PBS buffer containing 100 μM GSH and 50 μM GSNO was added to each vial, which was enough to submerge the entire coating area, to extract leachable selenium species from the LbL. The vials were then capped, wrapped with aluminum foil, and kept at room temperature for 5 d. Every 24 h, the extracting solutions were collected and the vials were refilled with fresh PBS buffer containing the same concentrations of GSH and GSNO. After 5 d extraction, the coatings were digested using nitric acid to quantify the remaining Se in the LbL. The extracts and digesting solutions were brought up to a volume of 25 mL for eventual ICP-MS measurements.

***In Vivo* Toxicity Study.** Samples for *in vivo* toxicity study were prepared following ISO standards 10993-11 and ISO 10993-12. LbLs containing 10 bilayers were coated on the inner surfaces of glass shell vials (1.7 cm ID, 6.5 cm, Fisherbrand®, Fisher Scientific Inc., Pittsburgh, PA) with a surface area calculated to be 28.9 cm^2. The vials were filled with 12 mL phosphate buffered saline or vegetable oil to reach a surface-volume-ratio of 2.4 cm^2 mL^{-1}. The vials were capped and incubated at 37 ˚C with constant agitation for 72 h. Systemic toxicity and irritation tests were performed following ISO 10993-11 and

ISO 10993-10, respectively.

NO Detection. Substrates coated with $(SePEI/Alg)_n$ LbL films were inserted into a PBS test solution (2 mL, pH = 7.4) containing GSNO and GSH. The NO produced was purged from the solution with N_2 flow and detected using a chemiluminescence NO analyzer (NOA) (Sievers 280, Boulder, CO). The amount of NO evolved from the solution was calculated based on the calibration curves of the NOA, which were obtained regularly by plotting the integrated NOA signal (ppb·s) during calibration vs. the introduced amount (moles) of NO into the system via nitrite reduction in an acidified potassium iodide solution. To prevent unwanted RSNO decomposition from external thermal or photo stimuli,[5] all NOA tests were performed at room temperature using amber reaction vessels. Lights in the laboratory were also turned off when these experiments were conducted. EDTA was added to the testing solution in order to eliminate any GSNO decomposition catalyzed by trace metal ions, e.g., Cu(II).

***In Vitro* Blood Test.** Fresh heparinized (5 U mL^{-1}) sheep whole blood was obtained from ECMO Laboratory in the Medical School at the University of Michigan. Three mL of blood was carefully transferred into a 15 mL polypropylene centrifuge tube. A glass slide coated with $(SePEI/Alg)_{10}$ was gently positioned in the blood. The tube was sealed and wrapped with aluminum foil to avoid light exposure. During the entire procedure, the blood surface was kept below the top of the coating to prevent any accidental contact with bare glass. After 24 h incubation at 4 °C in the dark, the slide was removed and rinsed with PBS buffer to wash off any loosely adsorbed blood residue. A control slide was

immersed in 3 mL PBS and processed following the same procedure. The ability of the LbL to generate NO from GSNO was then examined by the chemiluminescence method described above.

Preparation of Polymeric Substrates. Silicone tubing (0.64 mm ID/1.19 mm OD, 2 cm), purchased from Helix Medical Inc. (Carpinteria, CA), and 5 Fr double lumen polyurethane catheter (Cook, Denmark) were cut into 1-inch segments. The open ends of these segments were sealed with RTV 3140 SR followed by curing under ambient conditions overnight. Before immersion in polyelectrolyte solutions for LbL deposition, the polymeric substrates were cleaned by sonicating in deionized H_2O and ethanol for 20 min each. The silicone rubber surfaces were soaked in PBS overnight before priming treatments, whereas the polyurethane substrates were directly coated with $(SePEI/Alg)_n$ without a precursor layer.

2.3. Results and Discussion

2.3.1. Synthesis of RSe derivatized polyelectrolyte (SePEI)

To integrate catalytic activity into an LbL structure, a small molecule organoselenium species, e.g., 3,3'-diselenodipropionic acid (SeDPA), must be covalently linked to a polycation or polyanion without significantly compromising the capability of the polyelectrolyte to interact with its oppositely charged counterpart. Polyethyleneimine was selected due to its abundant primary amine sites within the structure which can be reacted

readily with an activated carboxylic acid group. An EDC/NHS mediated coupling reaction was adapted from a previously reported procedure (Scheme 2.2).[1] After separation from the reaction mixture, the modified PEI shows a light yellow color acquired from the diselenide bond indicating a successful immobilization of SeDPA onto the polymer.

Although SeDPA has two carboxylate groups capable of reacting with PEI, sometimes only one of the two carboxylic acids forms the desired amide bond, leaving an unreacted half molecule attached to the polymer through a diselenide bond with the reacted half. When the diselenide bond is reduced by GSNO or GSH during the NO generation reaction, the unreacted half molecule may leach out and could ultimately cause serious toxicity concerns. Consequently, the SePEI was reduced with $NaBH_4$ after the coupling reaction to break all the diselenide bonds into selenols, as indicated by the disappearance of the distinctive yellow color from the diselenide species. The reduced SePEI was then exhaustively dialyzed to remove any SeDPA halves detached from the polymer. After dialysis, the polymer concentrate regains its yellow color indicating that the selenols are oxidized back to diselenides during the dialysis.

As summarized in Table 2.1, the loading of RSe sites on PEI can be adjusted by controlling the reaction stoichiometry between SeDPA and PEI. SePEI3, SePEI7 and SePEI12, termed with respective to the weight percentage of elemental Se, were obtained. Also, the ratio of reacted $–NH_2$ and –COOH in the final product was back calculated indicating that only a portion of primary amines in PEI were coupled with RSe catalyst.

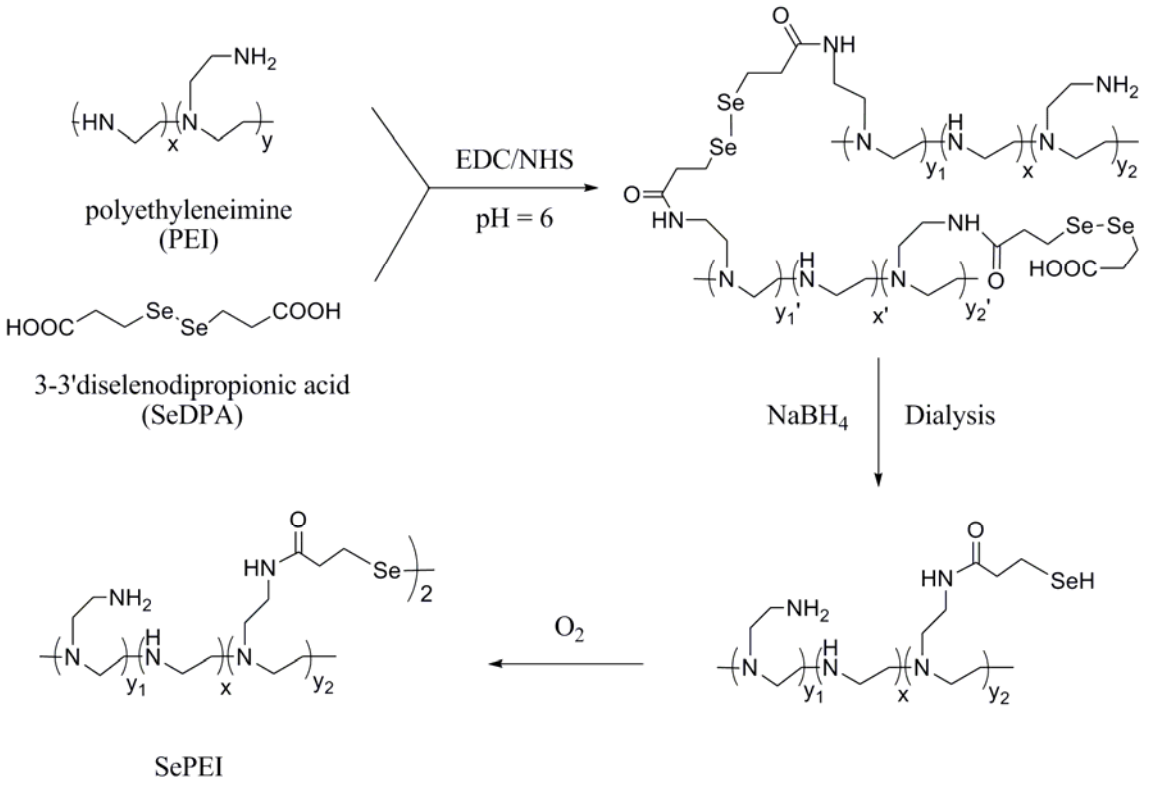

Scheme 2.2. Scheme of SePEI preparation by an EDC/NHS coupling reaction between SeDPA and PEI. Unreacted SeDPA halves are liberated by dissecting the diselenide bond with $NaBH_4$ and removed through exhaustive dialysis. The reduced RSeH is oxidized back to diselenide by ambient O_2 during dialysis, forming crosslinks between PEI chains.

Actually, it is necessary to keep some of the primary amines ionizable so that the modified polymer can still interact effectively with polyanions to form the LbL film.

	n(PEI-NH_2) (mmol)	n(SeDPA) (mmol)	Product NH_2:COOH	Se *wt* %
SePEI3	**2.3**	**0.25**	**1 : 0.065**	**2.8±0.2 %**
SePEI7	**1.2**	**0.25**	**1 : 0.16**	**6.6±0.1 %**
SePEI12	**0.6**	**0.25**	**1 : 0.3**	**11.5 %**

Table 2.1. Summary of SeDPA/PEI coupling stoichiometry and the composition of corresponding products. The moles of primary amine sites in PEI reactant are calculated based on a 1:2:1 ratio of primary, secondary and tertiary amines.

The attachment of SeDPA onto PEI inevitably impacts the properties of the polycation. Indeed, SePEI12 formed an insoluble precipitate after dialysis. This may be attributed to the greater consumption of ionizable amine sites which significantly contributes to the good solubility of PEI in water. Furthermore, the coupling of SePEI introduces more hydrophobic alkyl components to the PEI and therefore lowers its hydrophilicity. SePEI7, due to its higher RSe content and high solubility, was used throughout the entire dissertation work to construct NO generation LbL films and is generally termed as

"SePEI" for simplicity.

2.3.2. Preparation of LbL from SePEI and different polyanions (PA)

In order to deposit an LbL film, the positively charged polymer, i.e., SePEI in this context, has to interact with a polymeric species bearing negative charges. Several synthetic and natural anionic polymers (Figure 2.2b-g) were therefore allowed to pair with SePEI. The criterion used to select the best candidate was the amount of SePEI deposited on the quartz cuvette within a given number of coating cycles. In this study, FITC labeled SePEI (SePEI-FITC) was used to render the coating spectroscopically visible. The labeled SePEI shows a maximum absorbance at 500 nm due to the FITC chromophore. Hence, the absorbance from the resulting LbL was measured at the same wavelength. The quartz cuvette was first filled with a weakly basic CHES buffer (pH = 9.3) containing PDDA, a strong polyelectrolyte species bearing permanent ammonium ions, to enhance the ionization of the surface hydroxyl groups on the quartz. Then, the polyanions were allowed to interact with the PDDA layer and the coating cycle was repeated one more time to form a $(PDDA/PA)_2$ priming layer before SePEI was used to replace PDDA (see Figure 2.2a) to continue the LbL deposition. For each polyelectrolyte pair, UV-Vis measurement was taken after 4 and 8 (SePEI/PA) bilayers were coated. The absorbance change within these 4 bilayers was used to compare the interaction between SePEI and different PA species.

As shown in Figure 2.3, an increase of UV absorbance was observed for all the PAs

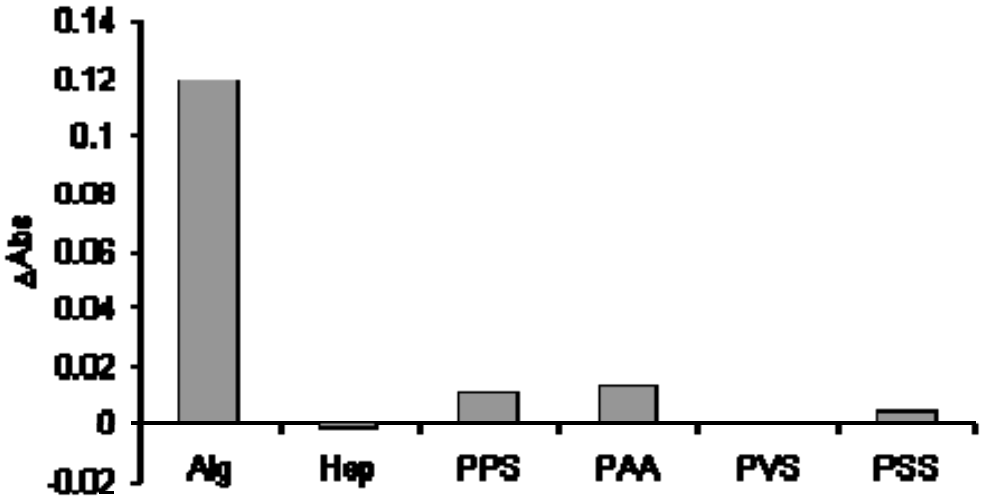

Figure 2.3. UV-Vis absorbance change at 500 nm for different SePEI/PA pairs between the 4th and the 8th coating cycles.

except heparin, indicating formation of polyelectrolyte LbLs. However, the ΔAbs varied markedly dependent on the polyanionic species: PSS only weakly interacted with SePEI giving a ΔAbs just above zero; PPS, PAA and PVS gave medium UV increases (0.01 ~ 0.02); Alg demonstrated the strongest capability of associating with SePEI, as indicated by a ΔAbs as high as 0.12. In general, the polysaccharide polyanions adsorb more SePEI than their polyvinyl counterparts carrying the same anionic functionality, i.e., Alg and PPS gave higher ΔAbs than PAA and PVS, respectively. So far, there is still a lack of sound theories that can be strictly followed to interpret these disparate complexation behaviors across different polyelectrolyte pairs. This is because the interaction between two oppositely charged species is highly susceptible to a number of factors such as molecular weight, ionic groups, chain stiffness and charge density, etc.[6] As a consequence, it is very

difficult to conduct systematic structure-interaction studies by varying only one parameter while keeping the others the same. However, it is reasonable to postulate that the relative rigid polysaccharide chain, compared with the polyvinyl backbone comprising freely rotating C-C single bonds, may prevent the polysaccharides from effectively matching their negative charges with the ammonium groups on SePEI. This ineffective interaction may result in more unbalanced charges which reciprocally adsorb more polyions in the next deposition step, despite the binding between the polyion pair being somewhat weaker. Notably, Hep showed a negative ΔAbs, implying that some of the SePEI molecules were desorbed from the quartz surface upon interacting with the Hep chains in the polyanionic solution. This is probably caused by the formation of a soluble polycation-polyanion complex. Based on these results, Alg was finally chosen to construct the NO generation LbL in attempts to maximize the amount of RSe catalyst immobilized in the film for a given number of coating cycles.

2.3.3. Stepwise growth of $(SePEI/Alg)_n$ LbL on quartz

The successive adsorption of $(SEPI/Alg)_n$ on quartz cuvette can be discerned by visually examining the quartz substrates after every immersion in Alg solution. After the 4^{th} cycle, the quartz slide became cloudy and continuously lost its transparency as more bilayers were deposited. The presence and propagation of this cloudiness suggest formation of a heterogeneous film structure which is attributed to the fast adsorption kinetics.[7] When the substrate is alternately immersed into SePEI and Alg solutions, the

polyions associate at the interface at such a fast rate that many defects are trapped and chain rearrangement does not have sufficient capacity to "heal" the defects in time before another coating cycle. In good agreement with these visual observations, UV-Vis spectra of the LbL films exhibit a steady background absorbance increase owing to the heterogeneity of the multilayer. Upon baseline subtraction, the UV-Vis spectra display consecutive increments after each coating cycle with a maximum absorbance at 503 nm (see Figure 2.4).

The absorbance at 503 nm was then extracted to plot against the number of bilayers in the LbL (see Figure 2.5). Interestingly, the UV-Vis data exhibits an "S" shape rather than a uniformly linear or exponential type curve that is typically observed in LbL assembly.[8-10] The slope of the curve is very flat initially but becomes steeper from the 4^{th} bilayer and then flattens again from the 6^{th} bilayer. Such a variation suggests a possible surface morphology evolution of the LbL, given that the SePEI is electrostatically attracted by the existing multilayer on the substrate. Therefore, SEM snapshots of $(SePEI/Alg)_n$ were taken to assess surface features at various stages of the coating process. The initial $(PDDA/Alg)_2$ precursor layer is found to provide a smooth and even coverage on the quartz substrate (Figure 2.6a). One (SePEI/Alg) bilayer only slightly roughens the surface with scattered islands that are hardly distinguishable from the background owing to their small dimensions (Figure 2.6b). When more layers of the polyelectrolytes are deposited, the tiny islands quickly develop into coalesced large particles with a maximum

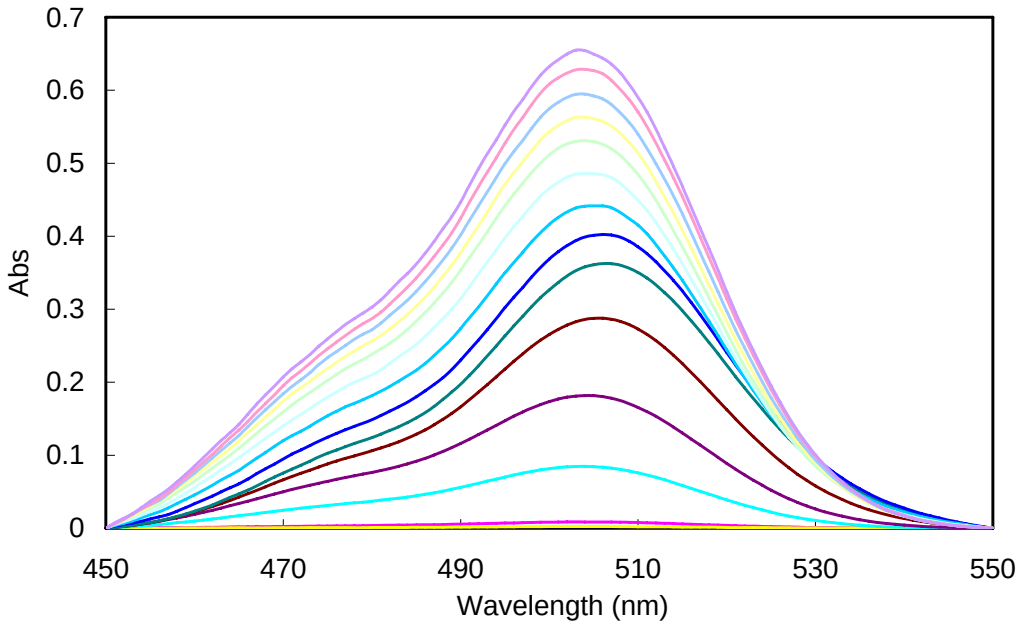

Figure 2.4. UV-Vis scan of (SePEI/Alg)n LbL after every coating cycle (n=15).

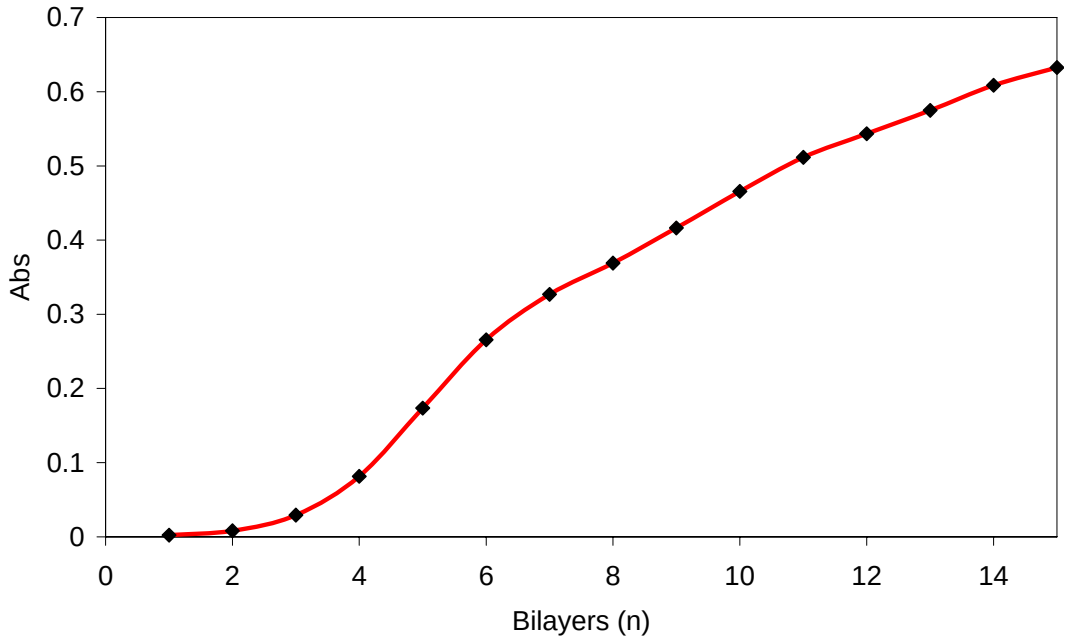

Figure 2.5. Absorbance at 503 nm of $(SePEI/Alg)_n$ after every bilayer assembled.

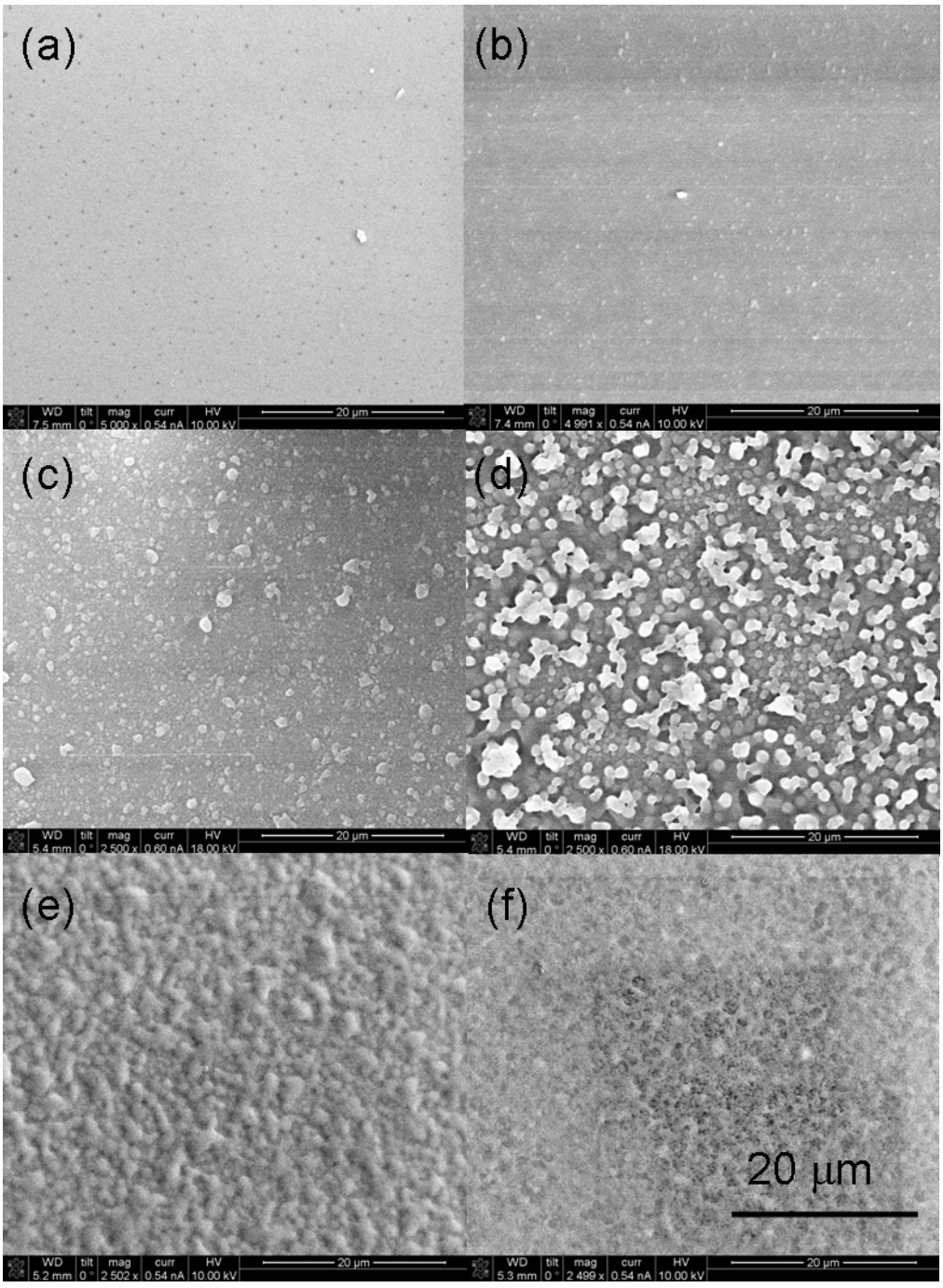

Figure 2.6. SEM of $(SePEI/Alg)_n$ on quartz slide: (a) $(PDDA/Alg)_2$ precursor layer; (b) $(SePEI/Alg)_1$; (d) $(SePEI/Alg)_2$; (d) $(SePEI/Alg)_3$; (e) $(SePEI/Alg)_4$; (f) $(SePEI/Alg)_5$.

diameter of ca. 2 μm, which considerably roughen the surface (Figure 2.6c-d). This observation supports the same heterogeneous LbL structure implied by the UV-Vis study. In fact, a recent study has reported that LbL coatings do not start growing as a successive superposition of interacting polymer layers, and polyelectrolyte adsorption is kinetically stopped by the surface potential reversal other than at full coverage of the substrate. In this case, the PEI crosslinked by the diselenides possesses a bulkier conformation compared with linear polyelectrolytes, which further sterically impedes the effective interaction of the SePEI with the substrate. As a result, little adsorption of SePEI can accumulate enough positive charge to reverse the surface potential, which explains the slow increase in UV-Vis adsorption for the first couple of coating steps. A full coverage of the surface is finally realized after 4 bilayers (Figure 2.6e); however, the earlier coarse structure can still be vaguely recognized from the bumpy surface contour. Continuous deposition of polyelectrolytes significantly smoothes the bumpiness and leads to more modest surface irregularities (Figure 2.6f). The transition from discrete particles to continuous layer as well as the subsequent smoother surface can be attributed to the propensity of polyelectrolytes to bridge over the underlying defects. Based on the SEM data, we speculate that the over-adsorption of SePEI from the 4^{th} to 6^{th} bilayer is chiefly a matter of greater surface roughness which increases the surface area. After the 6^{th} bilayer, the growth enters a "self-regulated" regime where the structure and properties of the LbL converge into a state determined by the nature of the polyelectrolyte pair.

2.3.4. Enhanced early stage growth of $(SePEI/Alg)_n$ on quartz substrates by $(PDDA/Alg)_2$ precursor layer

Quartz is usually treated as naturally negatively charged due to its silanol surface groups which deprotonate effectively under basic conditions. However, the ionization of a weak base such as PEI is hindered by high pH. Therefore, adsorption of a layer of PDDA at a pH ≈ 9 can enhance the ionization of silanol groups while stabilizing the surface charge by forming ion pair with quarternized ammonium on PDDA. Indeed, the priming $(PDDA/Alg)_2$ layer does promote the adsorption of the following (PEI-FITC/Alg) LbL. As shown in Figure 2.7a, the quartz slide pre-adsorbed with $(PDDA/Alg)_2$ shows a higher absorbance from FITC-SePEI than slide without priming treatment. Notably, this enhancement only occurs in the early stage (up to 5 bilayers) of the LbL growth. When more bilayers are coated, the difference between SePEI-FITC absorbed on the primed and unprimed slides remains the same. This trend can be viewed more clearly in Figure 2.7b. This is not surprising by considering that the original $(PDDA/Alg)_2$ primed surface, although it attracts more SePEI in the first couple of cycles, is eventually fully covered by (SePEI/Alg) bilayers. From then on, the LbL enters a substrate-independent regime so that the adsorption of polyelectrolyte is dominated by the existing LbL.

2.3.5. Annealing of $(SePEI/Alg)_n$ LbL

The kinetically limited layer-by-layer adsorption results in a heterogeneous film structure as reflected by its cloudy appearance. An annealing process is therefore

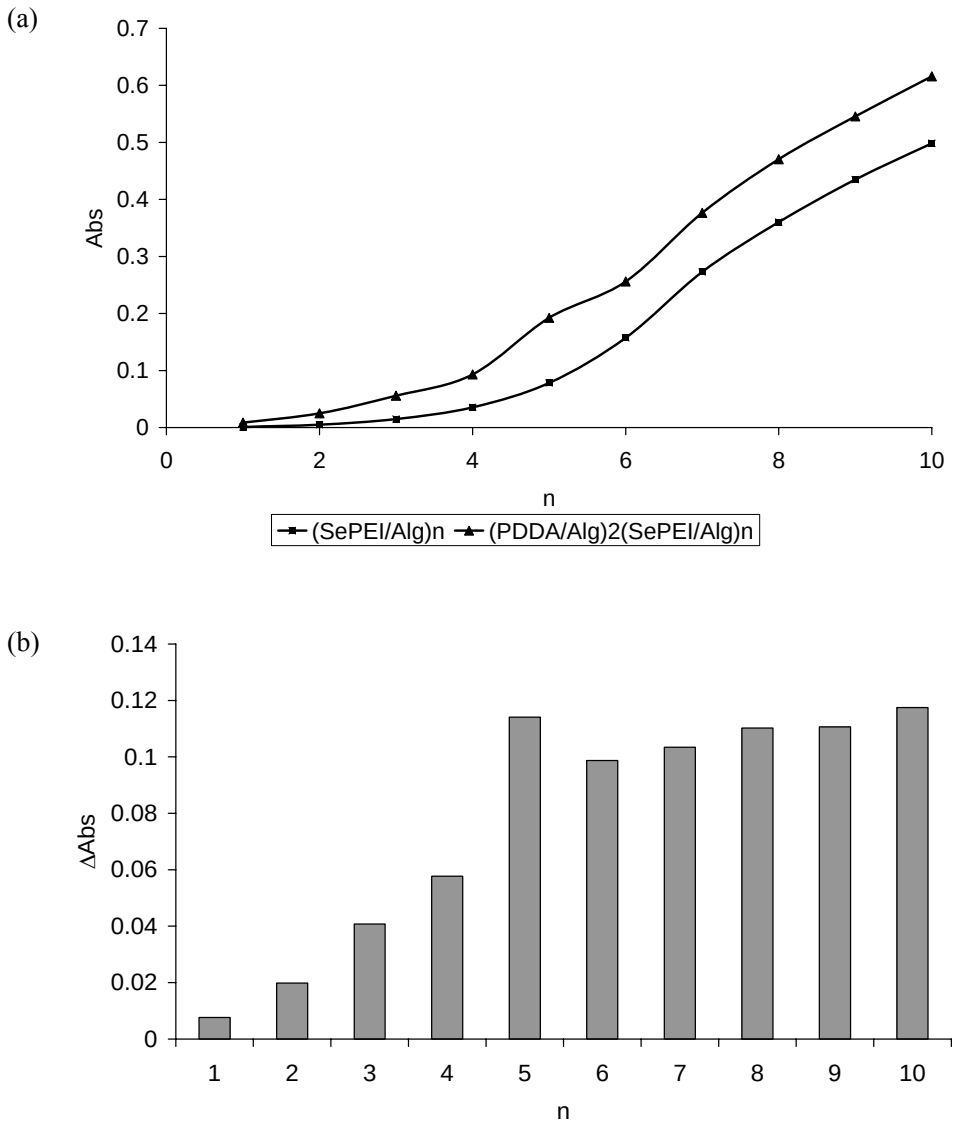

Figure 2.7. (a) UV-Vis absorbance at 503 nm for $(SePEI\text{-}FITC/Alg)_n$ coated on unprimed (solid square) and $(PDDA/Alg)_2$ primed (solid triangle) quartz slides; (b) Absorbance difference between $(SePEI\text{-}FITC/Alg)_n$ on unprimed and primed quartz slides for a given number of bilayers. $\Delta Abs = Abs(primed) - Abs(unprimed)$.

required to reduce the existing defects through self-rearrangement of polymer chains. Although the chain mobility in an LbL film is almost completely lost in the dry state, it can be regained to a certain degree upon rewetting.[7] We find that a $(SePEI/Alg)_5$ annealed in PBS containing 100 μM GSH can revert to a film with greater clarity (see Figure 2.8). The annealed LbL retains 92.2% of its original FITC absorbance suggesting that the observed improvement in film clarity is not due to delamination of the multilayer.

In contrast, the specimen annealed in PBS without the presence of GSH only partially loses its cloudiness. The presence of GSH likely facilitates the healing process by reducing most of the diselenide crosslinks and hence renders SePEI chains more flexible to rearrange into a more thermodynamically stable conformation. The SEM images taken at low magnification clearly show that the fuzzy appearance of freshly coated LbL surface develops into a denser layer embedded with coarse clumps up to 10 μm in diameter after annealing (see Figure 2.9). Such a surface conformational change further verifies the occurrence of chain rearrangement.

2.3.6. Characterization of annealed $(SePEI/Alg)_n$

The stability of $(SePEI/Alg)_n$ LbL is critical for a long lasting catalytic activity. Delamination of the multilayer will gradually reduce the surface NO generation and therefore weaken the anti-thrombotic efficiency. Also, the delaminated organoselenium species will provoke potential toxic side effects. To assess the stability of the NO generating LbL, an annealed $(SePEI\text{-}FITC/Alg)_5$ multilayer was soaked in PBS buffer in

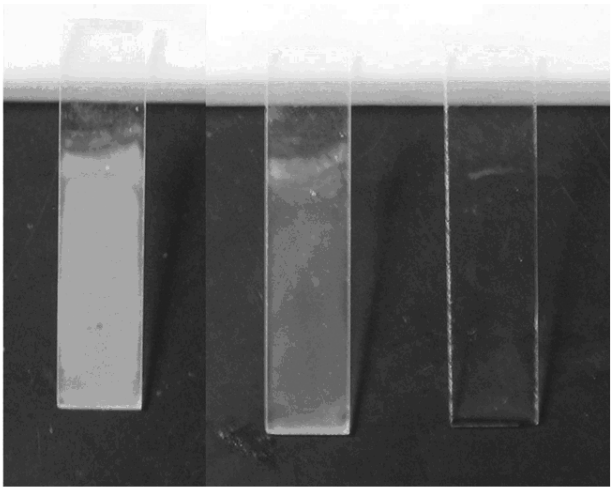

Figure 2.8. Appearance of a freshly coated $(SePEI/Alg)_5$ (left), $(SePEI/Alg)_5$ annealed in PBS buffer without addition of GSH for 12 hours (middle), and $(SePEI/Alg)_5$ annealed in PBS containing 100 μM GSH for 12 hours (right).

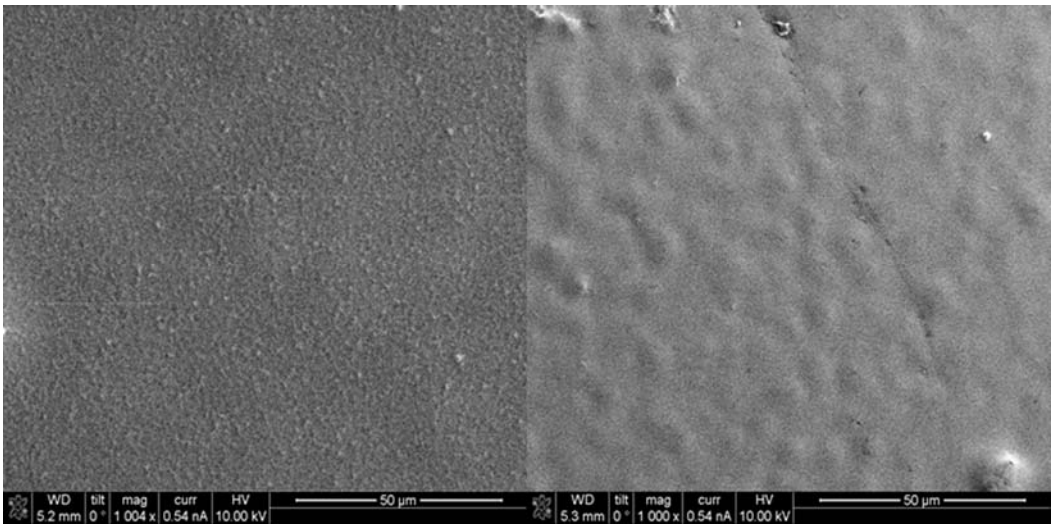

Figure 2.9. SEM of a $(SePEI/Alg)_5$ coated on quartz slide before (left) and after (right) annealed in PBS containing 100 μM GSH.

presence of exaggerated amounts of GSH and GSNO. The PBS/GSH/GSNO mixture was refreshed on a daily basis to maximum the reaction time. After a 4-day exposure in PBS containing 100 μM GSH and 50 μM GSNO, the multilayer preserves 95.3% of its original UV-Vis absorbance from the FITC tracer within the film (see Figure 2.10). Compared with the previously annealing experiment in which the LbL lost 7.8% UV-Vis absorbance within a period of 12 h, the annealed LbL indeed shows an improved stability.

The annealed $(SePEI/Alg)_n$ LbLs were also characterized via contact angle. Figure 2.11 shows the static contact angles of the films at each deposition step with pure water measured in atmospheric air at room temperature. In the early stage, the LbL exhibits similar contact angles regardless of which polyionic species is the outermost layer. This can be explained by the prevalent occupancy of the surface by the initial $(PDDA/Alg)_2$ precursor layer due to the poor coverage of the $(SePEI/Alg)_n$. From the 3rd coating cycle onward, the contact angles fluctuate periodically between 64.1 ± 3.3° for the SePEI as the outermost layer and 56.7 ± 3.1° for Alg as the outermost layer. The relatively lower contact angle of Alg outlayer is primarily due to the large amount of hydroxyl groups on the polysaccharide. This back-and-forth change of surface tension further verifies the LbL buildup of the film by alternate deposition of SePEI and Alg.

The chemical composition of the $(SePEI/Alg)_n$ LbL was studied using X-ray photoelectron spectroscopy (see Figure 2.12). The peak at 57 eV was identified as Se 3d electron, which confirms the successful immobilization of RSe species within the multilayer. Slight amounts of Cl and P were also found in the film, probably from the

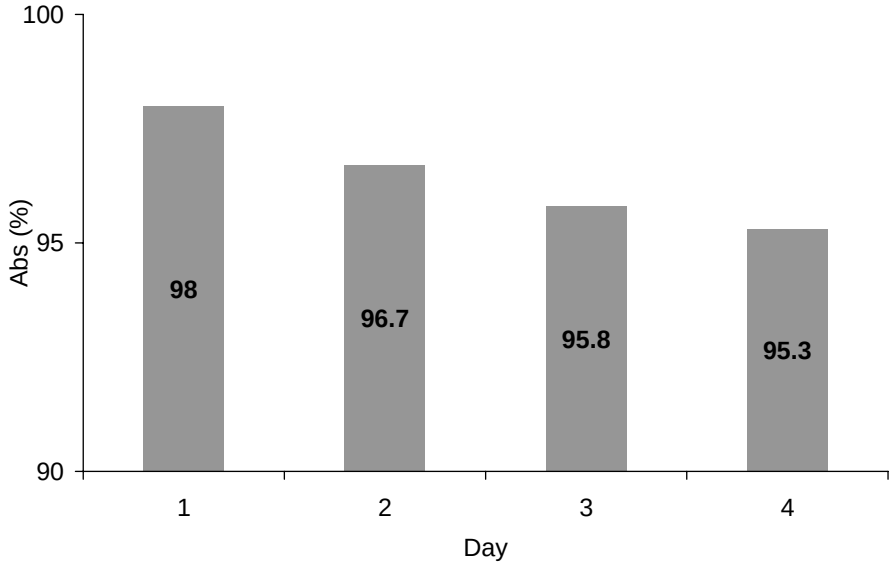

Figure 2.10. Stability studies on a $(SePEI/Alg)_5$ coated on the inner wall of a quartz cuvette. The cuvette was filled with PBS containing 50 μM GSNO and 100 μM GSH. After every 24 hours, old soaking solution was decanted and the cuvette was refilled with fresh PBS containing same given concentrations of GSNO and GSH. The absorbance at 503 nm (which is due to FITC chromophore) was monitored after every refill.

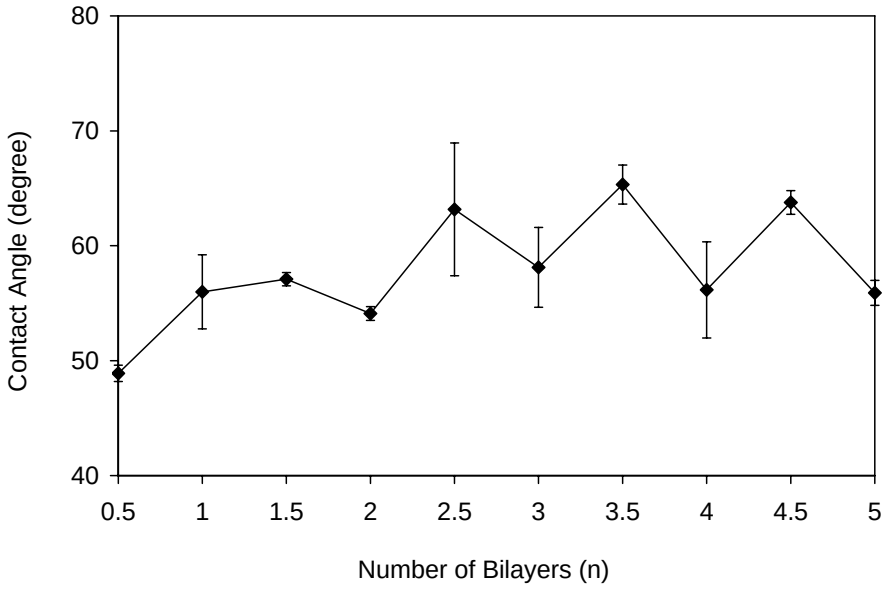

Figure 2.11. Contact angles measured from films of a different number of adsorbed layers of polyelectrolytes. Integral numbers represent films with Alg as the outmost layer; otherwise, SePEI is the outmost layer.

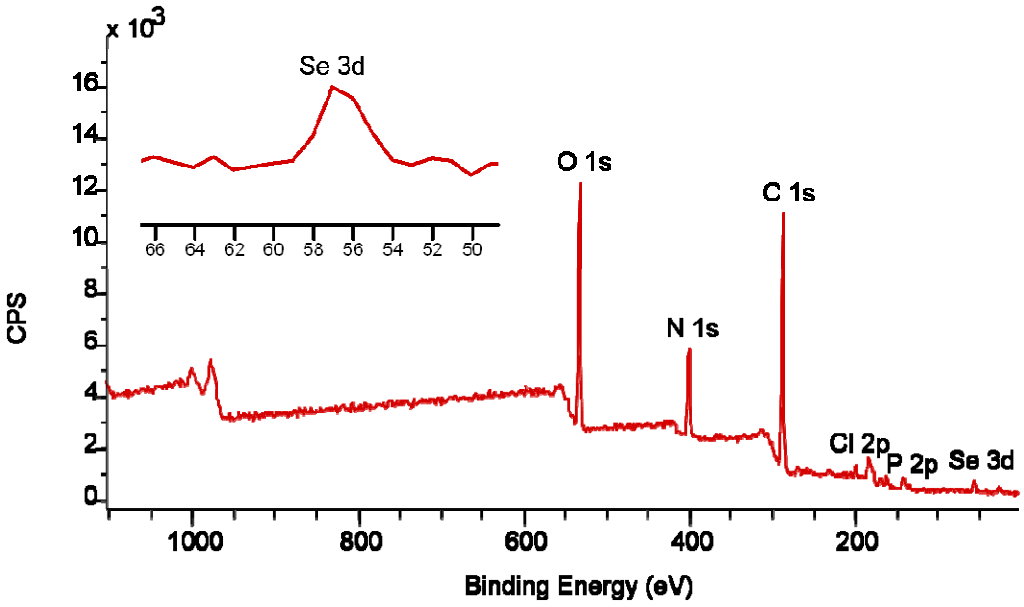

	C	N	O	Se	P	Cl
A%	62.41	13.90	21.42	0.94	0.88	1.46

Figure 2.12. X-ray photoelectron spectroscopy of a $(SePEI/Alg)_{15}$ coated on quartz substrate. Inset: zoom in spectrum showing Se 3d peak.

$H_2PO_4^-$ and Cl^- small ions in the buffer in which the LbL was deposited. The stoichiometry between SePEI and Alg was derived based on the atomic percentage of N and O assuming that all the N and O were contributed by the polyamine and polysaccharide, respectively. Interestingly, the amine:carboxylate ratio was calculated to be 3.89. This indicates that the deposition of SePEI and Alg does not follow a stoichiometric (i.e., a 1:1 ratio) pattern. Similar to low molar mass weak acid and base, the polymeric counterparts may undergo a partial ionization dependent on the local environment. In this circumstance, the uncharged repeat units do not participate in forming an ion pair with the oppositely charged component and hence the stoichiometry between two constituent polyelectrolytes will deviate from an ideal 1:1 ratio.

The partial ionization of SePEI is also reflected by the split of its N1s envelope observed in the core scan. As shown in Figure 2.13, the N1s electron is composed of two peaks, one centers at 399 eV while the other at 402 eV. The peak at higher binding energy is empirically assigned to cationic N atom due to the stronger binding of electron by the local positive charge. To better estimate the ratio of cationic and neutral amines, the N1s envelope was curve fitted into 6 components: cationic primary amine, neutral primary amine, cationic secondary amine, neutral secondary amine, tertiary amine, and amide. Integration of each component reveals that only 27.5% of the SePEI amines are in their ionized form. Such a low ionization degree is expected for branched PEI in which secondary and tertiary amines distribute densely along the polymer backbone. Protonation of one amine site can therefore invoke considerable electrostatic repulsion to

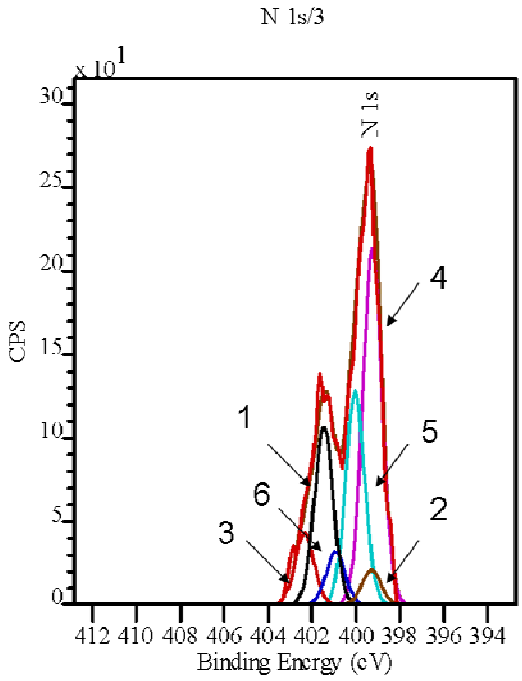

	Components	B.E.	A %
1	$-NH_2(+)$	401.5	19.60
2	$-NH_2$	399.1	3.84
3	-NH-(+)	402.4	7.91
4	-NH-	399.2	39.24
5		400.0	23.54
6	-NH-CO-	400.9	5.88

Figure 2.13. Curve fitting of N1s envelope in XPS core scan. The spectrum was smoothed twice using Savitzky-Golay approach with a smooth width of 5. Six components were simulated including the amides resulting from the coupling of SeDPA to the PEI. The cationic amines were marked with (+) to distinguish from their unionized counterparts.

.

the amines within close proximity. Indeed, the pKa values of different amine sites within branched PEI were reported to be 9.2, 8.2, 5.8 and 4.3, respectively.[11] Most of the cationic amines are likely contributed by the uncoupled primary amines locating at the end of the branches of PEI molecules, which are far away from each other and thus invoke less repulsive interaction upon protonation. If this partial ionization of SePEI is taken into account, the ratio of cationic amines and carboxylates is close to a 1:1 ratio. This explains the appearance of only a trace amount of small counterions in the film, although the total amine is in great excess to the carboxyl groups of the Alg species.

2.3.7. Preliminary toxicity evaluation of $(SePEI/Alg)_n$

For all materials targeting an ultimate biomedical application, special attention must be paid with the regard to their biological safety. Specifically for this NO generating LbL, the organoselenium species which is required for catalytic activity may also cause potential side effects if leached into the biological system. Although selenium is widely known as an essential trace element in the diet, deficiency of the element is associated with many health conditions such as immune dysfunction, cardiovascular disease, depression, and oxidative stress.[12] However, the toxicity of selenium has also been well recognized and correlated to the oxidation state of selenium.[13] The upper limit of selenium intake for humans from all sources is 400-450 μg per day as recommended by several expert panels.[12] An overdose beyond this limit may be seriously toxic, and fatalities have been reported, albeit very rarely.[13,14]

Accordingly, the $(SePEI/Alg)_n$ LbL was assessed for its toxic risk caused by any leachable selenium species from the film. The leaching test was performed on a $(SePEI/Alg)_{10}$ by extracting the film under exaggerated reaction conditions for 5 d. Then, the extracted LbL was completely digested using fuming nitric acid to quantify the remaining selenium in the film. The abundance of selenium element within the $(SePEI/Alg)_{10}$ was determined to be ca. 2.9 μg cm^{-2} (0.036 μmole cm^{-2}) (see Table 2.2). After the 5 d extraction, only 3.0% of the Se leached out from the multilayer intro the extracting solution. It is noteworthy that the average daily dietary intake of selenium in the United States is consistently above 55 μg/d and a super-nutritional level (> 100 μg/d) is suggested to optimize its anti-oxidation potency. If applied on medical devices with limited surface area, e.g., on a vascular stent, the LbL contains several micrograms of selenium in total which would be equal to only a small fraction of normal dietary intake.

The exact Se species that leaches from the LbL films has not been identified; however, it is possibly that this leaching is attributed to the instability of aliphatic organoselenium species. Diselenides are known to undergo alkaline hydrolysis in basic conditions.[15] Therefore, it is possible that SeDPA is slowly destabilized by the basic local environment created by the amine sites on PEI. Also, the anionic selenolate intermediate is a very good nucleophile and a strong reductive species. This species can undergo a series of unwanted side reactions and easily become oxidized into higher oxidation states by various oxidizing species.

	C_L (μg/mL)	C_T (μg/mL)	%	C (μg/cm^2)
1	0.05	1.41	3.4	2.9
2	0.04	1.40	2.8	2.9
3	0.04	1.41	2.8	2.9

C_L: Se concentration in extracting solution.
C_T: Se concentration in digesting solution.
%: percent Se leached out from the LbL during the 5 d extraction period.
C: Se content per unit area in $(SePEI/Alg)_{10}$.

(1) % is calculated using:

$$\%=100*\frac{C_L}{C_L+C_T}$$

(2) C is calculated following:

$$C=\frac{\text{total Se}}{\text{film area}}=\frac{(C_L+C_T)*25\text{ ml}}{12.4\text{ cm}^2}$$

Table 2.2. Selenium quantification and leaching test of $(SePEI/Alg)_{10}$ as measured by ICP-MS. $(SePEI/Alg)_{10}$ was coated on glass shell vials (1.5 cm ID, 3.5 cm). The coating area was calculated to be 12.4 cm^2. The coating area was submerged in 4 mL PBS buffer containing 100 μM GSH and 50 μM GSNO to extract leachable selenium species from the LbL. The vials were then capped, wrapped with aluminum foil and kept at room temperature for 5 d. The extracting solutions were collected very 24 h and the vials were refilled with fresh PBS buffer containing same given concentrations of GSH and GSNO. After the 5 d extraction period, the LbLs were digested using 100% fuming nitric acid. Both extracting and digestion solutions were then brought into 25 mL solutions using volumetric flask and ICP-MS was employed to determine Se concentrations in the solutions.

In vivo toxicity tests were also conducted using animal models. Phosphate saline and vegetable oil were selected to extract the LbLs taking into account that the leachable compounds may have various affinities with different extracting vehicles. The aqueous and oil phase extracts were administrated to two groups of five mice via intravenous and intra-peritoneal injection, respectively. Within an observation window of 28 d, neither group of mice tested develops any systemic toxic symptoms such as weight loss (see Figure 2.14), prostration or any neurological signs. The oil phase extract was also given to a rabbit model intradermally to test the local tissue response. Within 72 h, the dosed areas did not display any clinical sign of irritation such as rash, inflammation and swelling, etc. excluding presence of any irritants in the extraction solution (see Figure 2.15). All these toxicity evaluations, albeit still at a preliminary stage, show that this $(SePEI/Alg)_n$ is very promising for biomedical applications.

2.3.8. Nitric oxide generation by $(SePEI/Alg)_n$ from *S*-nitrosoglutathione

The catalytic activity of $(SePEI/Alg)_n$ deposited on quartz slides was investigated by measuring NO generation from GSNO with GSH as reducing agent via chemiluminescence. Figure 2.16b shows a typical chemiluminescence result obtained from a $(SePEI/Alg)_5$. Nitric oxide production is initiated instantly upon introducing the slide into the test solution and rapidly plateaus at a sustained NO level. When the slide is removed, the NO generation ceases almost entirely, indicating the catalytic GSNO breakdown occurs predominantly in the LbL film on the slide. Repeated immersion and

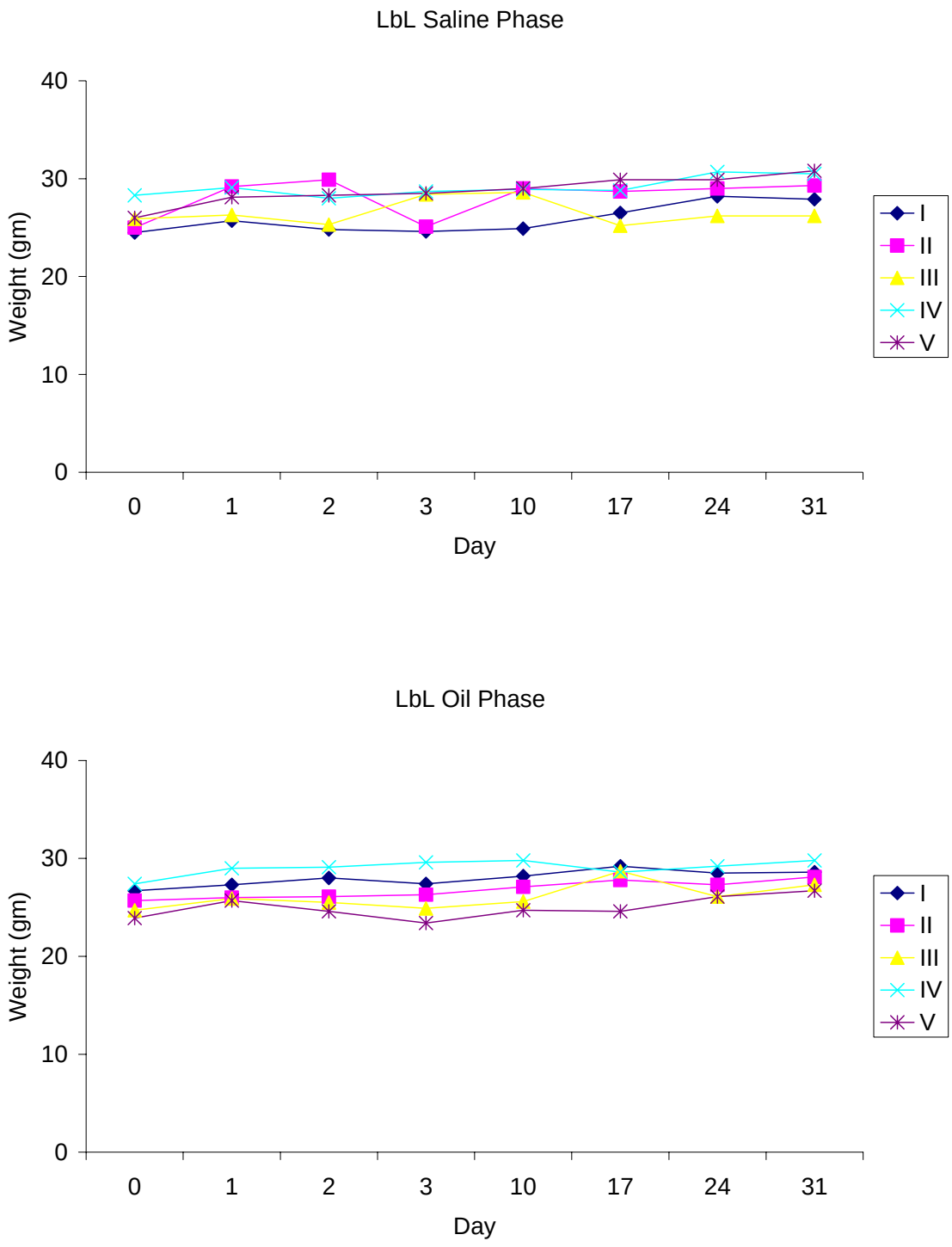

Figure 2.14. Measured weights of the mice injected with saline (top) and oil phase (bottom) extracts. In each group, five mice were tested, as denoted using Roman numerals I-V.

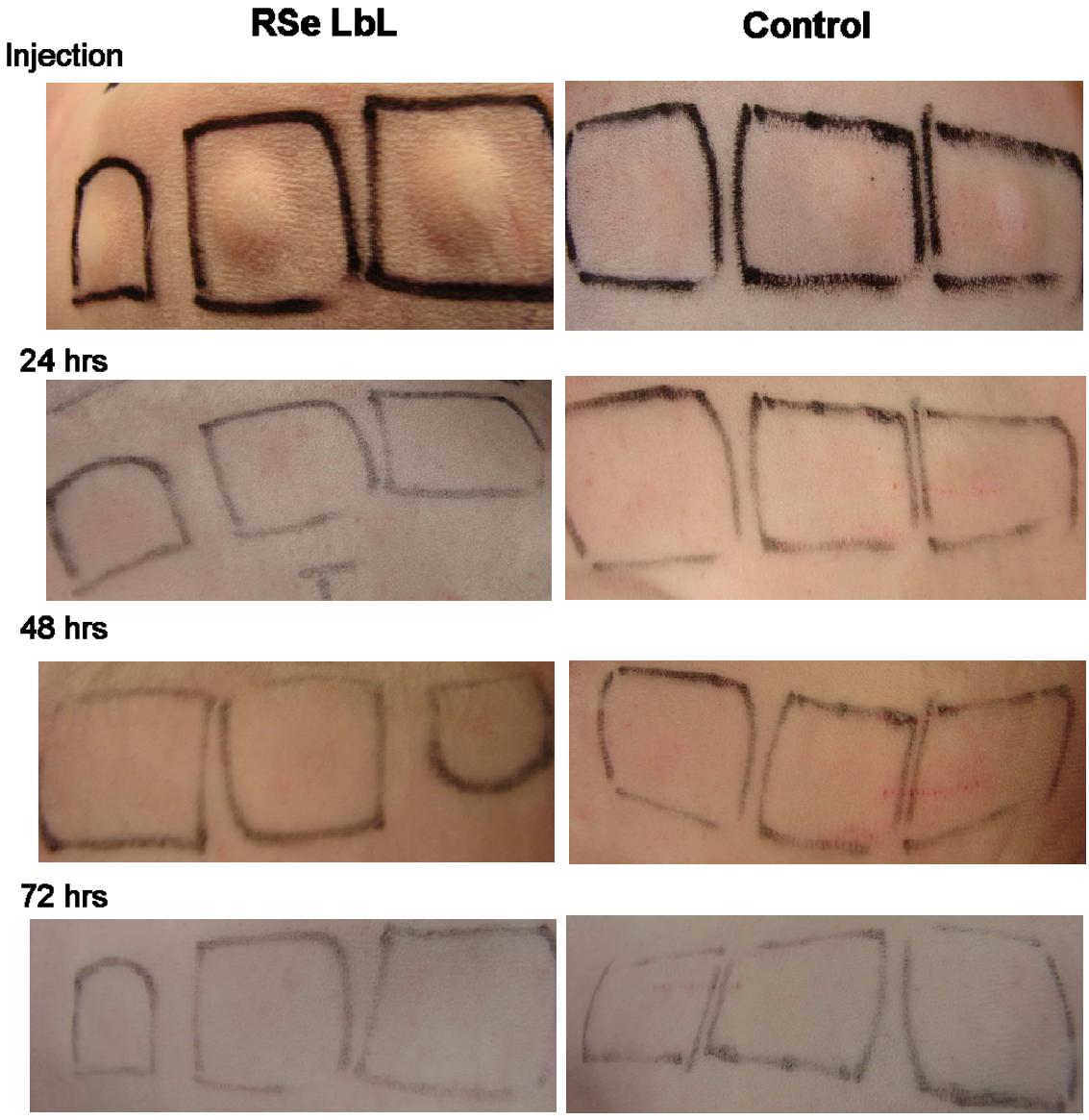

Figure 2.15. Pictures of the three test spots where the oil phase extracts were injected subcutaneously in the rabbits.

removal of the slide replicate the up-and-down NO generation pattern. The NO flux degrades slightly over time which is likely attributed to the consumption of the GSNO in the bulk test solution. Although GSNO can directly react with GSH to produce nitroxyl and potentially compete with the catalytic GSNO decomposition employed in our experiments,[16] we believe that the reaction rate for nitroxyl formation is much slower and the RSe catalyst dependent GSNO decomposition is the primary reaction by which GSNO is consumed in the reaction mixture. The marginal baseline increase after slide removal suggests only a very small amount of catalyst leaches from the LbL film into the test solution during the measurements, with no severe delamination of the catalytic multilayer observed. Indeed, the return to baseline in the chemiluminescence experiments after removing the LbL coated substrate is a very sensitive means to probe the degree of leaching, since any loss of RSe species will induce a homogenous reaction which is much faster than the heterogeneous surface reaction mediated by the LbL. An assembly that had not been annealed was also tested (see Figure 2.16a). When the slide was removed, approximately 60% of the NO flux remained without the presence of the substrate in the NO generating solution, implying that some catalytically active species had been released into the test solution from the coating. Such results further confirm the enhanced stability of the LbL assembly that is induced by the annealing step.

It should be also recognized that a solid polymer matrix would likely block the free diffusion of the reactive GSNO and GSH species from penetrating into such a coating. If the inner RSe catalytic sites are not accessible to GSNO substrate and GSH reducing agent,

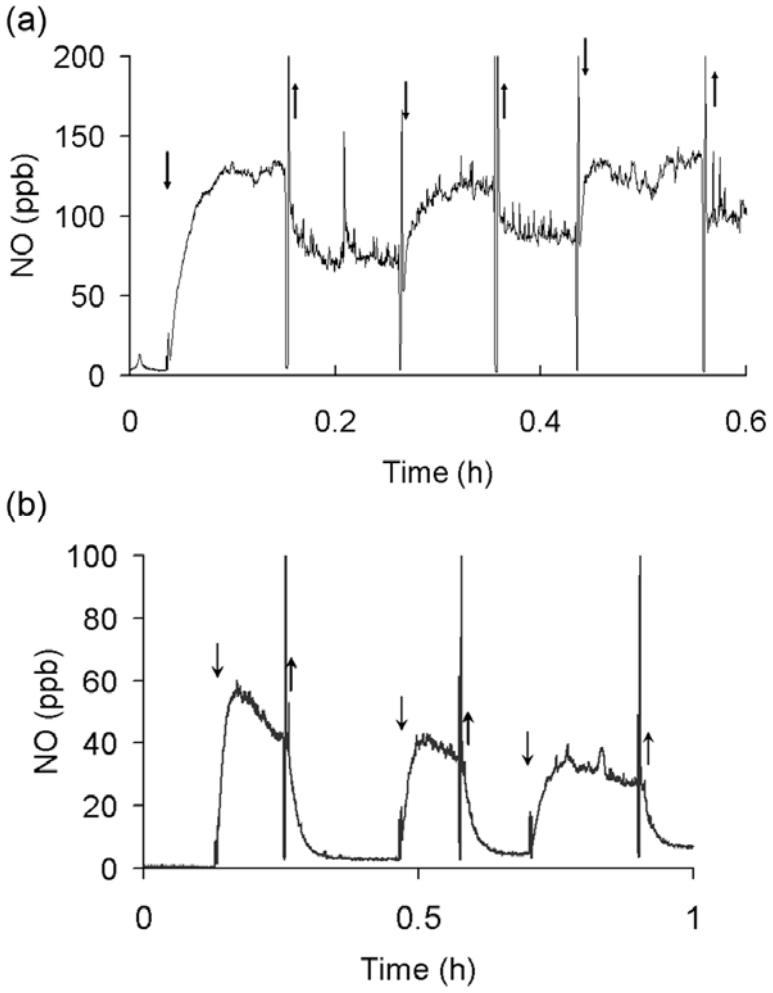

Figure 2.16. NOA studies of (a) fresh prepared (un-annealed) and (b) annealed $(SePEI/Alg)_5$ in PBS containing 50 μM GSNO and 50 μM GSH.

the amount of NO generation would be solely dictated by reactions at the outer surface of the polyelectrolyte coating but not the number of bilayers within the LbL film. However, if the film is truly permeable to GSNO and GSH, there should be an increase in observed NO production for thicker films. Hence, $(SePEI/Alg)_n$ with various numbers of catalytic bilayers were tested to evaluate the accessibility of the RSe sites within the LbL. Figure 2.17a clearly shows the maximum NO flux increases from 56 ppb for $(SePEI/Alg)_5$ to 106 and 146 ppb for $(SePEI/Alg)_{10}$ and $(SePEI/Alg)_{15}$, respectively. Meanwhile, the background solution phase NO generation (after slide removal) does not show a significant increase for the greater number of bilayers deposited. This proves that the enhanced NO production is indeed derived from the access to the RSe catalyst in the underlying layers of the LbL coating. The correlation between the maximum NO flux observed in NOA studies and UV-Vis adsorption of LbL with various numbers of bilayers is nearly proportional (see Figure 2.17b). Such a result implies a very open film structure in which most of the immobilized RSe species are able to contribute to GSNO breakdown even for films with 15 bilayers. This is an attractive feature of this new NO generating coating in that the degree of NO generation from given RSNO/RSH concentrations can be controlled by the number of bilayers deposited.

In a longer term study, ten separate aliquots of PBS buffer (2 mL in each aliquot) containing the same initial concentrations of GSNO and GSH (50 μM and 100 μM, respectively) were allowed to react successively with a single quartz slide coated with a $(SePEI/Alg)_{10}$ (see Figure 2.18). The LbL was kept in each test solution until the NO

(a)

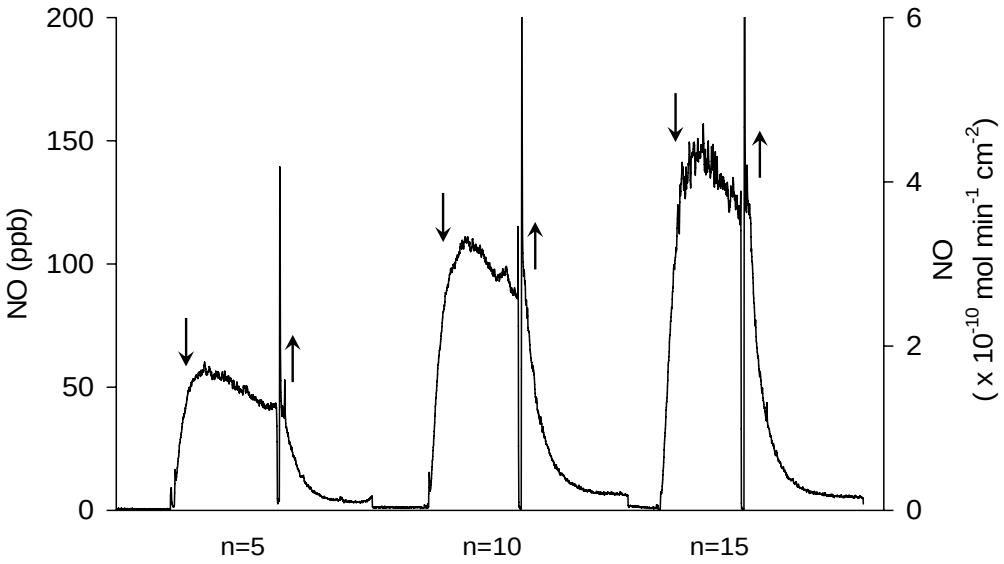

(b)

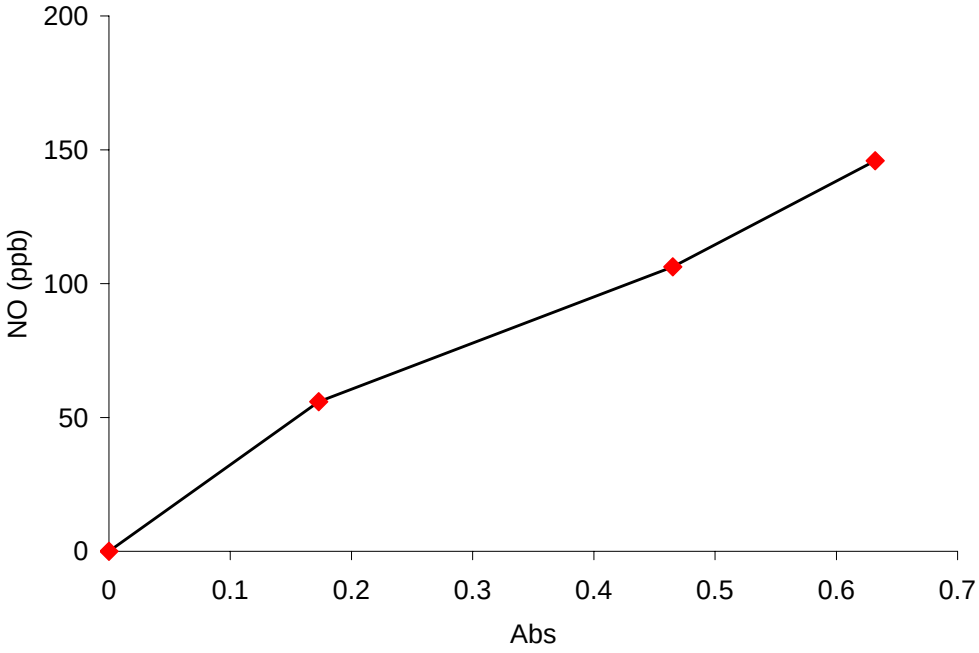

Figure 2.17. (a) NO generation by $(SePEI/Alg)_n$ on quartz with various number of bilayers in PBS containing 50 μM GSNO, 50 μM GSH and 0.1 mM EDTA. The slide was immersed (↓)/removed (↑) as indicated by the arrows. (b) NO flux vs. UV-Vis absorbance of $(SePEI/Alg)_n$ at 503 nm.

production fully stopped and subsequently transferred to the next test solution. After continuously reacting for 40 h in total, the LbL still exhibited significant catalytic activity. The conversion rate of GSNO was calculated separately for all 10 reactions, revealing that the GSNO in each batch was completely depleted. The estimated Se content in the LbL was 0.11 μmol, while the total GSNO decomposed was 1 μmol. It is obvious that the $(SePEI/Alg)_n$ can decompose more GSNO than the amount of Se immobilized in the multilayer film, further proving that the reaction is catalytic in nature. The extended reaction time also resulted in a slower kinetics. Compared with the 1st batch, the maximum NO flux in the 10th experiment decreases about 60%, while the time required to decompose all the GSNO is almost doubled.

The organoselenium immobilized LbL was also tested *in vitro* to preliminarily evaluate its activity after prolonged contact with sheep whole blood (see Figure 2.19). Without spiking additional GSNO, the endogenous GSNO and other RSNO species in the blood decrease rapidly due to the consumption by the catalyst. After a 24 h contact, the LbL was thus partially covered by thrombus (since NO generation ceases without more substrate). When the blood clots were carefully peeled off using tweezers, the LbL underneath still displayed significant catalytic activity in generating NO from a fresh GSNO/GSH solution and was able to fully convert all the GSNO added in the reaction. However, the LbL in contact with blood displayed a lower NO generating activity (ca. 50% less) compared with the control which had been in contact only with PBS buffer. Several experimental aspects may account for this activity decay. It is possible that part of

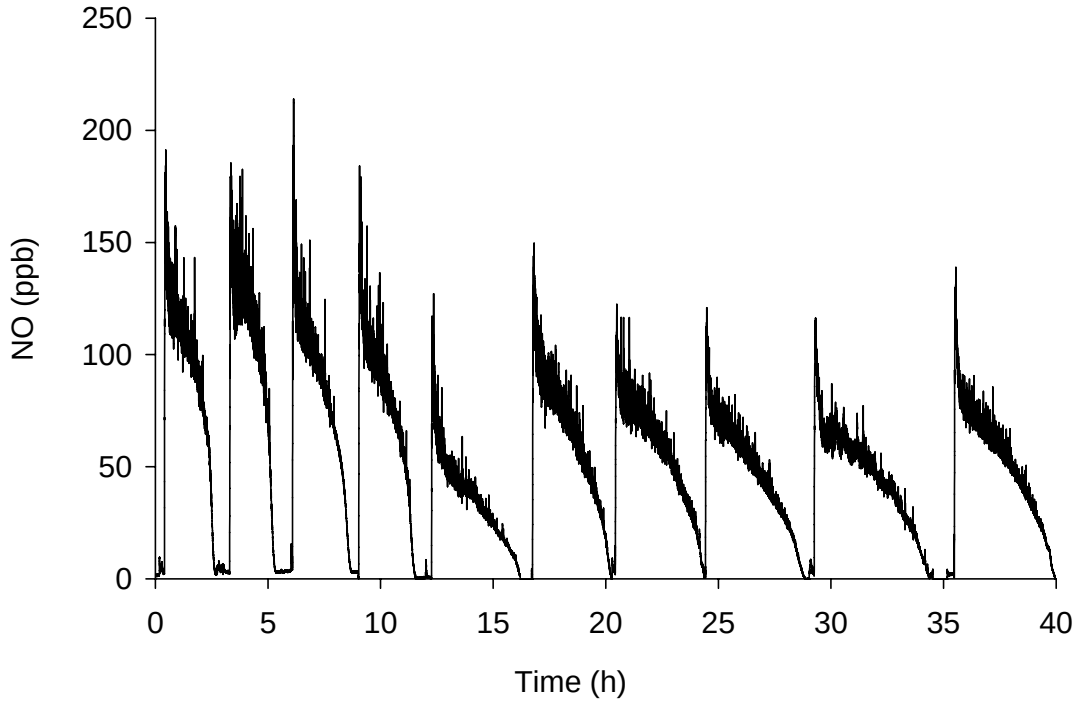

Figure 2.18. Long term NO generation by a slide coated with $(SePEI/Alg)_{10.}$ Ten batches of PBS (2 mL each) containing 50 μM GSNO and 100 μM GSH were allowed to react with the catalytic LbL successively.

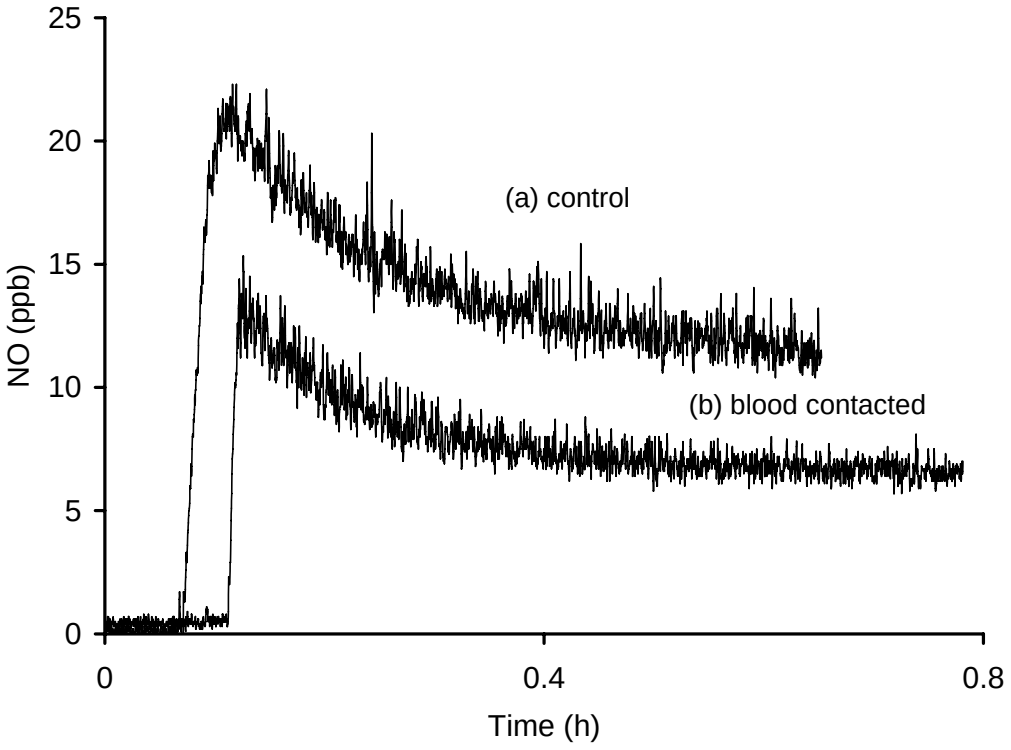

Figure 2.19. NOA of $(SePEI/Alg)_{10}$ after 24 h incubation in (a) PBS; (b) sheep whole blood. Please note that both measurements were stopped before the added GSNO was depleted. The NOA curves here represent the average NO generation rate rather than total amount of NO produced.

the multilayer is delaminated simultaneously upon the clot removal and herein reduces the catalyst quantity in the assembly. Further, protein adsorption on the LbL surface may also impede diffusion of GSNO/GSH reactants into the coating and this results in slower reaction kinetics. Nevertheless, the *in vitro* blood contact study strongly suggests that $(SePEI/Alg)_n$ LbL coatings can preserve significant activity after exposure to blood components for an extended time period.

2.3.9. Application of $(SePEI/Alg)_n$ LbL on polymeric surfaces.

The primary motivation for this study is the potential application of this RSe immobilized LbL approach to render biomedical materials/devices more biocompatible via spontaneous generation of NO from endogenous NO precursors. Toward this goal, it is important to demonstrate that the $(SePEI/Alg)_n$ film can be coated on biomedical grade silicone rubber and polyurethane, both are widely used to make biomedical devices. Several methods were examined to create surface charge on silicone rubber, including silanization with 3-aminopropylsilane (APS), adsorption of PDDA, and adsorption of SePEI. The treated silicone surfaces were characterized by contact angle measurement. As shown in Figure 2.20, the contact angles of treated surfaces range between 114.8° and 116.8°, which are 4-6° lower than the control silicone rubber that was immersed in PBS for the same period of time. Such decreased surface energy proves that all these three priming methods induce a certain degree of hydrophilicity to the surface, presumably due to the ammonium ions on PDDA or ionizable amines on PEI and APS. However, the

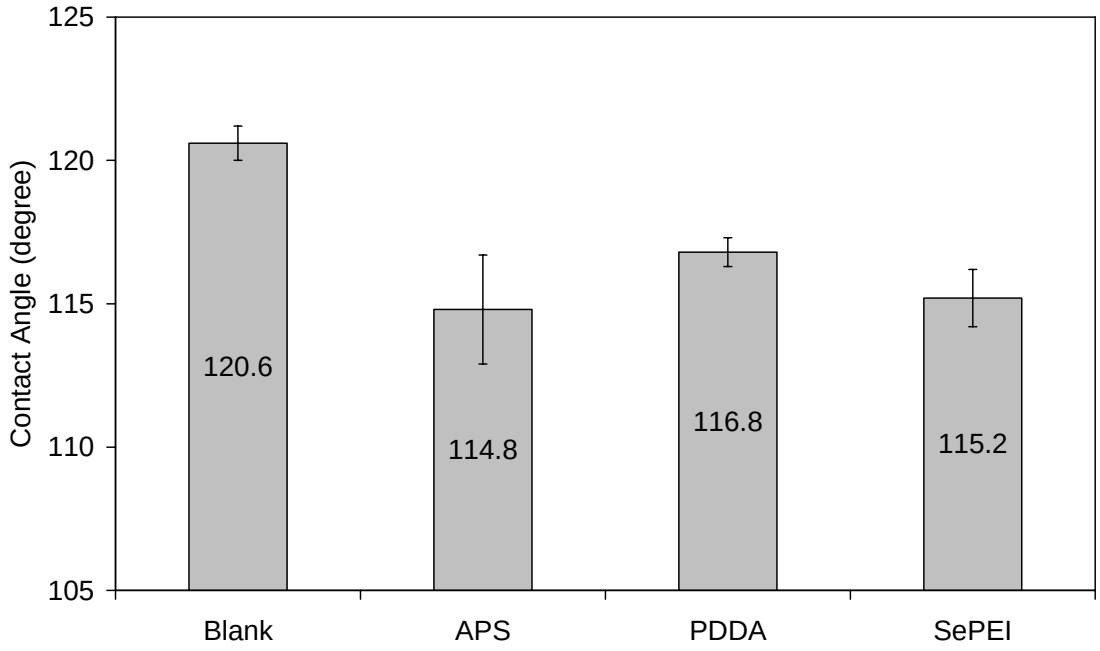

Figure 2.20. Contact angle measurements on silicone rubber surface adsorbed with different polymer. Glass slides were dip-coated with RTV Silicone Rubber (20% in THF) and cured in ambient condition overnight before utilized as flat silicone substrates. The silicone substrates were then immersed in solutions containing 3-aminopropylsilane (APS), PDDA, and SePEI for 2 hours. Another slide was immersed in PBS for the same amount of time and used as blank. The contact angles were measured using the same method described in the experimental section.

contact angle after treatments are larger than 90°, implying the overall surface nature is still very hydrophobic. This indicates that the amount of priming species adsorbed on the surface is very limited. The surface charge of the treated silicone tubing was reversed by a layer of Alg and further stabilized with $(PDDA/Alg)_2$ before $(SePEI/Alg)_n$ LbL film was assembled. UV-Vis revealed the same "S" shape growth pattern and little disparity in respective of the amount of SePEI deposited in the resulting LbLs, regardless of the various surface charging methods employed (see Figure 2.21). The LbL assembly was also applied on the surface of PU catheters without precoating with $(PDDA/Alg)_2$ precursor layer. Indeed, PEI can adsorb on polymeric surfaces via hydrophobic interaction to introduce cationic amine groups and initialize LbL growth.[17]

Figure 2.22 shows the NO generation from $(SePEI/Alg)_{10}$ coated on (a) silicone tubing and (b) PU catheter upon repeated immersion and removal of the LbL coated tubing into a PBS solution with 50 μM GSNO and 50 μM GSH. The coated devices with 10 bilayers exhibit similar up-and-down NO generation pattern, indicating that the LbL fabricated on polymeric surface without dense surface charge still possesses reasonable stability. In concert with the experiments performed on quartz slides, these results prove that the $(SePEI/Alg)_n$ behaves similarly even when applied on substrates with vastly different initial surface properties. The normalized NO fluxes observed when in contact with a 50 μM GSNO and 50 μM GSH solution are 2.4×10^{-10} and 1.8×10^{-10} mol min^{-1} cm^{-2} for silicone and PU substrates, respectively. These are comparable with the physiological NO levels ($0.5 - 4.0 \times 10^{-10}$ mol min^{-1} cm^{-2})[18] generated by healthy

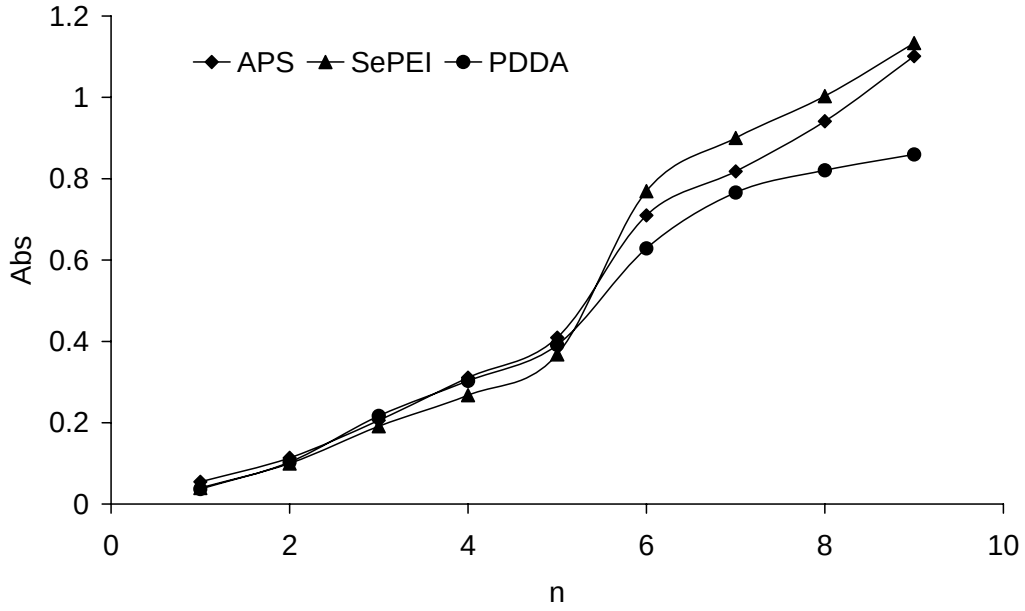

Figure 2.21. UV-Vis study of $(SePEI/Alg)_n$ buildup on silicone rubber treated with different charged polymers: silanization with APS, adsorption of PDDA, and adsorption of SePEI. The FITC labeled SePEI species was employed in this study. UV-Vis spectra were taken at 503 nm after every (SePEI-FITC/Alg) bilayer was deposited.

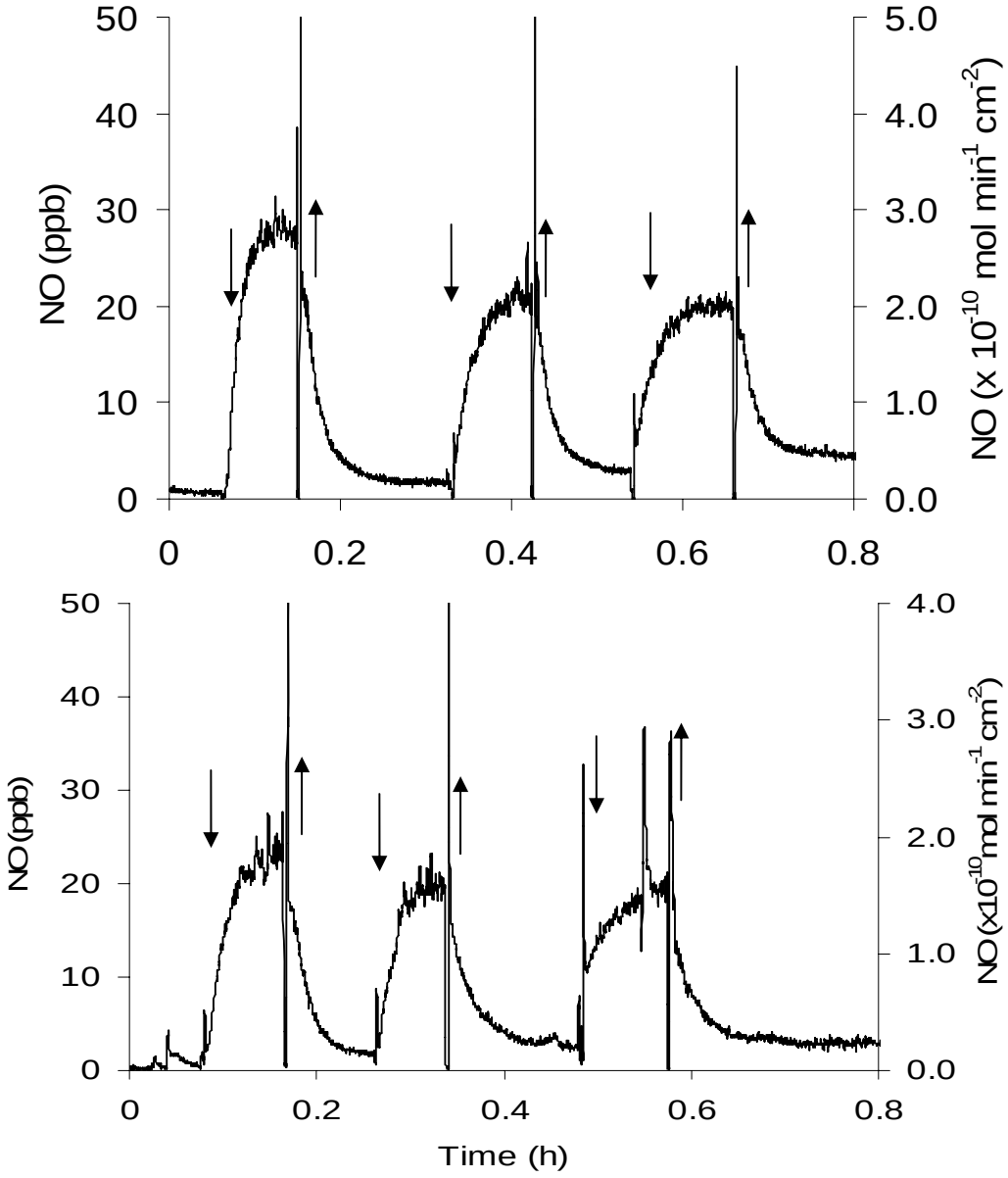

Figure 2.22. Nitric oxide generation from PBS containing 50 μM GSNO, 50 μM GSH and 0.1 mM EDTA by (a) $(SePEI/Alg)_{10}$ on silicone rubber tubing; (b) $(SePEI/Alg)_{10}$ on PU catheter without application of $(PDDA/Alg)_2$ precursor layer. The segment of polyurethane catheter or silicone rubber tubing was immersed (↓)/removed (↑) as indicated by the arrows.

endothelium cell lining the blood vessels. While the NO levels that would be generated when devices are in contact with fresh flowing blood will vary depending on the levels of RSNOs and free thiols (i.e., GSH and cysteine), recent studies have shown that NO generating polymer coatings based on copper catalysts, that carry out the same reactions as the RSe used here, do reduce thrombus formation on catheter surfaces when implanted in pig arteries for up to 20 h (compared to controls in the same animals).[19]

2.4. Conclusions

In summary, a novel strategy to immobilize catalytic organoselenium species via a shown capable of forming an LbL structure with Alg as the counter-polyelectrolyte. An annealing treatment is required to further stabilize the multilayer. The LbL shows overall neutrality with PEI and Alg interacting with their ionized amine and carboxylate sites in a nearly 1:1 ratio. The RSe catalysts immobilized within the LbL were capable of generating NO from GSNO, an endogenous NO precursor, for an extended time period. The surface confined polyelectrolyte matrix exhibits sufficient permeability to GSNO and GSH small molecules to access catalytic sites deep within the structure. Even after prolonged contact with blood, the LbL still preserves significant catalytic activity. Our preliminary studies using silicone rubber and polyurethane substrates clearly demonstrate that this NO generating surface can be easily adapted onto currently commercialized biomedical polymers used for vascular grafts, catheters, etc. It is noteworthy that the

mechanical LbL coating process could be very time consuming if more bilayers are demanded, albeit the coating mechanism is rather simple. Usually a manually coated LbL contains only up to 20 bilayers, which already takes ca. 10 h to complete. Layer-by-Layer deposition method has been described. The RSe immobilized PEI was Therefore, research described in Chapter 3 of this thesis will focus on the benefit of using an automated coating apparatus to prepare thicker LbL films with more bilayers to generate biological NO flux from lower concentrations of GSNO and GSH.

2.5. References

1. Cha, W.; Meyerhoff, M. E. *Biomaterials* **2007**, *28*, 19-27.

2. Cha, W.; Meyerhoff, M. E. *Langmuir* **2006**, *22*, 10830-10836.

3. Jacob, C.; Maret, W.; Vallee, B. L. *Proc. Natl. Acad. Sci. U. S. A.* **1999**, *96*, 1910-1914.

4. Haughland, R. P. *Handbook of Fluorescent Probes and Research Chemicals*; 6th ed.; Molecular Probes: OR, 1996.

5. Williams, D. L. H. *Acc. Chem. Res.* **1999**, *32*, 869-876.

6. Bertrand, P.; Jonas, A.; Laschewsky, A.; Legras, R. *Macromol. Rapid Comm.* **2000**, *21*, 319-348.

7. Yang, S. G.; Zhang, Y. J.; Zhang, X. Y.; Guan, Y.; Xu, J.; Zhang, X. L. *Chemphyschem* **2007**, *8*, 418-424.

8. Jiang, X. M.; Chen, Z. C.; Lv, D. S.; Wu, Q.; Lin, X. F. *Macromol. Chem. Phys.* **2008**, *209*, 175-183.

9. Garza, J. M.; Schaaf, P.; Muller, S.; Ball, V.; Stoltz, J. F.; Voegel, J. C.; Lavalle, P. *Langmuir* **2004**, *20*, 7298-7302.

10. Lavalle, P.; Gergely, C.; Cuisinier, F. J. G.; Decher, G.; Schaaf, P.; Voegel, J. C.; Picart, C. *Macromolecules* **2002**, *35*, 4458-4465.

11. Crea, F.; Crea, P.; De Robertis, A.; Sammartano, S. *J. Chem. Eng. Data* **2007**, *52*, 279-285.

12. Rayman, M. P. *Lancet* **2000**, *356*, 233-241.

13. Quadrani, D. A.; Spiller, H. A.; Steinhorn, D. *Vet. Hum. Toxicol.* **2000**, *42*, 96-98.

14. Williams, R.; Ansford, A. *Pathology* **2007**, *39*, 289-290.

15. Klayman, D. L. *Organic selenium compounds: their chemistry and biology*; Wiley-Interscience: New York, 1973.

16. Wong, P. S. Y.; Hyun, J.; Fukuto, J. M.; Shirota, F. N.; DeMaster, E. G.; Shoeman, D. W.; Nagasawa, H. T. *Biochemistry* **1998**, *37*, 5362-5371.

17. Moby, V.; Boura, C.; Kerdjoudj, H.; Voegel, J. C.; Marchal, L.; Dumas, D.; Schaaf, P.;

Stoltz, J. F.; Menu, P. *Biomacromolecules* **2007**, *8*, 2156-2160.

18. Vaughn, M. W.; Kuo, L.; Liao, J. C. *Am. J. Physiol. Heart Circ. Physiol.* **1998**, *274*, H2163-H2176.

19. Wu, Y. D.; Rojas, A. P.; Griffith, G. W.; Skrzypchak, A. M.; Lafayette, N.; Bartlett, R. H.; Meyerhoff, M. E. *Sens. Actuators, B* **2007**, *121*, 36-46.

CHAPTER 3

FABRICATION OF NITRIC OXIDE GENERATION LAYER-BY-LAYER ASSEMBLY USING AUTOMATED APPARATUS

3.1. Introduction

In Chapter 2, an LbL possessing immobilized RSe sites that showed substantial NO generation activity from RSNOs was demonstrated. A carboxylate derivatized RSe catalyst, SeDPA, was coupled onto PEI and the modified polycation was manually assembled into a thin film containing 5 to 20 (SePEI/Alg) bilayers. Quantification using ICP-MS revealed that the amount of RSe species immobilized within a $(SePEI/Alg)_{10}$ is only about 0.036 μmole cm^{-2}.[1] Therefore, high concentrations of GSNO and GSH (e.g., 50 μM each) were used in the experiments reported to enhance the NO generation so that the NO generation trend can be better observed. Nevertheless, it would be more meaningful to present the catalytic activity of such LbLs using physiologically relevant levels of GSNO and GSH. The GSH level in plasma is reported to be about 20 μM,[2] while the concentration of GSNO is suggested to be within a micromolar range.[3] A manually coated $(SePEI/Alg)_{10}$ was tested accordingly using 2.5 μM GSNO and 20 μM GSH and yielded a NO flux of only 0.2 x 10^{-10} mol cm^{-2} min^{-1} (see Figure 3.1). This

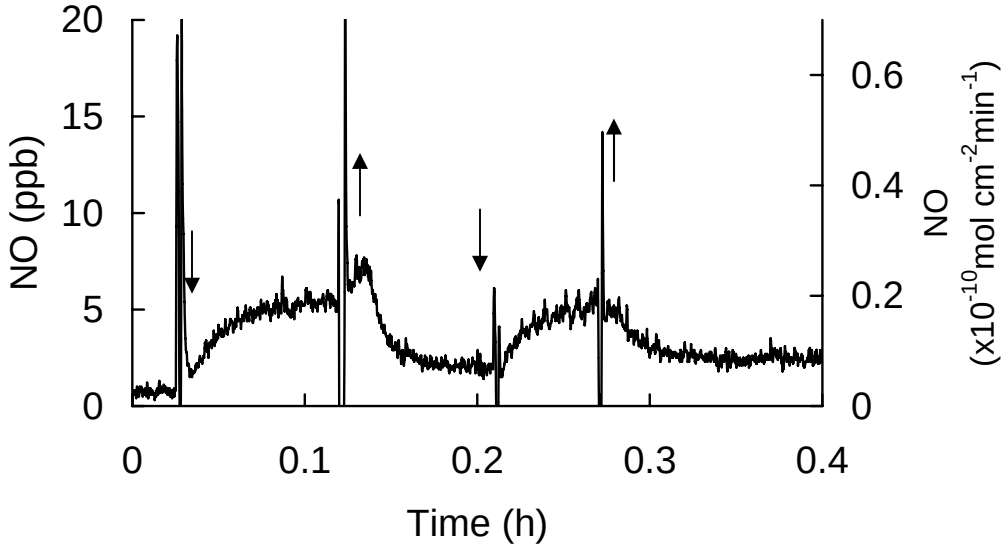

Figure 3.1. Nitric oxide generation by $(SePEI/Alg)_{10}$ from 2.5 μM GSNO and 20 μM GSH at 37˚C. A piece of glass slide coated with the LbL was immersed into the test solution and then removed as indicated by the (↓) and (↑) arrows.

NO flux is still lower than the 0.5-4 x 10^{-10} mol cm^{-2} min^{-1} basal NO flux from healthy endothelial cells.[4] To promote greater NO generation, more catalytic sites need to be incorporated in the LbL. In other words, more bilayers have to be assembled. Although the LbL technique is widely appreciated for its simple processing, the fabrication can be very time-consuming and it is therefore not suitable for manual preparation if a large number of bilayers are needed. For example, deposition of an LbL consisting of 50 bilayers takes almost 24 h of nonstop work, assuming that the substrate is immersed in each polyelectrolyte solution for 10 min. Therefore, automation of the coating process will be beneficial to free manual labor as well as to provide more consistency.

In this chapter, we report our achievements in preparing LbLs using an automatic coating apparatus to assemble as many as 100 bilayers. With physiological concentrations of GSNO and GSH, these LbLs generate NO fluxes comparable to that of natural human endothelial cells. Even with a hundred bilayers, the LbL structure shows excellent stability under exaggerated reaction conditions. The surface morphology of the LbLs was also examined using electron microscopy.

3.2. Experimental

3.2.1. Materials

Polyethyleneimine (PEI, M_w 25 kD), sodium alginate (Alg, M_w 12-80 kD), and glutathione (GSH) were purchased from Sigma-Aldrich (St. Louis, MO) and used as received. Organoselenium immobilized PEI (SePEI) and *S*-nitrosoglutathione (GSNO) were synthesized as described previously.[1] All solutions were prepared with 18 MΩ cm^{-1} deionized distilled water obtained from a Milli-Q system (Millipore Corp., Billerica, MA). Five Fr Cook® double lumen polyurethane catheters were obtained from Accord Biomaterials Inc. (Ann Arbor, MI).

3.2.2. Preparation of $(SePEI/Alg)_n$ Layer-by-Layer assembly

The quartz slide was cleaned using piranha solution (3:7 v/v H_2SO_4/H_2O_2 mixture) for 30 min before use to fully remove surface impurities. *(Caution: this solution is*

extremely corrosive.) The LbL multilayer was prepared by immersing a quartz slide alternately into SePEI and Alg solutions (1 mg mL^{-1}) for 10 min each. In order to assemble more bilayers in a single LbL assembly, an automatic coating instrument StratoSequence 6 (Nanostrata Inc., Tallahassee, FL) was employed. The automatic fabrication protocol differs from the manual method primarily in its extended washing step, in which the substrate is sequentially immersed in three batches of PBS for 1 min each after adsorption of one layer of polyelectrolyte (see Scheme 3.1).

3.2.3. Characterization of NO generation LbLs

NO Detection. Nitric oxide generation from $(SePEI/Alg)_n$ LbLs coated on metal substrates was quantitated as described in Chapter 2.

SEM. Surface morphology of the polyelectrolyte multilayers was examined on a FEI Nova Nanolab Scanning Electron Microscope via the detection of secondary electrons. The specimens were dried in a N_2 atmosphere overnight and then gold coated using a SPI Sputter Coater at 18 mA for 60 s for better imaging.

Se Leaching Test and Quantification of Total Se in the LbL. A piece of $(SePEI/Alg)_{100}$ with a known surface area was placed in a vial filled with 10 mL of PBS buffer containing 100 μM GSH, 50 μM GSNO and 0.1 mM EDTA to extract any leachable selenium species. The vial was then capped, wrapped with aluminum foil, and incubated at 37 °C. Every 24 h, the extracting solution was collected and the vial

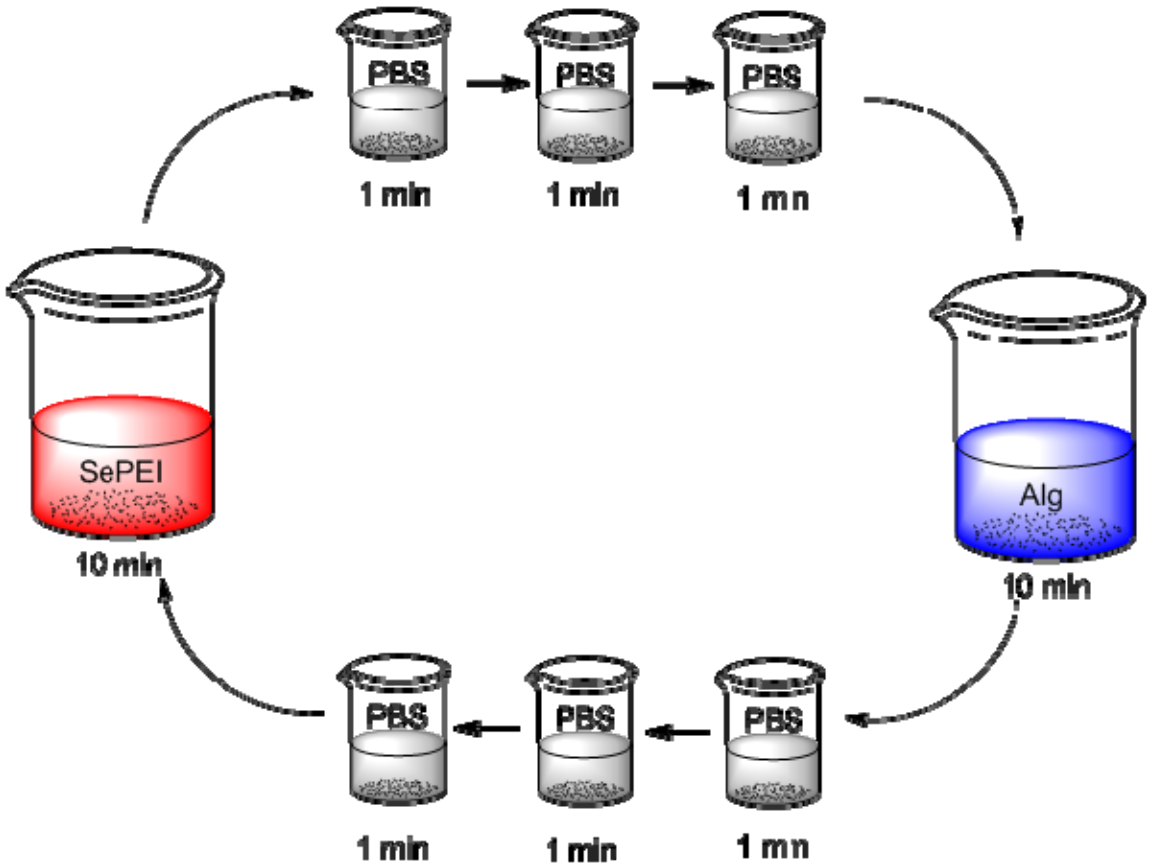

Scheme 3.1. Schematic representation showing the automatic LbL deposition procedure.

was refilled with fresh PBS buffer containing the same concentrations of GSH, GSNO and EDTA. After 3 d extraction period, the extracts were combined and brought to 50 mL using a volumetric flask. The extracted coating was then digested using 10 mL fuming nitric acid and brought to a final volume of 100 mL. The extract and digesting solution were then sent for ICP-MS measurements to determine the Se concentrations.

***In Vivo* Implantation.** To evaluate the *in vivo* performance of the $(SePEI/Alg)_{100}$, the LbLs were deposited on 5Fr Cook® polyurethane catheters without any priming treatment. The cannular tip of the catheter was automatically sealed during the coatings by the LbL. Before implantation, a catheter was cut down to 1 cm long segments and tested for its NO generation activity. Another intact catheter was then implanted in the jugular vein of a New Zealand rabbit for 4 h. The catheter was then explanted, cut into 1 cm long segments, and assessed for its post-surgery catalytic activity.

3.3. Results and Discussion

Layer-by-Layer assemblies, in spite of their simple and straightforward fabrication, are highly sensitive to the coating parameters in terms of their structure and physical properties. This is because the surface charge reversal is a consequence of the kinetically controlled adsorption of the polyelectrolyte, rather than a thermodynamically dictated process. Therefore, transition from a manual fabrication to an automatic protocol may also alter the NO generation behavior of the resulting LbL. Although it

takes 6 minutes longer to complete one bilayer in the automatic method, the extensive washing indeed turns out to be beneficial in producing more stable LbLs. As discussed in Chapter 2, the manually coated LbL has to be annealed in a GSH solution for hours to obtain a stable structure that shows a clear up-and-down NO generation pattern. This is because the LbL is formed by a kinetically controlled process. If the freshly prepared multilayer structure is not given enough time to cure, it is unstable and tends to reorganize if the coating remains wet.[5] For the NO generation LbL, such reorganization is always associated with leaching of the RSe species, which potentially can cause serious toxicity issues. However, the automatically coated LbL shows excellent stability even without the annealing process (see Figure 3.2). Assemblies containing 40 and 100 bilayers were tested immediately after deposition to give NO generations of 140 and 420 ppb, respectively. The NO productions quickly diminished to less than 10 ppb when the coatings were removed from the GSNO and GSH reservoir, indicating that the NO was predominantly produced within the LbL. These observations prove that the LbLs are very stable and the annealing treatment is not necessary for LbLs prepared with the automated dip method. This is most likely attributed to the prolonged washing during which the polyelectrolyte chains were allowed to reorganize into a more stable conformation. Notably, the $(SePEI/Alg)_{40}$ and $(SePEI/Alg)_{100}$ multilayers display similar residual NO productions, which clearly demonstrates that the stability of the LbL is not compromised even after hundreds of assembling cycles.

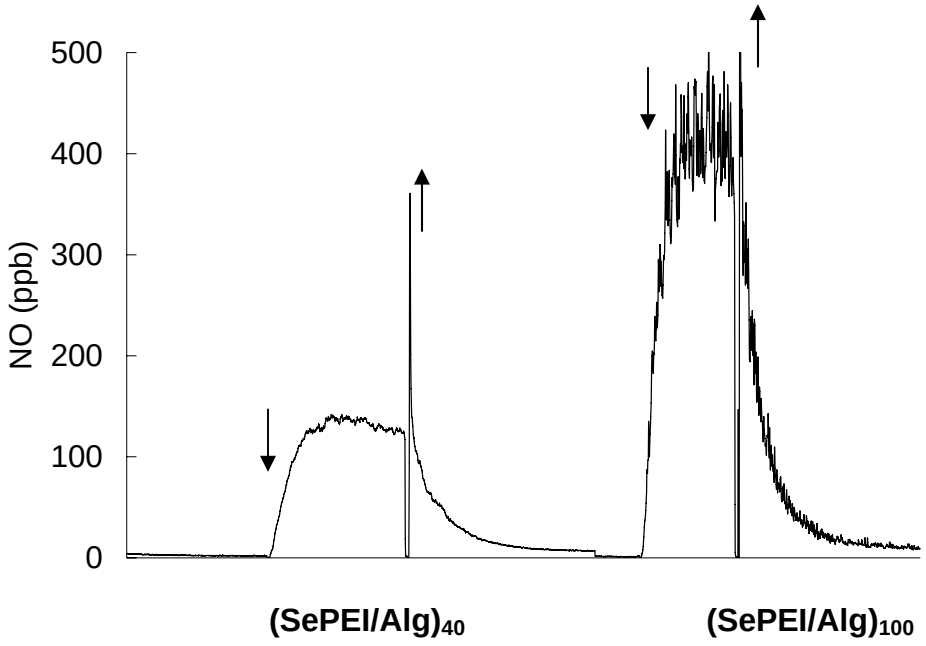

Figure 3.2. Nitric oxide generation from 50 μM GSNO and 50 μM GSH by $(SePEI/Alg)_{40}$ and $(SePEI/Alg)_{100}$. The (↓) and (↑) arrows indicate that the LbL was immersed into or removed from the test solution. The coating areas are estimated to be about 3.3 cm^2.

The NO generation was also plotted against the number of bilayers in the LbL (see Figure 3.3). When more bilayers were assembled into the LbL, the catalytic activity of the coating increased correspondingly, reflected by an almost linear trend of the NO flux produced from the same concentrations of GSNO and GSH. This observation is in accordance with the data obtained from manually coated LbLs (see Figure 2.17 in Chapter 2). Such a result implies a very open film structure in which most of the

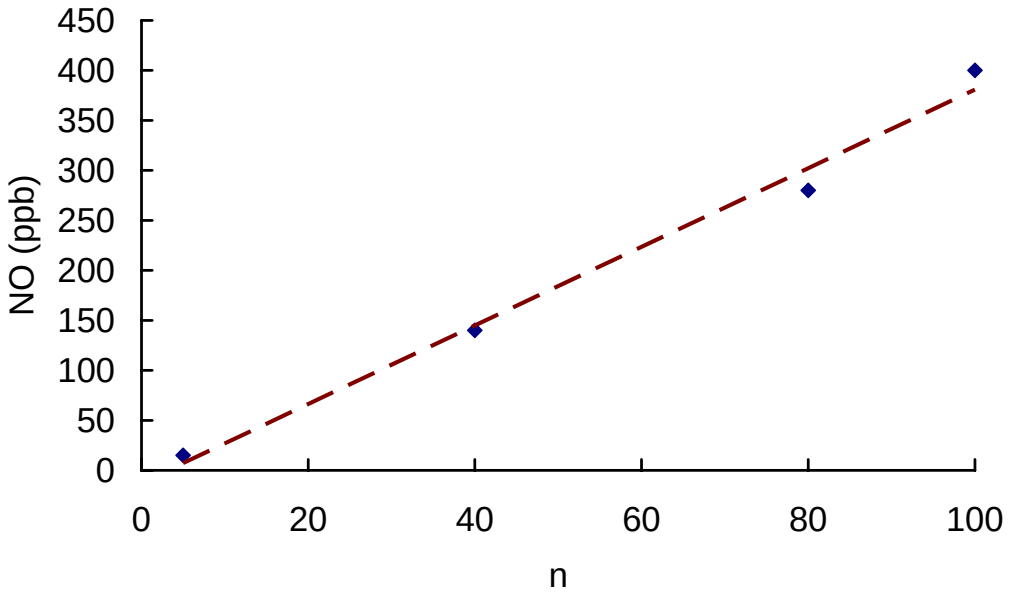

Figure 3.3. Correlation between number of bilayers (n) and NO generation from 50 μM and 50 μM GSH.

immobilized RSe species are able to contribute to GSNO breakdown. This is an attractive feature expected from the LbL technique; i.e., that the degree of NO generation from given RSNO/RSH concentrations can be controlled by the number of bilayers deposited.

The primary goal of using an automatic apparatus and preparing an LbL with many bilayers is to immobilize more catalytic sites so that enough NO can be generated from the typical concentrations of GSNO and GSH present in the biological environment. Hence, a $(SePEI/Alg)_{100}$ was evaluated for NO generation capability using 2.5 μM GSNO and 20 μM GSH at room temperature. According to chemiluminescence, the

multilayer generated NO at a flux of 1.6 x 10^{-10} mol cm^{-2} min^{-1} (see Figure 3.4). This value is within the range of 0.5 and 4 x 10^{-10} mol cm^{-2} min^{-1}, which is the estimated NO flux generated by healthy endothelium cells.[4] The sample was then preserved in PBS buffer at 4°C with its activity followed up periodically using the same experimental configuration. The activity shows a sluggish decrease over time; however, the coating retained at least 85% of its original activity after 17 d (see Figure 3.5). This result, in conjunction with the production of a biological level of NO, suggests that such an LbL has potential to be used on long term cardiovascular implants.

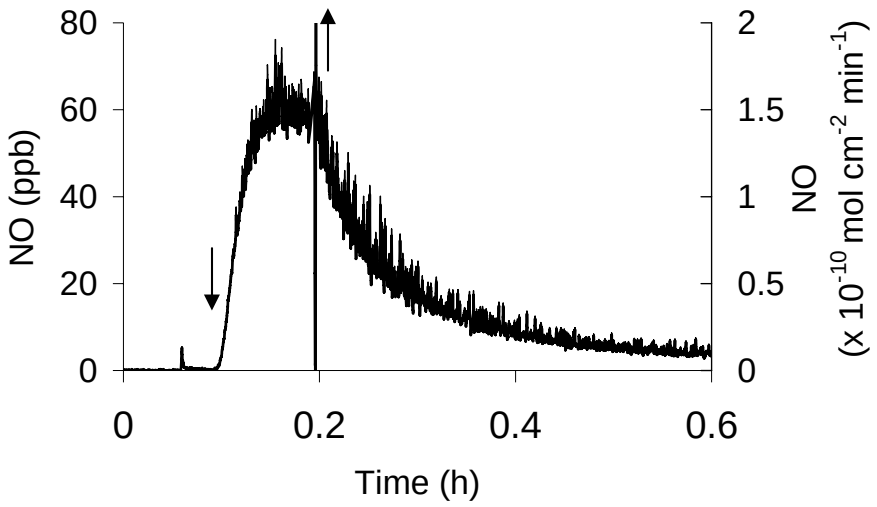

Figure 3.4. Nitric oxide generation by $(SePEI/Alg)_{100}$ from 2.5 μM GSNO and 20 μM GSH at room temperature. The (↓) and (↑) arrows indicate that the LbL was immersed into or removed from the test solution.

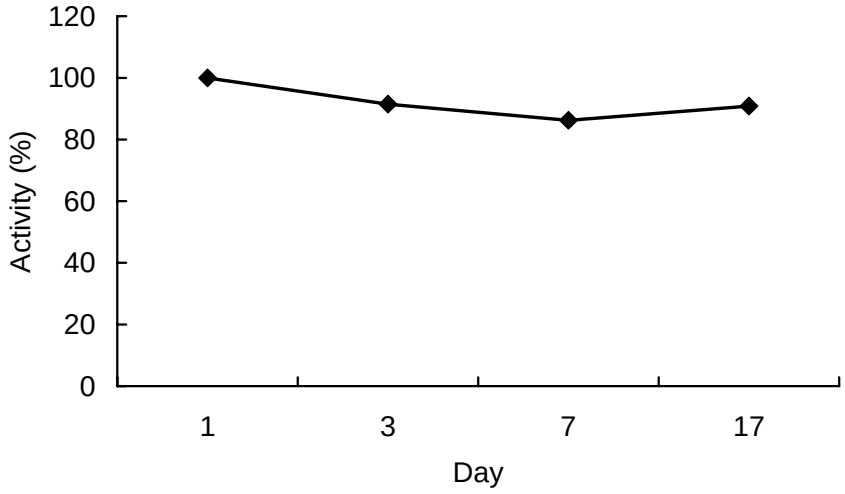

Figure 3.5. Long term activity of $(SePEI/Alg)_{100}$, tested using 2.5 μM GSNO, 20 μM GSH and 0.1 mM EDTA at room temperature.

Although the $(SePEI/Alg)_n$ LbL shows good catalytic activity and stability *in vitro*, exposure to blood rich in reactive biological species may have an adverse impact on the catalysts. Therefore, the $(SePEI/Alg)_{100}$ was constructed on a PU catheter which was then implanted in a rabbit vein. The NO generation activities were evaluated before and after the implantation (see Figure 3.6). Before implantation, the LbL gave a peak NO flux of 1.5×10^{-10} mol cm^{-2} min^{-1} from 1 μM GSNO and 20 μM GSH. After 4 h, the catheter was explanted and found to be covered by blood clots. The reason for such a failure of this NO generation coating in terms of thromboresistancy might be very complicated and will be discussed further in the conclusion section of this chapter.

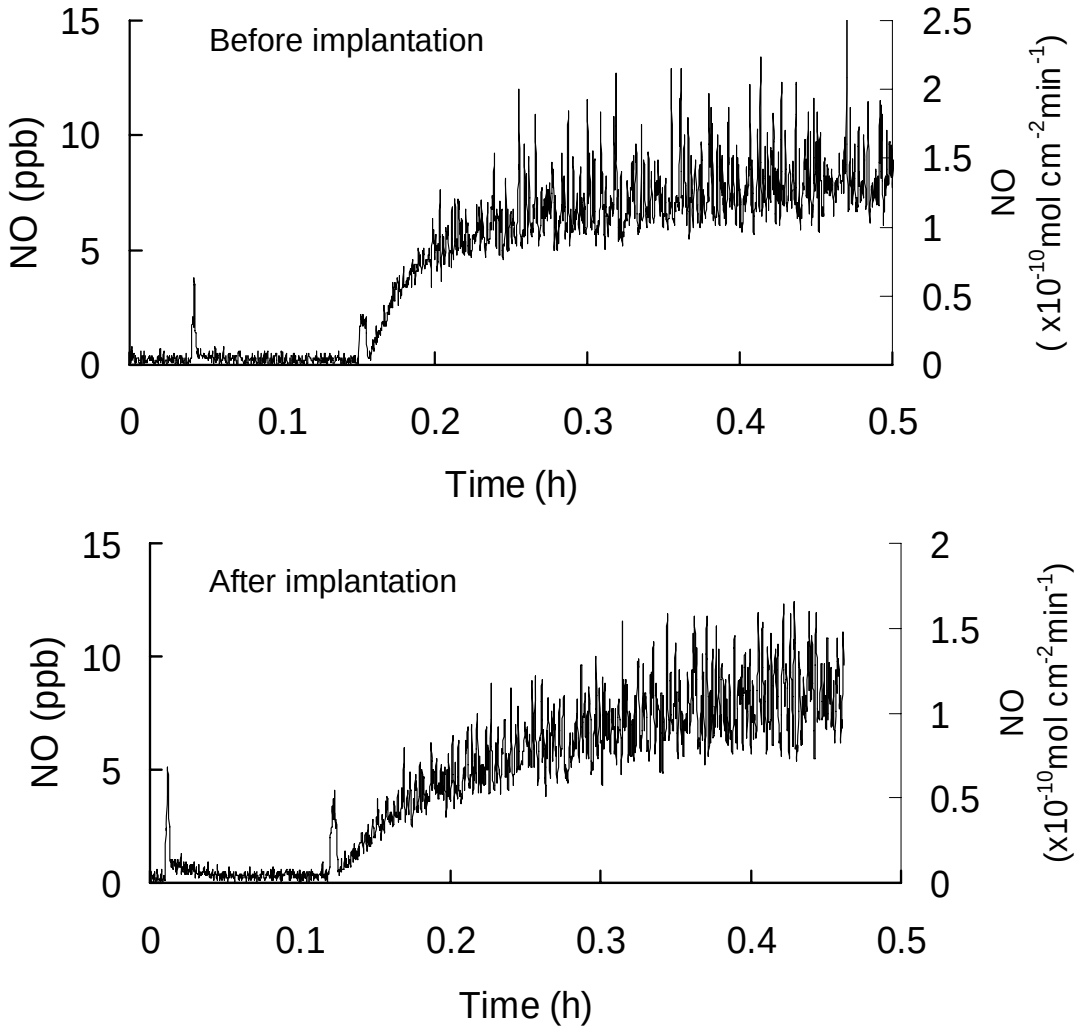

Figure 3.6. Nitric oxide generation by $(SePEI/Alg)_{100}$ coated on a PU catheter before (top) and after (bottom) implantation in a rabbit vein for 4 hours. The NO generation was measured using 1 μM GSNO and 20 μM GSH at 37 °C.

After removal of the clot, the catheter was gently washed and tested for NO generation. Under the same conditions, an NO flux of 1.2 x 10^{-10} mol cm^{-2} min^{-1} was produced by this explanted LbL, which was very close to the flux before implantation. This result highlights a very encouraging fact that LbL does survive the sheer stress of the flowing blood and its catalytic efficiency is preserved even in direct contact with the blood components.

The surface morphology of coatings comprising 50 and 100 bilayers was imaged by SEM. Notably, the drying process is a critical parameter dictating the surface texture. When coarse evacuation or air-blowing was applied, the LbLs often exhibited rough surfaces with bumps and holes. In contrast, smoother surfaces were observed on samples capped in vials to let water evaporate naturally. As shown in Figure 3.7, $(SePEI/Alg)_{50}$ exhibits a very smooth and featureless appearance under the microscope; however, $(SePEI/Alg)_{100}$ shows a surface texture resembling an orange peel. We speculate this unevenness is related to the diselenide crosslinks within the SePEI, because the LbL constructed using PEI without diselenide coupling displayed a very smooth surface (data not shown). Another possibility is that the polyions in the LbL form a scattered microcrystalline region upon drying,[6] although the polyelectrolyte complexes commonly show amorphous structures owing to their fast binding.

The potential toxicity concern of these automatic coated LbL was also assessed by measuring the leachable RSe species from the coating under exaggerated reaction

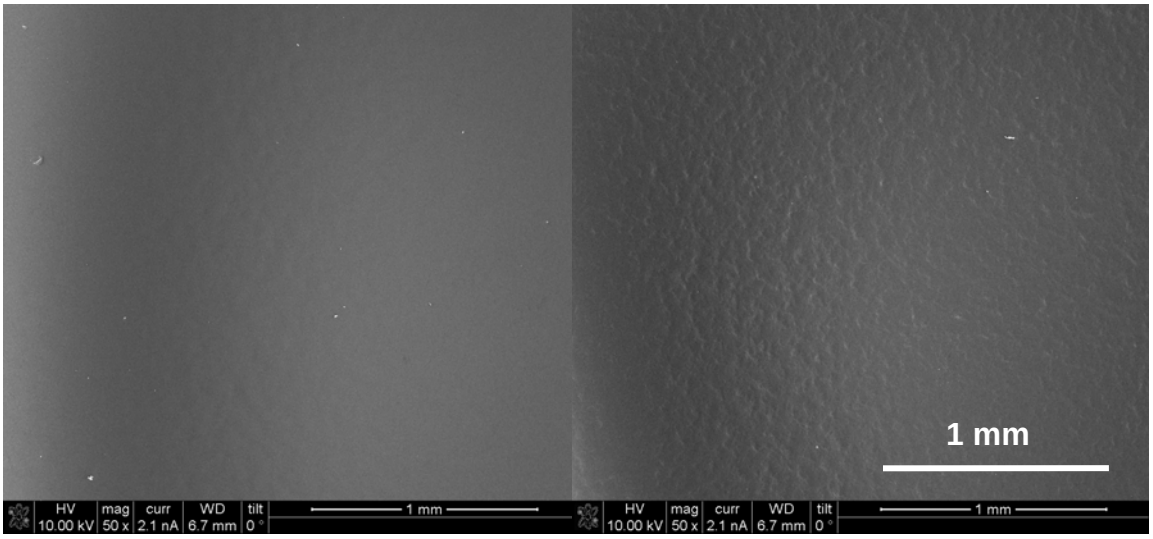

Figure 3.7. SEM snapshot of $(SePEI/Alg)_{50}$ (left) and $(SePEI/Alg)_{100}$ (right).

conditions. A piece of $(SePEI/Alg)_{100}$ with a surface area of 3.8 cm^2 was extracted with PBS containing 50 μM GSNO, 50 μM GSH and 0.1 mM EDTA. Approximately 3.1% Se was found released into the extracts after three days. Such a leach rate is very similar to the Se leaching observed in manually coated LbL, indicating that the increase of coating cycles does not compromise the cohesion between the oppositely charged polyelectrolytes in the LbL. This discovery implies an "unlimited" multilayer growth in terms of the structural stability of the resulting LbL. The total abundance of Se element in the LbL was also determined to be ca. 93.9 μg cm^{-2}. It is not surprising that this concentration is much higher than the 2.9 μg cm^{-2} Se that was found in the manually coated $(SePEI/Alg)_{10}$; however, one may also notice that this 30 fold increase is not proportional to the increase of the number of bilayers. This is because the manual and

automatic coating protocols should be viewed as two distinctive systems due to the sensitivity of the LbL to the exact deposition process.

3.4. Conclusion

In this chapter, LbLs with up to 100 bilayers were realized using an automatic coating apparatus. As expected, a physiologically relevant level of NO can be generated from low concentrations of GSNO and GSH if enough catalytic sites (i.e., the number of bilayers) were deposited on the substrate. We also successfully demonstrated that the catalytic activity was sustainable over an extended period of time, which indicates these NO generation LbLs are suitable for long term cardiovascular implants.

Despite of all these positive aspects regarding this automated preparation of NO generating LbLs, there are still many unresolved issues. Most importantly, whether the NO flux generated by these LbLs is enough for thrombosis prevention still needs further proof. Recently, the lowest NO flux required to maintain an extracorporeal circulation loop free of thrombosis was suggested to be about 13×10^{-10} mol cm^{-2} min^{-1}.[7] Intuitively, one can see that this flux threshold is device-dependent, i.e., a larger device tends to need a higher surface NO supply to be thromboresistant. It should also be noted that the hemocompatibility of the EC layer involves synergic efforts of several anti-platelet and anti-coagulant species. If present alone, the NO flux probably needs to reach a higher dose to completely suppress the coagulation response. The ultimate answer for this

question lies in evaluating these $(SePEI/Alg)_n$ LbLs *in vivo* using suitable substrates and animal models. Clearly, this generic NO generation LbL, as described in Chapter 2, allows for the selection of a substrate of any nature and dimension to fit the needs for a given *in vivo* implantation.

In our preliminary *in vivo* implantation, the LbL coated catheters were found covered by blood clots after explantation. It is still premature to draw any conclusions about the efficacy of this NO generation surface. First of all, the RSNO level in the blood is highly dependent on each individual animal, and is a critical variable dictating the NO generation rate. Presence of other prothrombotic surface features such as a rough surface contour and selective protein binding may further offset the NO potency. It will be necessary to conduct more detailed investigations to better understand the surface biochemistry of the $(SePEI/Alg)_n$ multilayer and hence to fine tune its surface physicochemical properties.

3.5. References

1. Yang, J.; Welby, J. L.; Meyerhoff, M. E. *Langmuir* **2008**, *24*, 10265-10272.

2. Kelm, M. *Biochim. Biophys. Acta Bioenerg.* **1999**, *1411*, 273-289.

3. Wu, Y. D.; Zhang, F. H.; Wang, Y.; Krishnamoorthy, M.; Roy-Chaudhury, P.; Bleske, B. E.; Meyerhoff, M. E. *Clin. Chem.* **2008**, *54*, 916-918.

4. Vaughn, M. W.; Kuo, L.; Liao, J. C. *Am. J. Physiol. Heart Circ. Physiol.* **1998**, *43*, H2163-H2176.

5. Yang, S. G.; Zhang, Y. J.; Zhang, X. Y.; Guan, Y.; Xu, J.; Zhang, X. L. *Chemphyschem* **2007**, *8*, 418-424.

6. Silva, H. S.; Uehara, T. M.; Bergarnaski, K.; Miranda, P. B. *J. Nanosci. Nanotechnol.* **2008**, *8*, 3399-3405.

7. Skrzypchak, A. M.; Lafayette, N. G.; Bartlett, R. H.; Zhou, Z. R.; Frost, M. C.; Meyerhoff, M. E.; Reynolds, M. M.; Annich, G. M. *Perfusion-Uk* **2007**, *22*, 193-200.

CHAPTER 4

CATALYTIC NITRIC OXIDE GENERATION ON STENT METAL SURFACES

4.1. Introduction

Percutaneous transluminal coronary angioplasty (PTCA) has become the major intervention for coronary atherosclerosis to remove the lipid/cholesterol deposits and restore the blood flow through the diseased arteries. During PTCA, a stent mounted on an angioplasty balloon is delivered to the target site and deployed via balloon inflation to open the vessel with the atherosclerotic plaque. The balloon is then withdrawn, while the stent is left behind as a scaffold to preserve the luminal patency of the newly widened vessel.

Clinical outcomes point to the beneficial impact from stent placement in preventing vessel recoil/re-closure.[1] However, the recipients are under risk of several stent-related complications, including sub-acute thrombosis which occurs in 1 to 3% of patients within 7 to 10 days of the procedure.[2] This complication has been largely mitigated by aggressive multidrug treatments with anti-platelet agents (e.g., clopidogrel, aspirin, and glycoprotein IIb/IIIa inhibitors, etc.) and anti-coagulants (e.g., heparin, and warfarin). However, well-documented side effects, such as gastrointestinal toxicity and internal bleeding, have also been associated with these antithrombotic treatments.[3,4] Nitric oxide, owing to its propensity to react with many biological species, has potential advantages over other

pharmacologic treatments in its highly localized effect and multi-pathway metabolism.[5] Therefore, it is of interest to demonstrate the applicability of the previously described NO generation LbL (see Chapter 3) to the stent relevant metallic surfaces.

In this chapter, three exemplary biomedical metallic materials (see Table 4.1) were selected to study the feasibility of fabricating $(SePEI/Alg)_n$ LbLs on their surfaces. Stainless steel 316L (SS) is the classic material to make stent struts owing to its well-suited mechanical properties. The low carbon content of this material tremendously reduces the possibility of *in vivo* corrosion, making this alloy very useful for long term implantation. Nitinol (NiTi), a shape memory alloy, is used to fabricate self-expanding stents which have a smaller diameter at room temperature and expand to their preset diameter at body temperature.[6] Titanium (Ti) is also studied in particular in this work, although pure Ti is not commonly used as the sole stent material. Due to its low ductility, Ti stents are more prone to fracture; however, such an inadequate mechanical property does not limit the metal from coronary stent applications. Indeed, coatings comprising titanium oxide and nitride have proved to be more biologically inert with reduced platelet and fibrinogen deposition.[7-9] Recently, Ti-based tantalum and niobium alloys have shown excellent hemocompatibility and hence are potentially useful as stent materials.[10] Similar to Chapter 3, a homemade automatic coating robot was employed to fabricate the catalytic NO generation thin films on these metal surfaces. The consecutive build-up of the multilayer was monitored by the mass of the polyelectrolytes deposited on the metal, as well as the Se content in the coating. The resulting metal based $(SePEI/Alg)_n$ were examined for their NO generation activity, surface morphology, and coating thickness.

Alloy	Constitution	Commercial products/manufacturer
Stainless Steel 316L	Fe 60-65% Cr 17-20% Ni 12-14% C < 0.03%	CYPHER® / Boston Scientific Corp. TAXUS® / Cordis Corp. Endeavor®/ Medtronic Inc. Xience®/ Abbott Laboratories Inc.
Nitinol	Ni 49.5-57.5% Ti 42.5-50.5%	PRECISE® / Cordis Corp. Sentinol® / Boston Scientific Corp.
Ti	Ti	Titan® Ti-N-O / Hexacath (France)

Table 4.1. Elemental constitutions and representative common stent alloys.

4.2. Experimental

4.2.1. Materials

Polyethyleneimine (PEI, M_w 25 kD), sodium alginate (Alg, M_w 12-80 kD), glutathione (GSH), and lysozyme from chicken egg white were purchased from Sigma-Aldrich (St. Louis, MO) and used as received. Bovine albumin fraction V solution was purchased from Invitrogen Corp. (Carlsbad, CA). Reagent grade acetone and ethanol were acquired from Fisher Scientific (Pittsburgh, PA). Sheets of stainless steel 316L, medical grade titanium, and nitinol were acquired from Accord Biomaterials Inc. (Ann Arbor, MI). *S*-Nitrosoglutathione (GSNO) and organoselenium immobilized polyethyleneimine (SePEI) were synthesized as previously described.[11] Phosphate-buffered saline (PBS, 10 mM, pH = 7.4) was prepared in the laboratory. All the solutions were prepared with 18 MΩ cm^{-1} deionized-distilled water via a Milli-Q filtration system (Millipore Corp., Billerica, MA).

4.2.2. Preparation of nitric oxide generation Layer-by-Layer on metal substrates

Metals were cut into 1 x 3 cm strips and sequentially sonicated in acetone, ethanol, and deionized water (10 min each) shortly before the LbL assembly process. A homemade automated LbL deposition system (see Chapter 3) was employed to ensure consistency of the deposition cycles across various samples. The LbL was coated by alternately dipping the metals in 1 mg mL^{-1} SePEI and Alg solutions (10 min each) with three intermediate PBS washings (1 min each) to remove loosely attached species prior to deposition of the next counter polyion layer. Such a coating cycle was repeated until the desired number of bilayers was reached. Upon completion of the LbL process, samples were dried in ambient air.

4.2.3. Characterization

NO Detection. Nitric oxide generation from $(SePEI/Alg)_n$ LbLs coated on metal substrates was quantitated as described in Chapter 2.

SEM. Surface morphology of the polyelectrolyte multilayers was examined on a FEI Nova Nanolab Scanning Electron Microscope via the detection of secondary electrons. The specimens were dried in a N_2 atmosphere overnight and then gold coated using a SPI Sputter Coater at 18 mA for 60 s for better imaging.

Quantification of Total and Leachable RSe Species in the LbL. Metals with a known surface area (usually 1or 2 cm^2) were coated with $(SePEI/Alg)_n$ and then extracted in 1 mL PBS buffer (pH = 7.4) containing 50 μM GSH, 50 μM GSNO, and 50 μM EDTA at 37 °C for any leachable organoselenium species. The extract solution was refreshed on a

daily basis to maximize reaction time. At the end of the 3 d extraction, the extracts were combined, brought to 25 mL using deionized distilled water and sent for ICP-MS analysis to determine selenium concentration in the solution. Metal strips from the previous selenium leaching study were separately submerged in fuming HNO_3 (*Caution: fuming HNO_3 is extremely corrosive.*), which resulted in a gradual delamination and digestion of the LbL film. A total of 5 mL of fuming HNO_3 was used and the bare metals were removed when the digestion was complete (~ 2 d at room temperature). The digestion solution was then brought to 250 mL with DI water and sent for ICP-MS analysis.

4.3. Results and Discussion

Different from the quartz substrates employed in Chapters 2 and 3, metals are completely opaque objects. This distinctiveness excludes spectroscopic characterization of the LbL structure by measuring the transmitted light. As a result, the build-up of the multilayer was confirmed via measuring the mass of the polyelectrolytes deposited on the metal surface. As shown in Figure 4.1, four pieces of SS and Ti were weighed separately and subsequently coated with 25, 50, 75 and 100 bilayers of (SePEI/Alg), respectively. Due to the limited quantity of substrate, only two pieces of NiTi were coated with 50 and 100 bilayers, respectively. The samples were then completely dried and their masses were acquired again. The mass of the LbL was then derived by subtracting the initial mass of the metal substrate from the mass after the LbL deposition, followed by normalization against the coating area. On all three metals, the mass of the LbL correlated positively with the number of bilayers. Remarkably, fitting the data into a linear trend yielded a similar slope across all three substrates, meaning the growth of the multilayer (i.e., the

amount of polyions deposited in a single bilayer) was not substrate specific within the range of 25 to 100 bilayers.

The successful construction of the multilayer structure was also proved by detecting the Se content within the LbL using ICP-MS. As shown in Figure 4.2, the elemental Se content within the multilayer also displayed a linear correlation with the number of bilayers. Meanwhile, it is not surprising that the Se concentrations in the LbLs are also substrate nonspecific, except for $(SePEI/Alg)_{100}$ coated on NiTi which slightly deviated from the Ti and SS data. One may notice that there are contradictory data obtained on NiTi, which seemed to absorb a lower amount of polyelectrolytes but contain more Se. It must be noted that the masses that were manipulated in aforementioned experiment were very small (only several milligrams), which makes the results shown in Figure 4.1 more susceptible to random errors and artifacts.

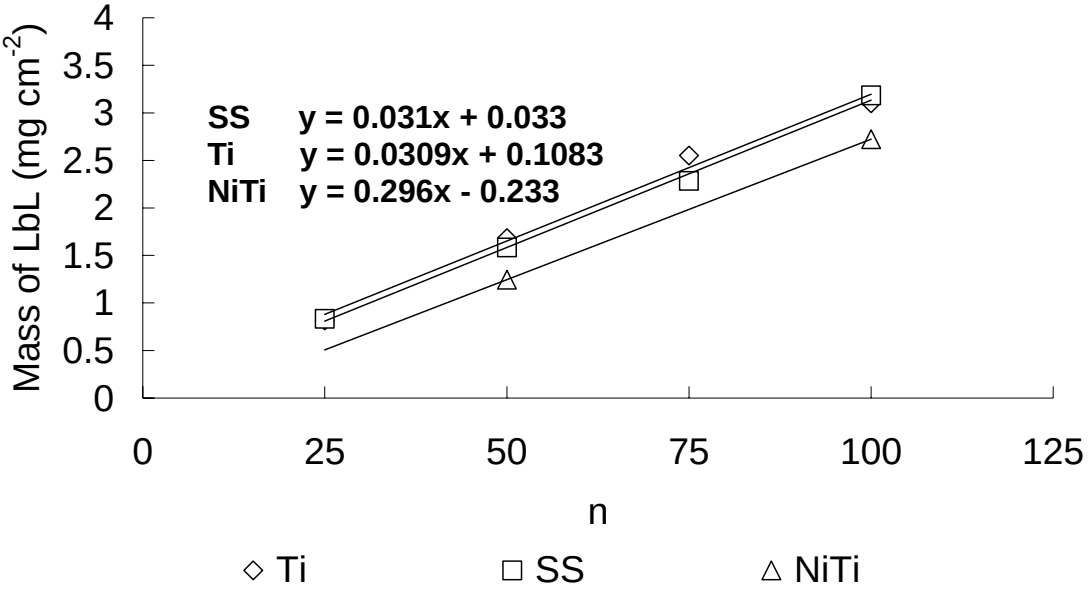

Figure 4.1. Mass of $(SePEI/Alg)_n$ coated on metal substrates (1 x 3 cm).

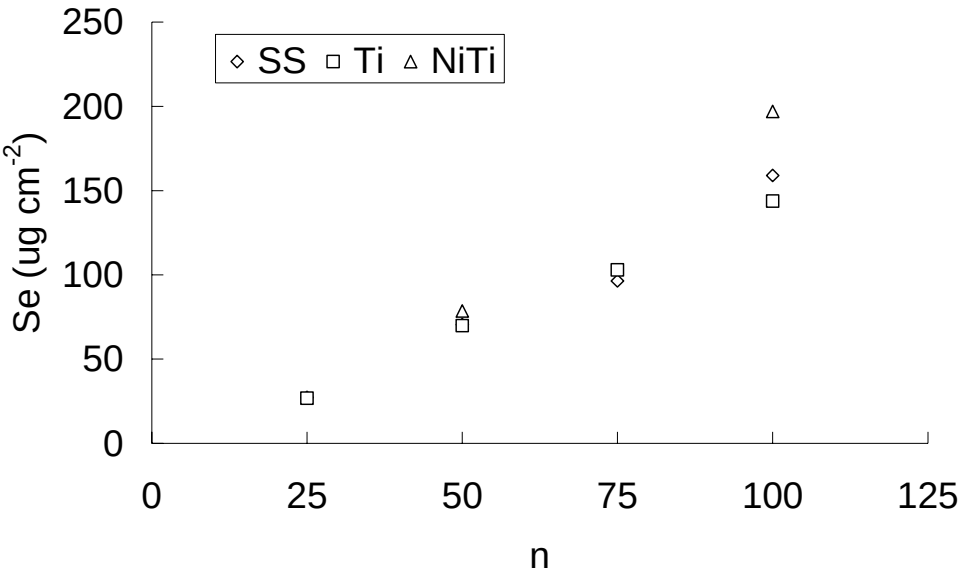

Figure 4.2. Se density within $(SePEI/Alg)_n$ coated on SS, Ti, and NiTi.

The catalytic activity of the LbL coated on metal substrates was first evaluated using excess GSNO and GSH to better elucidate the trend. It revealed that the LbLs coated on different metal substrates possessed similar NO generation capability (see Figure 4.3). With 50 μM GSNO and 50 μM GSH, the LbLs yielded a considerable NO production upon immersion in the reaction solution. When the catalytic multilayer was removed from the reaction reservoir, the NO generation almost completely ceased. The slight baseline increase indicated predominant heterogeneous NO production within the multilayer structure. The structural stability was also revealed by the leaching studies in which the leachable RSe species were extracted from $(SePEI/Alg)_{50}$ using exaggerated reaction conditions with 50 μM GSNO and 50 μM GSH. After 3 d extraction period, the LbLs coated on SS, Ti and NiTi lost 1.90%, 3.50% and 0.71% of its total Se content, respectively.

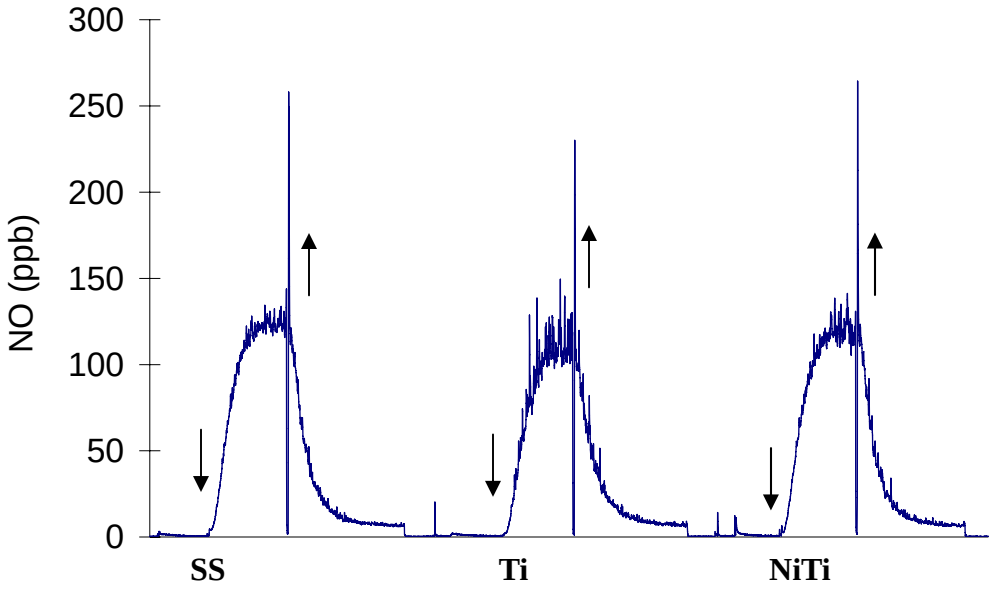

Figure 4.3. NO generation by $(SePEI/Alg)_{25}$ coated on SS, Ti and NiTi from 50 μM GSNO, 50 μM GSH and 50 μM EDTA. The metal pieces were immersed into/removed from the reaction cell as indicated by the (↑) and (↓) arrows.

The NO production from given amounts of GSNO and GSH was also plotted against the number of bilayers (see Figure 4.4). Surprisingly, the NO fluxes only slightly varied in a narrow range between 5 - 6 x 10^{-10} mol cm^{-2} min^{-1}, instead of scaling proportionally along the number of bilayers coated. This observation was obviously contradictory to the results shown in Figure 4.1 and Figure 4.2, both of which showed an increase in RSe catalyst deposited on the metal surfaces with increased number of bilayers. So far, the mechanism for such a saturated NO flux remains unclear. We speculate that it might relate to the internal structure of the LbL which dominates the diffusion of the GSNO and GSH through the polyelectrolyte matrix. As discussed in Chapters 2 and 3, the heterogeneous NO generation occurs not only on the surface of the LbL, but also within the multilayer structure which requires the reactant species to diffuse into the LbL. If the LbL

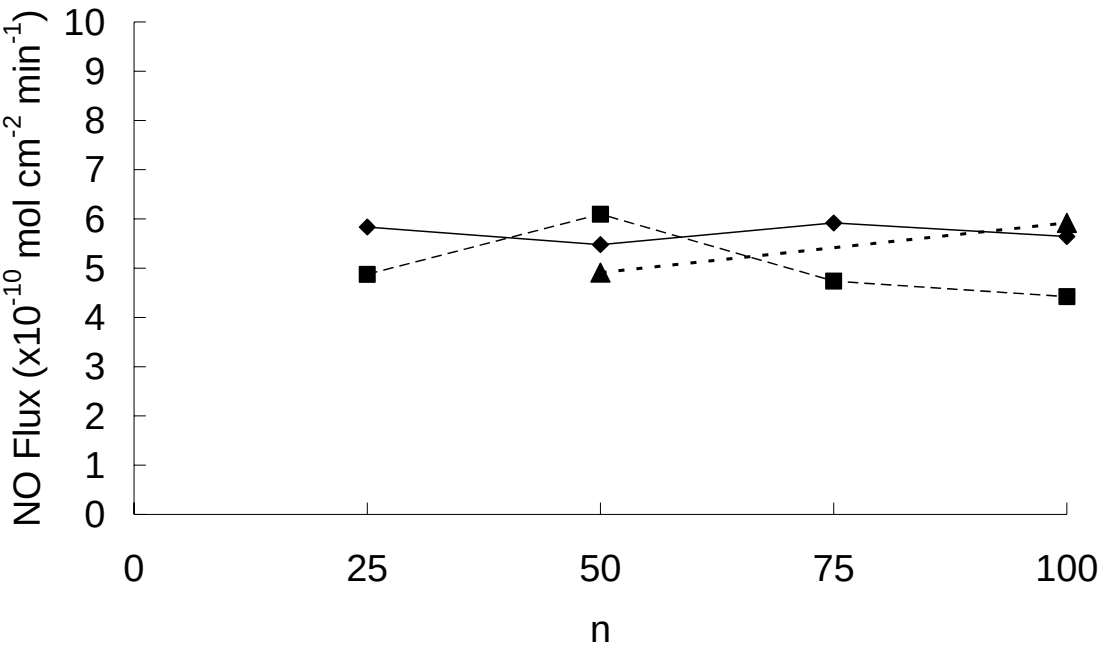

Figure 4.4. NO production from 50 μM GSNO, 50 μM GSH and 50 μM EDTA by $(SePEI/Alg)_n$ containing various number of bilayers.

possesses a highly open structure, GSNO and GSH can diffuse through the entire multilayer so that all the RSe sites within the LbL are able to contribute to the RSNO decomposition. In contrast, a dense structure tends to result in a limited permeability. In the case of metal substrates, the reactants appear to only penetrate a shallow layer within the coating, which excludes the catalytic sites buried in the deep interior from being involved in the reaction. As a result, the NO generation is determined by the permeable thickness and the RSe sites within that region rather than the total catalytic sites.

Nevertheless, these LbLs coated on metal surfaces were evaluated for their NO generation efficiency under typical biological conditions. With 1 μM GSNO and 20 μM GSH, the LbLs produced a NO flux of ca. 0.6 x 10^{-10} mol cm^{-2} min^{-1}, which is relevant to the biological NO flux from the EC monolayer as estimated to be 0.5 - 4 x 10^{-10} mol cm^{-2}

min^{-1} (see Figure 4.5).[12] This highlights the potential of this NO generation LbL to be used to render stent surfaces enhanced biocompatibility.

The plasma proteins comprise the largest group of polyelectrolytes in the blood, which can strongly interact with the highly charged LbL surface through electrostatic attraction and deposit on the surface via the same mechanism as the LbL assembly. Indeed, proteins themselves have been widely used as constituents to build LbL structures to achieve given biological activity on the modified surface.[13,14] To investigate the potential impact of surface protein adsorption, the SePEI based LbLs were placed in PBS buffers containing lysozyme (pI = 11) or albumin (pI = 4.5), which were selected to represent proteins bearing overall positive and negative charges at biological pH, respectively.[15] Compared with a control sample immersed in fresh PBS without any protein species, the LbLs in albumin and lysozyme preserved 97.4% and 98.5% of the NO generation capacity after 1 h exposure, respectively (see Figure 4.6). Apparently, the positively charged lysozyme was more likely to adsorb on the LbL surface; however such a surface fouling and the consequent surface charge reversal did not lead to a significant alteration in the NO generation activity of the LbL.

The surface texture of $(SePEI/Alg)_n$ coated on metal substrates was also evaluated using electron microscopy. As shown in Figure 4.7, the LbLs coated on SS, Ti, and NiTi displayed a relative smooth surface morphology. The $(SePEI/Alg)_{25}$ on SS was then cut to create a fresh edge so that the cross-section of the multilayer could be viewed. Under the microscope, the LbL was discovered to be a dense homogeneous coating with an estimated thickness of 20 μm. It is not surprising that the LbL did not possess a "layered" structure as its name implied. Indeed, the polyelectrolyte LbL has been well-recognized

as a fuzzy

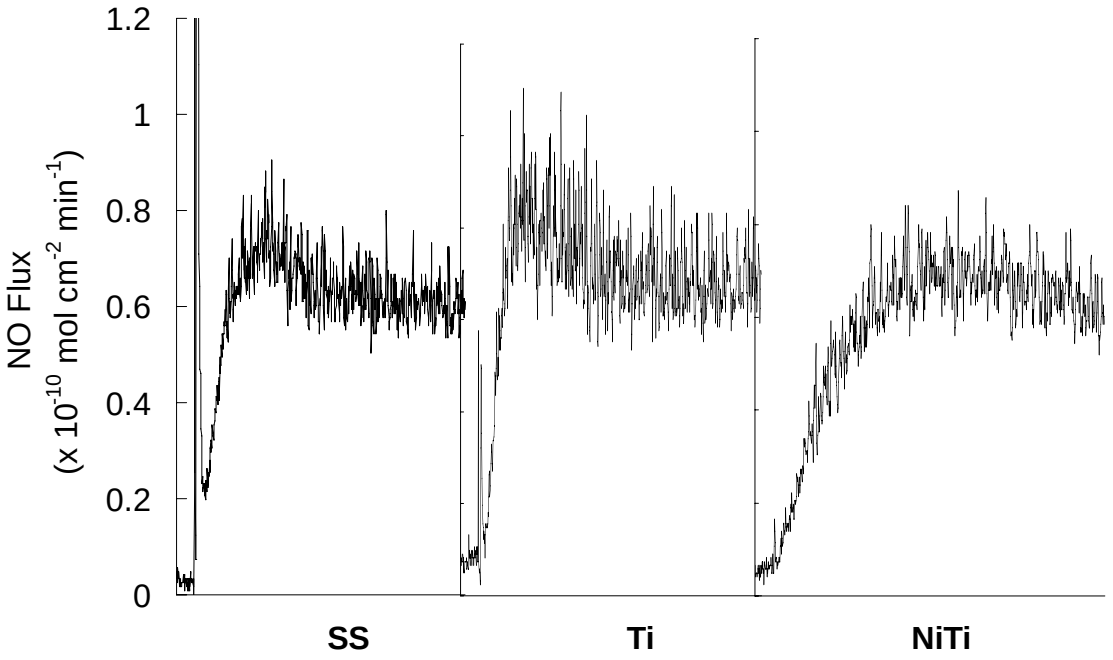

Figure 4.5. NO generation from biological relevant concentrations of GSNO and GSH at 37 ˚C by $(SePEI/Alg)_{25}$ coated on different metal substrates.

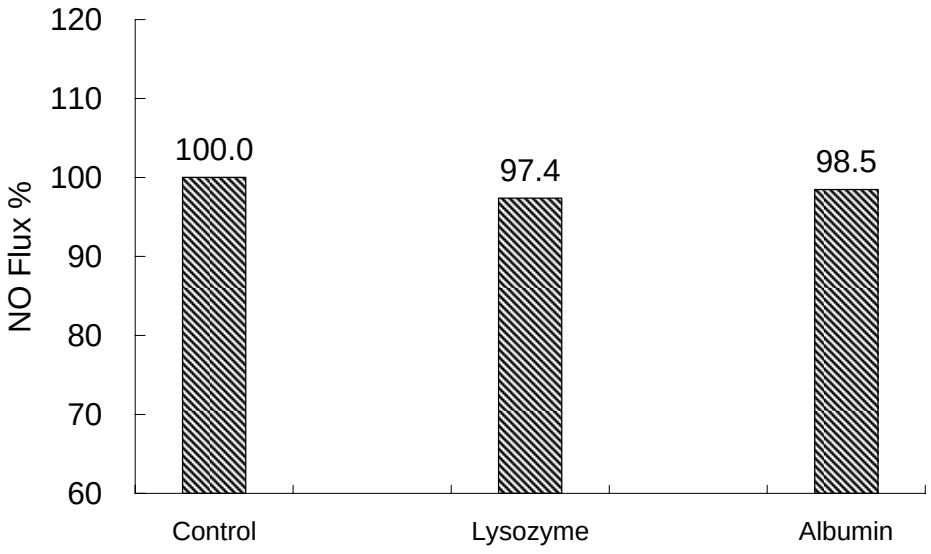

Figure 4.6. NO generation from $(SePEI/Alg)_{25}$ exposed to representative plasma proteins,

in comparison with the multilayer in contact with only PBS buffer.

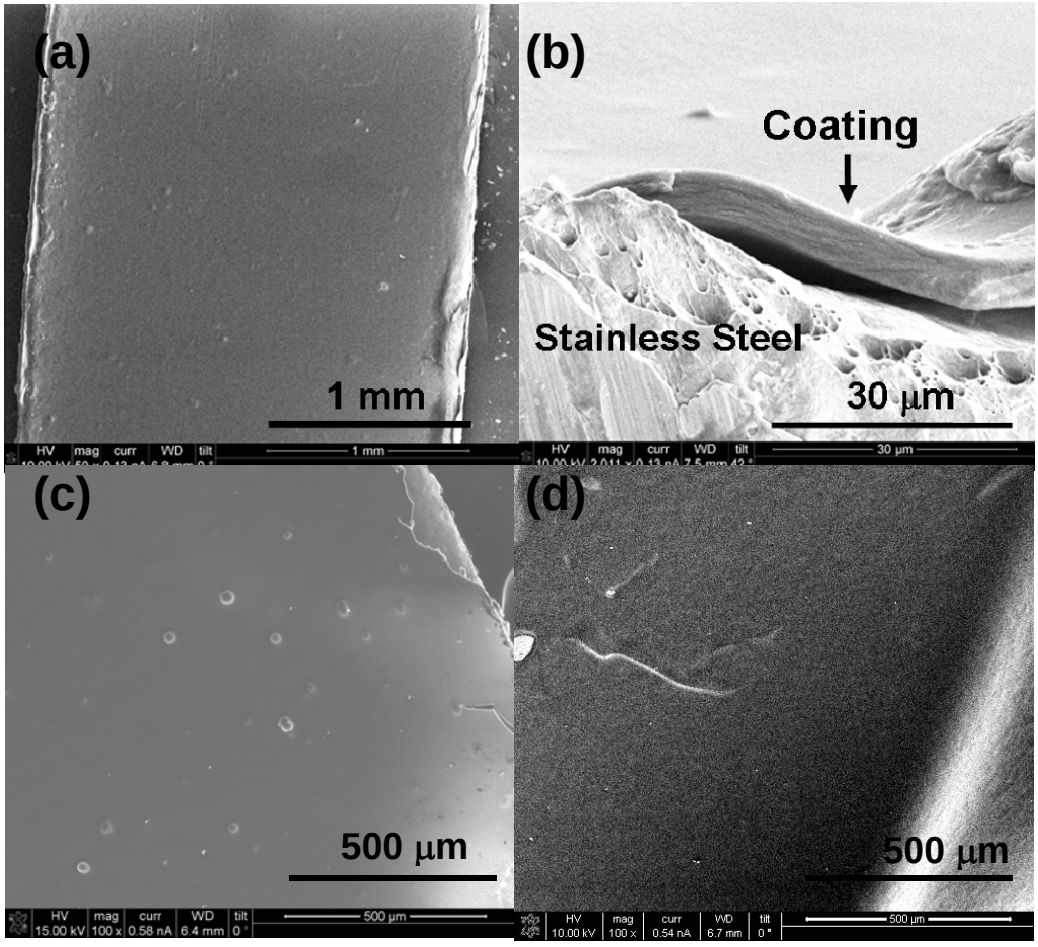

Figure 4.7. SEM pictures of the LbLs fabricated on metal surfaces: (a) $(SePEI/Alg)_{25}$ on SS; (b) cross-section of $(SePEI/Alg)_{25}$ coated on SS; (c) $(SePEI/Alg)_{50}$ on Ti; $(SePEI/Alg)_{50}$ on NiTi.

assembly of interpenetrated polymer chains.[16,17] It is also noteworthy that such a thickness was acquired from a coating which had been completely dried to meet the high vacuum conditions required by SEM. Under real reaction conditions, i.e., in buffers or biological fluids, the polyelectrolyte film is prone to swell. Indeed, a completely reversible swelling/deswelling cycle was observed on a LbL containing poly(allylamine hydrochloride) and poly(styrene sulfonate).[18] The average volume percentage of water in the swollen film could be as high as 50%, dependent on the type of constituent polyion species as well as the thickness of the LbL.

4.4. Conclusion

In this chapter, the previously described NO generating LbL coating was translated onto metal substrates. Stainless steel, nitinol and titanium were selected due to their dominating use in coronary stents. A consecutive deposition of SePEI and Alg polyelectrolytes was realized on these metal surfaces by monitoring the substrate mass during the coating procedure. Similar to the earlier work conducted using quartz substrates, the LbLs fabricated on metal substrates showed substantial structural stability and catalytic activity. However, the LbL coated on metal surfaces displayed a "saturated" NO flux which did not change accordingly as more bilayers were further deposited. We postulate that such a saturated NO production is very likely due to the limited permeability of the polyelectrolyte matrix when deposited on metal surfaces. Unfortunately, the relation between the permeability versus the polyelectrolyte species used to fabricate the

multilayer, as well as the coating conditions has not yet been thoroughly studied. This reality makes it less possible to intentionally tailor the coating parameters to promote the diffusion of reactants within the polymer matrix. Nevertheless, it has been reported that the permeability can be enhanced via exposing the LbL to certain organic solvents for an extended period of time.[19] Thus, it might be worthwhile to screen possible solvents for this purpose to "loosen up" the interpenetrated polymer chains without significantly impairing the structural integrity of the final LbL.

4.5. References:

1. Serruys, P. W.; Dejaegere, P.; Kiemeneij, F.; Macaya, C.; Rutsch, W.; Heyndrickx, G.; Emanuelsson, H.; Marco, J.; Legrand, V.; Materne, P.; Belardi, J.; Sigwart, U.; Colombo, A.; Goy, J. J.; Vandenheuvel, P.; Delcan, J.; Morel, M. A. *N. Engl. J. Med.* **1994**, *331*, 489-495.

2. Schoen, F. J.; Edwards, W. D. In *Cardiovascular Phathology*; 3rd ed.; Silver, M. D., Gotlieb, A. I., Schoen, F. J., Eds.; Churchill Livingstone: New York, 2001.

3. Ibanez, L.; Vidal, X.; Vendrell, L.; Moretti, U.; Laporte, J. R. *Aliment. Pharmacol. Ther.* **2006**, *23*, 235-242.

4. Derry, S.; Loke, Y. K. *Br. Med. J.* **2000**, *321*, 1183-1187.

5. Kelm, M.; Yoshida, K. In *Methods in Nitric Oxide Research*; Feelisch, M., Stamler, J., Eds.; John Wiley & Sons Ltd.: Chichester, England, 1996.

6. Stoeckel, D.; Pelton, A.; Duerig, T. *Eur. Radiol.* **2004**, *14*, 292-301.

7. Yang, P.; Huang, N.; Leng, Y. X.; Chen, J. Y.; Sun, H.; Wang, J.; Chen, F.; Chu, P. K. *Surf. Coat. Technol.* **2002**, *156*, 284-288.

8. Huang, N.; Leng, Y. X.; Yang, P.; Chen, J. Y.; Sun, H.; Wang, J.; Wan, G. J.; Zhao, A. S.; Ding, P. D. *Nucl. Instrum. Meth. Phys. Res., B* **2006**, *242*, 18-21.

9. Windecker, S.; Mayer, I.; De Pasquale, G.; Maier, W.; Dirsch, O.; De Groot, P.; Wu, Y. P.; Noll, G.; Leskosek, B.; Meier, B.; Hess, O. M. *Circulation* **2001**, *104*, 928-933.

10. Biehl, V.; Wack, T.; Winter, S.; Seyfert, U. T.; Breme, J. *Biomol. Eng.* **2002**, *19*, 97-101.

11. Yang, J.; Welby, J. L.; Meyerhoff, M. E. *Langmuir* **2008**, *24*, 10265-10272.

12. Vaughn, M. W.; Kuo, L.; Liao, J. C. *Am. J. Physiol. Heart Circ. Physiol.* **1998**, *43*, H2163-H2176.

13. Cai, K. Y.; Rechtenbach, A.; Hao, J. Y.; Bossert, J.; Jandt, K. D. *Biomaterials* **2005**, *26*, 5960-5971.

14. Zhavnerko, G. K.; Yi, S. J.; Kweon, S. M.; Ha, K. S. In *NATO Advanced Research Workshop on Frontiers in Molecular-Scale Sci and Technology of Fullerene, Nanotube, Nanosilicon, Biopolymer (DNA, Protein) Multifunct Nanosystems*; Buzaneva, E. V.,

Scharff, P., Eds. Kiev, Ukraine, 2001, p 79-90.

15. Claesson, P. M.; Blomberg, E.; Froberg, J. C.; Nylander, T.; Arnebrant, T. *Adv. Colloid Interface Sci.* **1995**, *57*, 161-227.

16. Lvov, Y.; Decher, G.; Mohwald, H. *Langmuir* **1993**, *9*, 481-486.

17. Lvov, Y. M.; Decher, G. *Kristallografiya* **1994**, *39*, 696-716.

18. Wong, J. E.; Rehfeldt, F.; Hanni, P.; Tanaka, M.; Klitzing, R. V. *Macromolecules* **2004**, *37*, 7285-7289.

19. Dong, W. F.; Liu, S. Q.; Wan, L.; Mao, G. Z.; Kurth, D. G.; Mohwald, H. *Chem. Mater.* **2005**, *17*, 4992-4999.

CHAPTER 5

LAYER-BY-LAYER ASSEMBLY WITH COMBINED NITRIC OXIDE GENERATION AND SURFACE IMMOBILIZED HEPARIN

5.1. Introduction

Years of study on the molecular basis of thrombotic response have revealed an extraordinarily complicated physiological system is involved, not merely the supersensitive platelets but also a series of coagulation proteins that undergo a self-amplified reaction cascade. Depending on the triggering mechanism (i.e., by tissue factors or surface adsorbed plasma proteins), the clotting cascade propagates along different routes but eventually converges into a common pathway in which prothrombin and factor X are activated into thrombin and factor Xa (FXa), respectively (see Figure 1.2 for details). In the natural hemostasis system, this common pathway is modulated by anti-thrombin III (AT-III), which effectively deactivates thrombin and FXa by co-interacting with heparin. Such awareness leads to the application of heparin as an anti-coagulant to mitigate thrombosis incidence after cardiovascular interventions.

The structure of heparin consists of a disaccharide repeat unit (see Figure 2.2c) composed of a trisulfated induronic acid and a glucosamine. The large number of sulfate and carboxylate groups result in a highly negatively charged polysaccharide

backbone, which is essential to the bioactivity of heparin. Indeed, the anti-coagulant electrostatically interacts with a binding domain enriched with lysine and arginine residues on AT-III to induce an allosteric activation of the enzyme, and subsequently accelerates the inhibition of thrombin and FXa (see Figure 5.1). Despite of the potent anti-coagulation efficacy, unfractionated heparin is marked by its poor bioavailability and adverse immune response, largely due to the non-specific interaction between the highly sulfated polysaccharide chain and the positively charged domains on the plasma proteins.[1] Low molecular weight heparin obtained from controlled depolymerization and/or fraction of the unfractionated heparin has emerged as a clinical substitute to manage thromboembolic disorders due to its improved bioavailability and reduced side effects.[2,3] However, systemic application of either unfractionated or low molecular weight heparin tends to elevate the bleeding complications.[4,5] As a result, surface-immobilized heparin has recently been pursued to create hemocompatible materials via a localized anti-coagulation effect.

The most widely used method to immobilize heparin is via amide bond formation between heparin and an aminated surface. In our group, unfractionated heparin has been attached on aminated PVC and PU, which were further applied as an outer layer of NO release coatings to achieve a dual anti-thrombotic activity.[6,7] Less frequently, the heparin chain is cleaved by nitrous acid at the glucosamine residues to produce an aldehyde end group[8], which can react with surface amines to form a Schiff base. More recently, heparin was electrostatically deposited into a surface thin film using the LbL method with other natural macromolecules such as chitosan,[9,10] hyaluronic acid[11] and albumin.[12] The anti-coagulation potency of surface-bound heparin has been assessed via

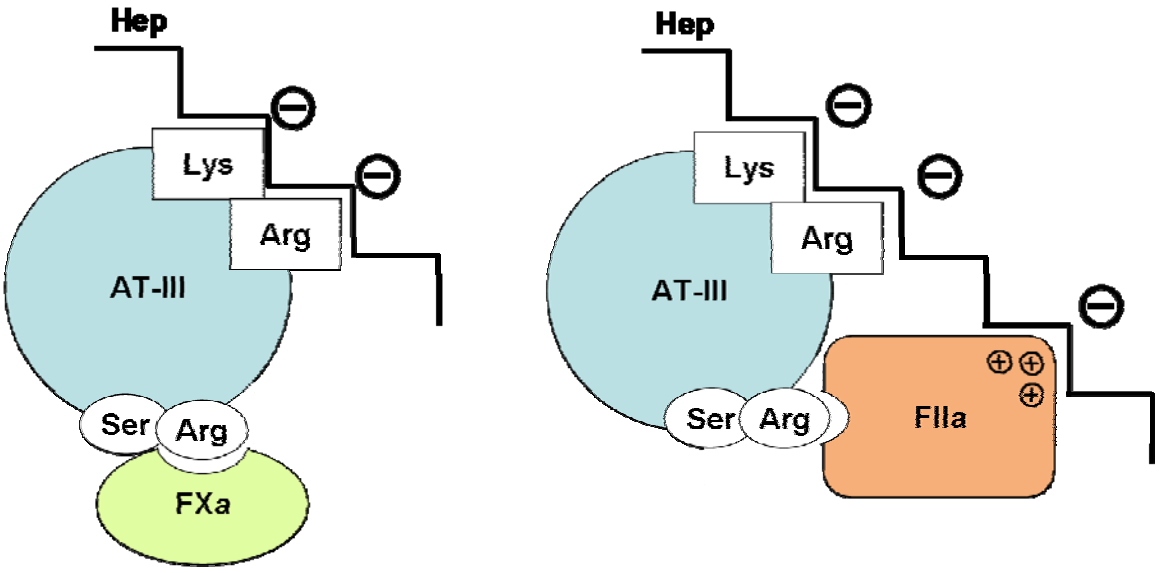

Figure 5.1. Schematic representation of the interactions among heparin, AT-III, FXa and thrombin (denoted as FIIa here). The Lys/Arg designation illustrates the heparin binding site of AT-III. The Ser/Arg residues represent the reactive sites of AT-III to FXa and thrombin. The effect of heparin on the reaction between AT-III and thrombin (right) involves formation of a ternary complex in which heparin interacts with both AT-III and thrombin electrostatically. In contrast, the inhibition of FXa does not require a direction interaction between Hep and FXa (left).[13]

direct methods such as FXa[6,7,14] and FIIa[15] chromogenic assays, or indirect methods such as aTPP,[9] PT[9] or platelet activity tests.[12]

In this chapter, novel LbLs with combined NO generation and surface heparin activity are reported. Previously, a $(SePEI/Alg)_n$ multilayer was prepared using an automatic coating apparatus and the resulting coatings proved capable of generating a physiological level of NO under typical biological conditions. The aforementioned $(SePEI/Alg)_n$ LbL is capped with an Alg outlayer and thus has excess negative charges on its surface. However, the LbL coating sequence can also be terminated after deposition of an ouyer layer of SePEI. In this circumstance, the SePEI outermost layer endows the mutilayer with a vast number of surfaceamine sites suitable to attach other active species. Herein, heparin was immobilized on the aminated LbL through two distinct methods: electrostatic deposition and covalent attachment. The anti-FXa activity of these heparin immobilized surfaces was assessed using a chromogenic assay. Further, it will be demonstrated that these heparinized LbLs are still capable of generating substantial amounts of NO from GSNO and GSH.

5.2. Experimental

5.2.1. Materials

Heparin sodium salt (Hep), sodium alginate (Alg, M_w 12-80 kD), glutathione (GSH), 1-(3-dimethylaminopropyl)-3-ethylcarbodiimide (EDC), 5,5'-dithiol-bis(2-nitrobenzoic acid) (DTNB), fluorescein-5-isothiocyanate (FITC), fluorescein-5-thiosemicarbazide (FTSC) and 2-(*N*-morpholino)ethanesulfonic acid (MES) were obtained from

Sigma-Aldrich (St. Louis, MO) and used as received. Bovine albumin (BSA) fraction V solution was purchased from Invitrogen Corp. (Carlsbad, CA). Human anti-thrombin III (AT-III) and bovine Factor Xa (FXa) were purchased from Haematologic Technologies Inc. (Essex Junction, VT). Chromogenix S-2222 was purchased from DiaPharma Group, Inc. (West Chester, OH). Organoselenium immobilized polyethyleneimine (SePEI), and *S*-nitrosoglutathione (GSNO) were synthesized as described previously.[16] All solutions were prepared with 18 MΩ cm^{-1} deionized distilled water obtained from a Milli-Q system (Millipore Corp., Billerica, MA).

5.2.2. Fabrication of NO generation LbL

The catalytic LbL was fabricated using a StratoSequence 6 (Nanostrata Inc., Tallahassee, FL). The substrates were mounted on the automatic coating apparatus and dipped alternately into SePEI and Alg solutions (1 mg mL^{-1} in PBS) for 10 min. Each deposition step was followed by a sequential washing in three batches of PBS for 1 min each to remove loosely adsorbed polymer and to minimize cross contamination of the coating solutions. The coating cycles were repeated until the desired number of bilayers was achieved.

5.2.3. Heparin immobilization

Heparin was immobilized on the LbL surface through two distinct mechanisms: 1) electrostatically interacting with positively charged SePEI; and 2) covalently bonding to the amine sites via amide formation. The physical adsorption of heparin was achieved by conducting a similar LbL procedure whereby the LbL was immersed in 1 mg mL^{-1} SePEI and heparin PBS solutions, repeatedly. Alternatively, heparin was covalently

attached to the LbL surface through reacting the carboxylate functional groups on the polysaccharide with the amine sites on SePEI. To do so, the automatic LbL deposition was stopped after deposition of an outmost layer of SePEI so that an amine-rich surface resulted (denoted as LbL-NH_2); otherwise, the multilayer was defaulted to have an Alg top layer. To facilitate the coupling reaction, 20 mg heparin was pre-activated with 8 mg EDC in 4 mL MES buffer (pH = 6) for 1 h. The Hep-EDC adducts were separated from the reaction by centrifuging the mixture through a membrane with a MWCO of 3K for 15 min. Then, the concentrate was redissolved into 1 mg mL^{-1} PBS solution in which the LbL-NH_2 substrate was subsequently immersed for a given amount of time.

5.2.4. UV-Vis detection

The immobilization of heparin on the LbL surface, as well as the stability of the resulting structure, was monitored using a UV-Vis spectrophotometer (Lambda 35, Perkin Elmer, MA). The FITC labeled SePEI and heparin species, denoted as SePEI-F and Hep-F, were employed exclusively in this study. SePEI was modified as previously described in Section 2.2.3., while heparin was labeled using an amine-derivatized fluorescein species, fluorescein-5-thiosemicarbazide (FTSC, ε=78,000 $M^{-1}cm^{-1}$). Specifically, 40 mg heparin and 3 mg EDC were dissolved in 4 mL PBS, in which 0.4 mL DMF containing 5 mg mL^{-1} FTSC was added. The mixture was allowed to react for 1 h and then washed with PBS using a centrifugal unit with MWCO of 3K. The labeled heparin shows a λ_{max} at 504 nm.

5.2.5. NO detection

Nitric oxide generation by the catalytic LbLs from GSNO in presence of GSH was

quantitated as described in Chapter 2.

5.2.6. Anti-FXa activity of immobilized heparin

The surface bioactivity of the heparinized LbL was determined using a chromogenic anti-FXa assay. A PU catheter segment coated with the heparinzed LbL was immersed in a microcentrifuge tube containing a solution composed of 224 μL PBS, 80 μL AT-III (103 μg mL^{-1}) and 80 μL BSA. After incubation at 37 ˚C for 2 min, 16 μL FXa (1 μg mL^{-1}) was added and the mixture was incubated for 1 min. Then, 40 μL S-2222 (2.5 mg mL^{-1}) was added into the reaction followed by incubation for another 10 min. The reaction was terminated by acidifying the solution with 160 μL acetic acid. Three aliquots of 100 μL reaction mixture were then transferred into a 96-well microtiter plate and the absorbance at 405 nm was measured by the microplate reader.

5.2.7. Diffusion of GSH through the NO generation LbL

The typical experimental set-up for monitoring the diffusion of GSH through the LbL is illustrated in Figure 5.2. A piece of dialysis membrane (MWCO 12 ~ 14 kD) coated with LbL on both sides was mounted between two diffusion cells: one was charged with 0.5 mM GSH/PBS solution (G cell) and the other was filled with fresh PBS buffer (P cell). Such a high concentration of GSH was used in order to accelerate the diffusion. Before the test, the $(SePEI/Alg)_n$ LbL was proved stable at this GSH concentration even after 12 h immersion (data not shown). Since GSH is prone to oxidize into the corresponding disulfide, the PBS buffer used in this study was pre-deoxygenated with house N_2 for 1 h. The set-up was then seated at room temperature with vigorous stirring

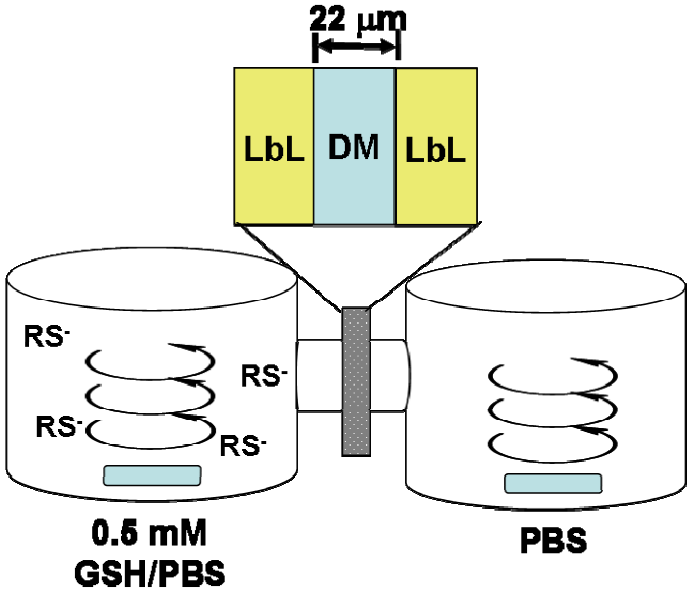

Figure 5.2. Diffusion experiment set-up. Film mounted between the two diffusion chambers was a piece of dialysis membrane (DM) coated with the NO generation LbL on both sides.

in both chambers for 12 h. The solution in the P cell was sampled in the beginning and at the end of the diffusion period to determine the amounts of GSH that diffused through the membrane. Three tests were performed in a row and the concentrations of GSH acquired were averaged. After each test, the cells were filled with fresh PBS and seated for 12 h to thoroughly extract any residual GSH trapped in the membrane and the LbL structure as well. The same piece of membrane was allowed to adsorb another layer of SePEI and then reacted with EDC activated heparin for 12 h. After the heparin immobilization, the membrane was soaked in PBS overnight to remove any unreacted and loosely bounded species. Subsequently, another three diffusion tests were performed on this heparin modified membrane using the same experiment set-up.

The thiol concentration in the P cell solution was quantitated using Ellman's reaction. Specifically, 100 μL sample solution or calibration standard was injected into a microtiter plate well followed by addition of 100 μL 5 mM DTNB in 100 mM phosphate buffer (pH = 8.0). The reaction was incubated at room temperature for 10 min and the UV-Vis absorbance at 414 nm was then measured using a microplate reader.

5.3. Results and Discussion

5.3.1. Deposition of $(SePEI/Hep)_m$ on the surface of $(SePEI/Alg)_n$ NO generation LbL

The structure of heparin is characterized by the large number of negative charges distributed along the polysaccharide backbone. This polyanionic structure, combined with the potent anticoagulant activity, makes heparin a frequent constituent in

hemocompatible LbL assemblies.[11-14] However, our attempts to fabricate a multilayer using heparin and SePEI directly on quartz surface did not succeed (see Section 2.3.2). Interestingly, however, a stepwise growth of $(SePEI\text{-}F/Hep)_m$ was observed on a quartz surface pre-coated with a $(SePEI/Alg)_{10}$ (see Figure 5.3a). The absorbance at 510 nm was extracted from the spectra and plotted against the number of dipping cycles, which reveals a linear correlation (see Figure 5.3b). In another experiment, the $(SePEI/Hep)_m$ LbL was also found to form on a surface pre-coated with $(PDDA/Alg)_2$ (data not shown). These results imply that heparin is more likely to form stable LbL with SePEI on the surfaces where a substantial amount of polyelectrolytes are already adsorbed. We speculate that this might be due to the relatively small molecular weight of heparin, as well as the slow early-stage growth of LbLs. Indeed, as previously discussed in Section 2.3.3, the LbL structure grows very slowly in the first couple of bilayers. It was then discovered by SEM that the quartz substrate was not fully covered by the LbL, presumably due to the low surface charge density. Rather, the polyelectrolytes first formed scattered particles which gradually merged into a continuous layer as the coating procedure continued, associated with amplification of the surface charge. Intuitively, it is relatively difficult for polyions with shorter chains (e.g., heparin) to undergo such a merging process due to their less outspreading structure.

The successful immobilization of heparin was confirmed by constructing the LbL using fluorescein labeled heparin and subsequently detecting the heparin content in the multilayer with a UV-Vis spectrometer (see Figure 5.4). The UV-Vis result shows a continuous increase at 510 nm as more coating cycles were performed. This observation provides a direct evidence for the presence of heparin in the multilayer. The

(a)

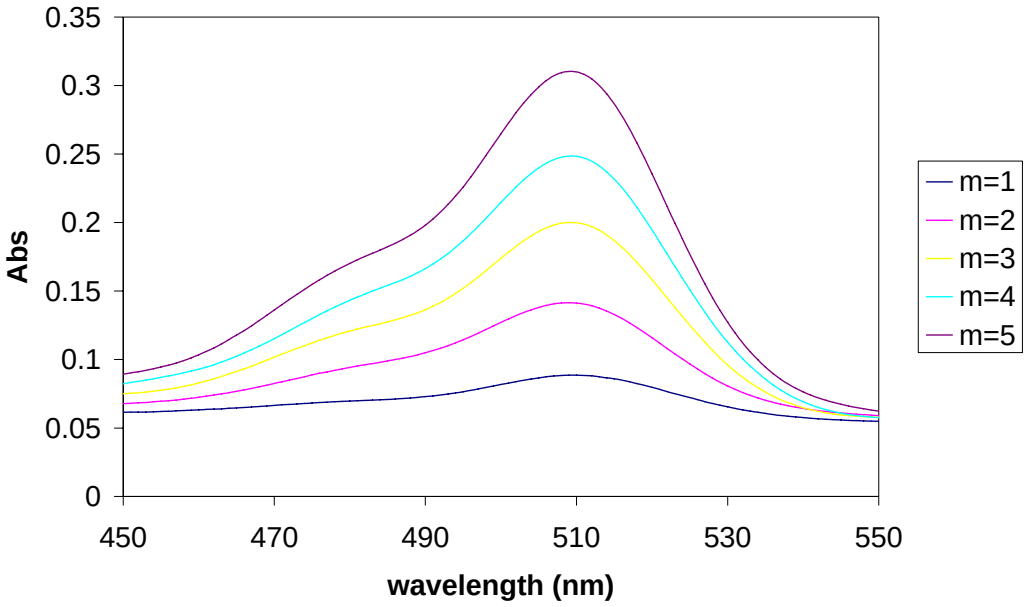

(b)

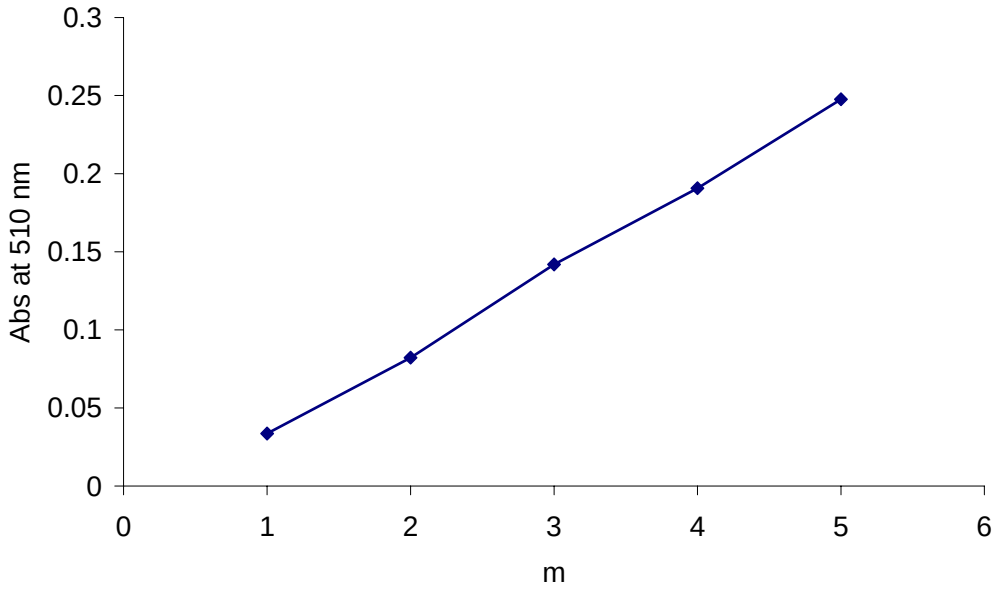

Figure 5.3. (a) UV-Vis absorbance of $(SePEI\text{-}F/Hep)_m$ deposited on a quartz cuvette pre-coated with $(SePEI/Alg)_{10}$; (b) correlation of the absorbance at 510 nm with the number of (SePEI-F/Hep) bilayers (n). Please note that the SePEI used in the $(SePEI/Alg)_{10}$ sublayer is not labeled with FTIC probe.

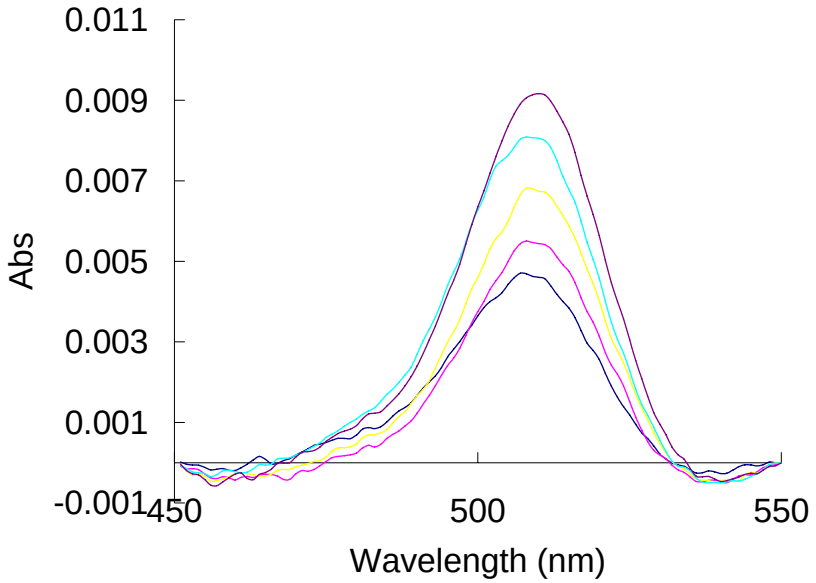

Figure 5.4. UV-Vis absorbance of $(SePEI/Hep\text{-}F)_m$ deposited on a quartz cuvette pre-coated with a $(SePEI/Alg)_{10}$.

stability of $(SePEI/Hep)_m$ was assessed under exaggerated reaction conditions by monitoring the decay of UV-Vis absorption (see Figure 5.5). After 48 h, the $(SePEI/Hep)_m$ multilayer proved to preserve 96.3% SePEI and 93.7% heparin in its structure. Notably, the stability of the $(SePEI/Hep)_m$ is very similar to the results previously obtained on $(SePEI/Alg)_{n,}$ which retained 96.7% SePEI after exposure to the same conditions for 2 d. This observation further indicates that the failure to build a $(SePEI/Hep)_m$ directly on the quartz surface is somehow related to the initiation of the LbL growth in the early stage of assembly.

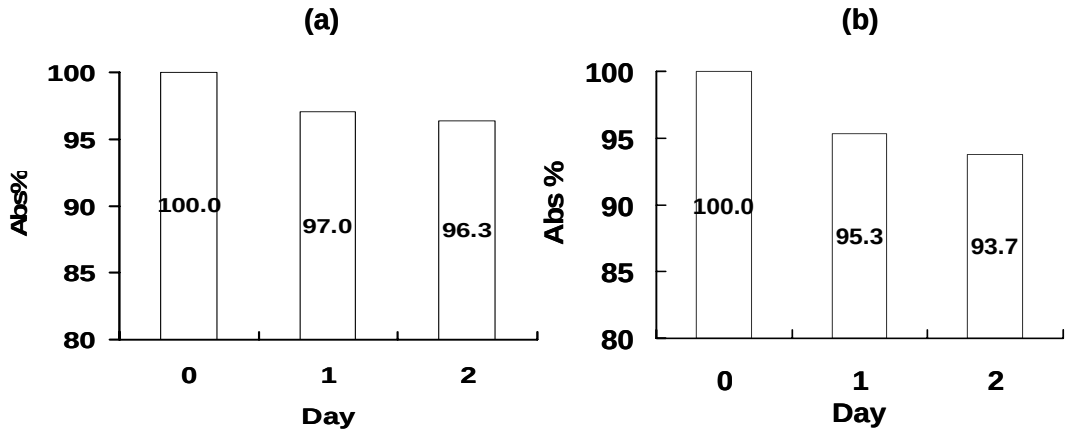

Figure 5.5. Stability studies of (a) $(SePEI\text{-}F/Hep)_5$ and (b) $(SePEI/Hep\text{-}F)_5$ coated on a $(SePEI/Alg)_{10}$. The cuvette was filled with PBS containing 50 μM GSNO and 50 μM GSH. After every 24 h, old soaking solution was decanted and the cuvette was refilled with fresh PBS containing same given concentrations of GSNO and GSH. The absorbance at (a) 500 nm and (b) 510 nm was monitored after every refill.

The surface heparin activity of these $(SePEI/Hep)_m$ LbL was assessed using an anti-FXa assay. The key reagent in the assay is a chromogenic substrate composed of a peptide sequence coupled with a chromophore, which gives a dramatic absorbance change when cleaved from the peptide by FXa. This chromogenic reaction can be effectively suppressed by heparin which can potentiate the deactivation of FXa by AT-III. Therefore, the UV-Vis absorption of the assay is inversely correlated to the heparin activity in the sample. Indeed, the calibration curve clearly demonstrates an inverse linear relationship between the heparin activity in standards and the absorbance at 405 nm (see Figure 5.6). In Figure 5.7, the anti-FXa activity of the $(SePEI/Hep)_2$ and $(SePEI/Hep)_4$ was determined to be 1.6 ± 0.4 mU cm^{-2} and 1.1 ± 0.1 mU cm^{-2} based on the calibration curve, respectively (see Figure 5.7). Not surprisingly, $(SePEI/Hep)_4$ showed a similar surface activity compared with $(SePEI/Hep)_2$, provided that only the heparin species in the top layer are able to interact with FXa and AT-III. This heparin activity is relatively low compared to results reported elsewhere,[6,7] which is very likely due to the consumption of the negative charges on the heparin chain by PEI in the LbL, which is critical for the binding between the polysaccharide and AT-III.

The catalytic activity of a $(SePEI/Alg)_{100}(SePEI/Hep)_4$ was evaluated and compared with a $(SePEI/Alg)_{100}$ control which does not top-coated with $(SePEI/Hep)_4$ (see Figure 5.8). Although the $(SePEI/Alg)_{100}(SePEI/Hep)_4$ has 4 more layers of SePEI, the catalytic LbL shows a NO generation similar to the control. This is probably because the catalytic activity is predominantly contributed by the underlying $(SePEI/Alg)_{100}$. Also, no significant baseline increase was observed upon removal of the sample from the testing solution, indicating an absence of serious RSe leaching.

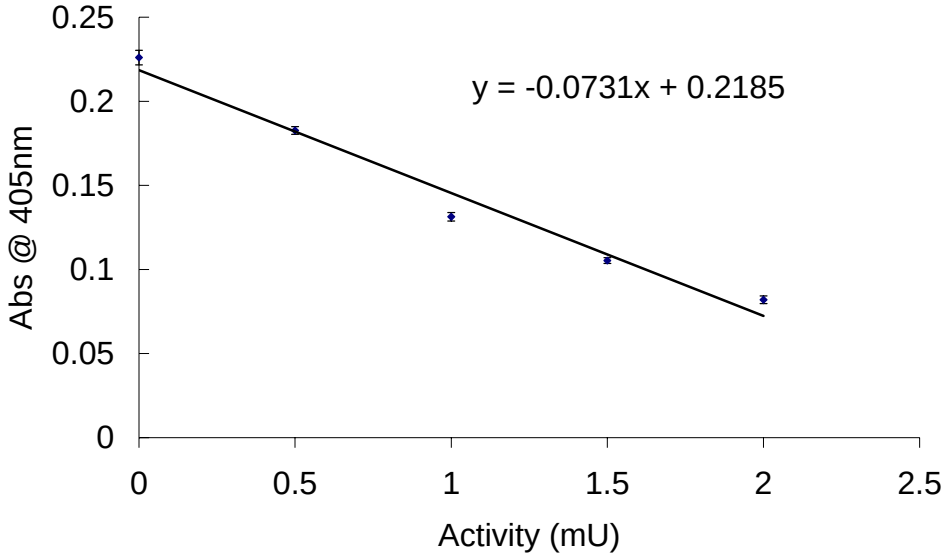

Figure 5.6. Calibration curve showing the relationship between heparin activity and the UV absorbance measured at 405 nm.

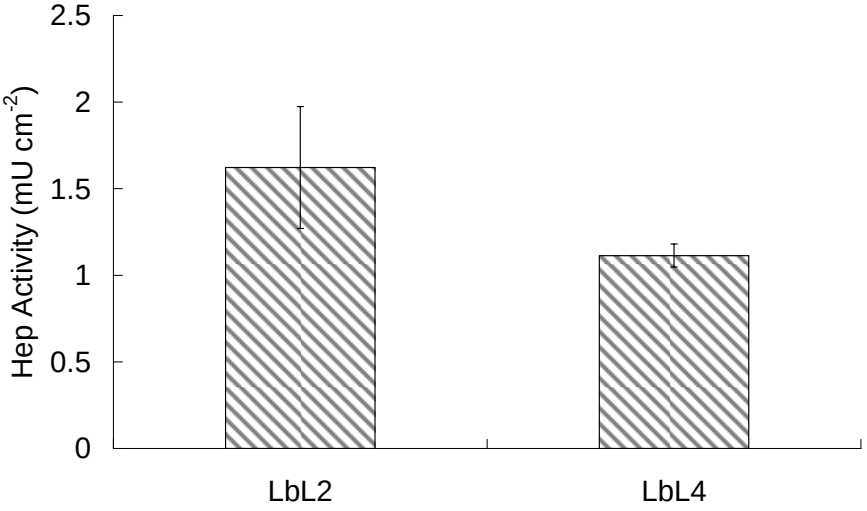

Figure 5.7. Surface anti-FXa activity of $(SePEI/Hep)_2$ (LbL2) and $(SePEI/Hep)_4$ (LbL4) fabricated on a $(SePEI/Alg)_{100}$.

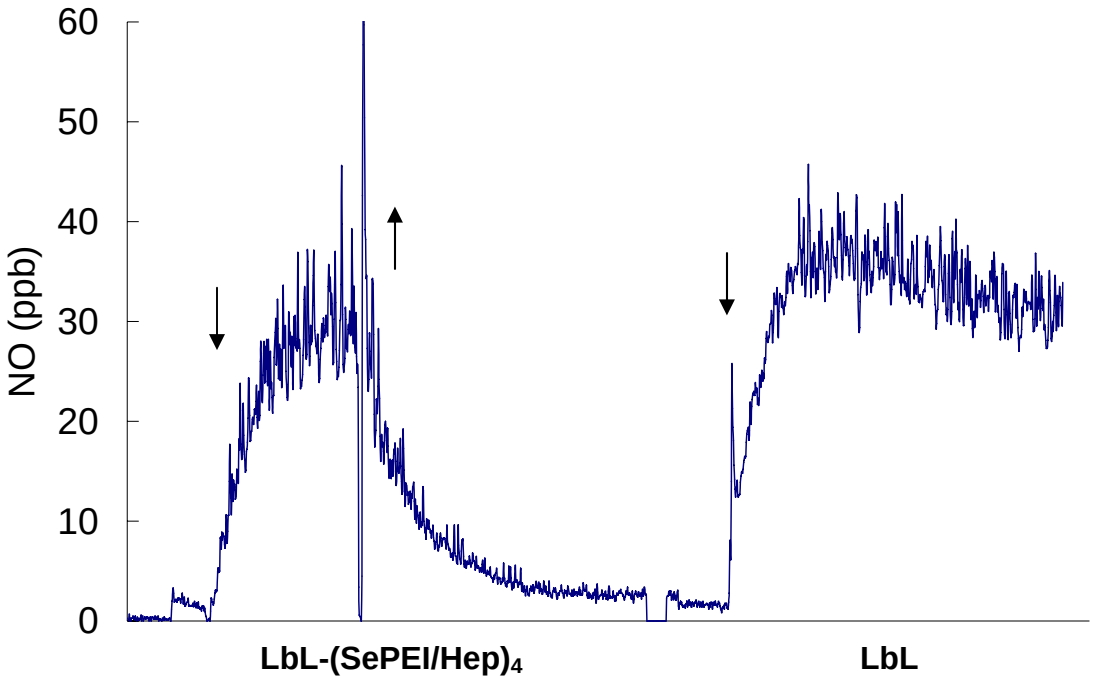

Figure 5.8. Nitric oxide generation by $(SePEI/Alg)_{100}(SePEI/Hep)_4$ from 50 μM GSNO and 50 μM GSH, compared with that of $(SePEI/Alg)_{100}$. Both coatings were fabricated on PU catheters (0.2 cm OD, 0.5 cm). The coating was immersed/removed as indicated by (↓) and (↑) arrows.

5.3.2. Covalent attachment of heparin on $(SePEI/Alg)_n$ LbL

Heparin can also be covalently attached to an aminated surface, i.e., a NO generation LbL with SePEI in the outermost layer (LbL-NH_2), via amide bonds. A $(SePEI/Alg)_{100}SePEI$ was thus allowed to react with a PBS solution containing 1 mg mL^{-1} EDC activated heparin, which was also labeled with a fluorescein probe. After 12 h, the coating was thoroughly washed and characterized using UV-Vis, which revealed a significant absorbance at 504 nm (see Figure 5.9). Compared with the electrostatic adsorption method (Figure 5.4), this absorbance increase is much higher, indicating that the heparin immobilization might not be limited to the surface. This can be due to the diffusion of some low molecular weight heparin fragments into the LbL structure. Such diffusion was later proved to be not fully reversible by immersing the heparinized LbL in

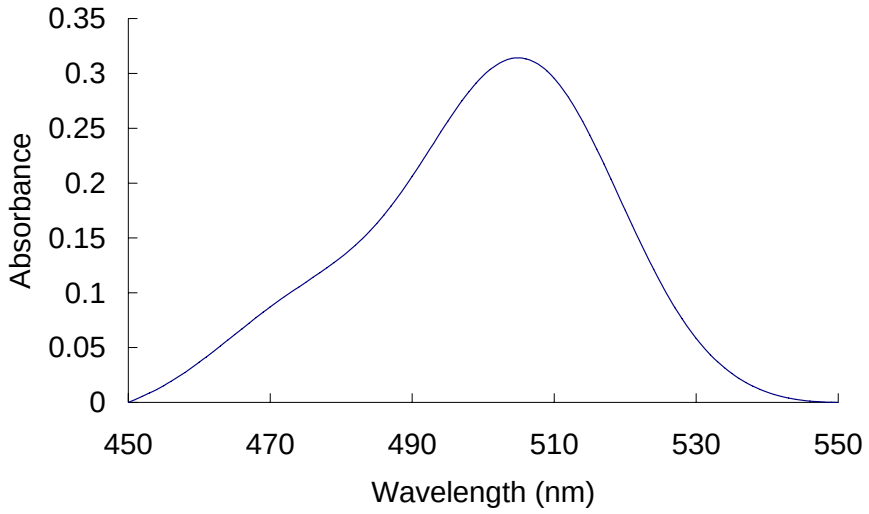

Figure 5.9. UV-Vis measurement of $(SePEI/Alg)_{100}SePEI$ after 12 h coupling with fluorescein labeled heparin.

PBS buffer and monitoring the absorbance change over time. As shown in Figure 5.10, the LbL lost only 44.2 % of the total heparin content after 10 d soaking in PBS. Nevertheless, this observation suggests that the heparin within the LbL is not covalently bonded.

The structural stability of $(SePEI/Alg)_n$ LbL during the heparin immobilization was also investigated by measuring the UV-Vis absorbance of a $(SePEI\text{-}F/Alg)_{100}SePEI$ before and after coupling with heparin. As shown in Figure 5.11, a slight absorbance decrease of ca. 12% was observed, indicating some of the FITC labeled SePEI was dissociated from the LbL. This is probably caused by the reorganization/dissolution of the polyelectrolytes within the LbL. Although the alternating deposition of polyanion and polycation is usually expected to be an irreversible process, partial dissolution of the LbL structure has been reported upon change in pH[17] or ionic strength.[18] Therefore, the heparin segments diffused into the multilayer, which are also charged species, may have an impact on the interaction between SePEI and Alg.

Figure 5.12 shows the anti-FXa activity of these covalently bound heparinized LbLs. Notably, the control sample, which is a $(SePEI/Alg)_{100}$ immersed in 1 mg mL^{-1} heparin solution for 12 h, proved active in FXa inhibition, which is probably because of the slow release of the heparin trapped in the multilayer film. As previously discussed, the heparin impregnated in the $(SePEI/Alg)_n$ LbL is slowly released upon prolonged exposure to PBS. Although the release has been demonstrated to be a very slow process (i.e., only several percent per day), it may still result in a surface anti-FXa activity due to the highly efficient enzymatic reaction involved in the assay. The $(SePEI\text{-}F/Alg)_{100}$(SePEI-Hep) surfaces demonstrate even higher anti-FXa activities which

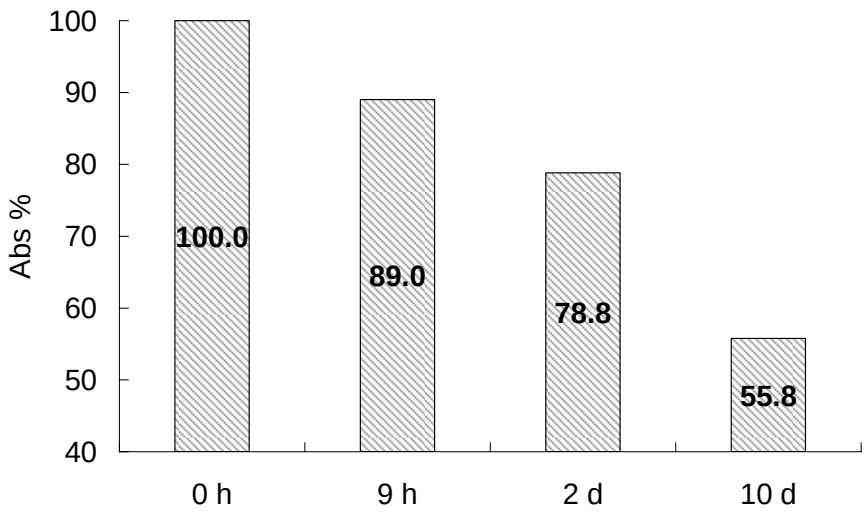

Figure 5.10. UV-Vis absorbance of $(SePEI/Alg)_{100}(SePEI\text{-}Hep\text{-}F)$ after immersing in PBS buffer for given amounts of time.

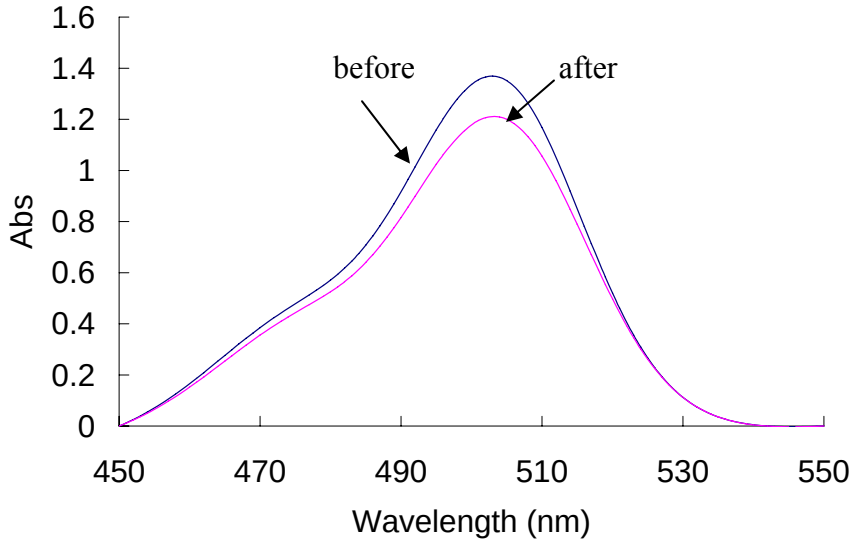

Figure 5.11. UV-Vis absorbance of $(SePEI\text{-}F/Alg)_{100}SePEI$ before and after coupling with heparin. Please note that the outmost SePEI layer does not carry fluorescein labels.

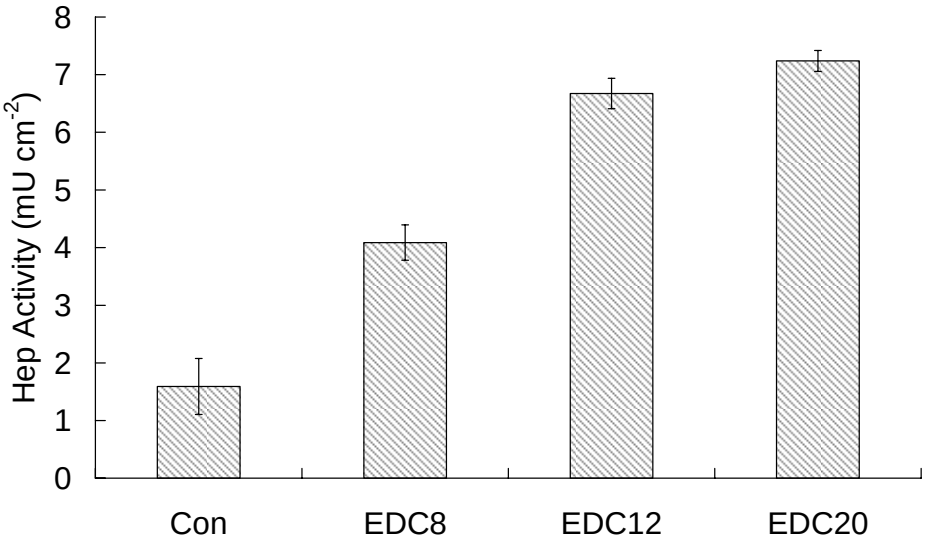

Figure 5.12. Anti-FXa activities of the covalently heparinized LbLs. "EDC8", "EDC12" and "EDC20" are used to denote the LbL that has been reacted with EDC activated heparin for 8, 12 and 20 hours, respectively. A $(SePEI/Alg)_{100}$ solely immersed in a heparin solution without any coupling reagent for 12 h was used as the control (Con).

scale according to the length of the coupling reaction time between the LbL-NH_2 and the EDC activated heparin. When the reaction time is extended from 8 h to 12 h and then 20 h, the resulting surface activity is increased from 4.1±0.3 mU cm^{-2} to 6.7 ±0.3 mU cm^{-2} and then to 7.2±0.2 mU cm^{-2}, respectively. In comparison with the control sample, this effectiveness in FXa inhibition indicates that the observed anti-FXa activity is at least partially due to by the surface immobilized heparin. It should be noted that the LbL-NH_2 surface adsorbs heparin through electrostatic interactions as well. Therefore, the surface activity should be contributed by not only the covalently attached but also the electrostatically adsorbed heparin molecules. In a long term activity study, surfaces with covalently immobilized heparin demonstrated significant anti-FXa activities even after 6 d immersion in PBS (see Figure 5.13).

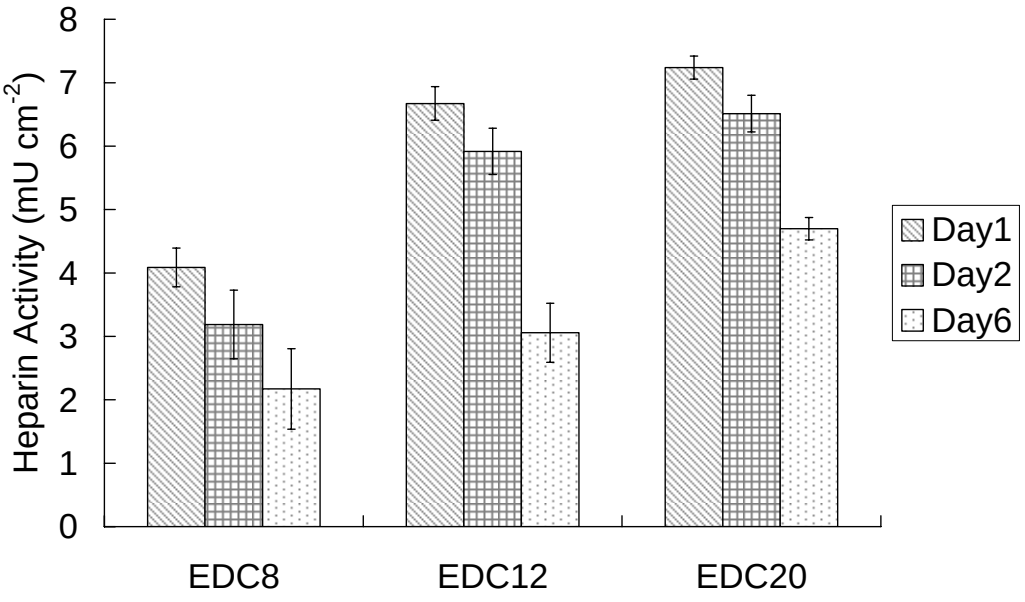

Figure 5.13. Long term surface anti-FXa activity of NO generation LbL with covalently attached heparin. EDC8, EDC12 and EDC 20 denote LbLs covalently reacting with EDC activated heparin for 8, 12, and 20 h.

In NO generation studies, a remarkable activity decrease was observed with the LbL which had been covalently coupled with heparin (see Figure 5.14). This activity reduction (ca. 50%) is much greater than the amount of SePEI previously discovered to dissociate from the LbL, implying that the NO generation efficiency was impeded by mechanisms other than the loss of catalytic sites in the multilayer. Nevertheless, LbL-Hep was still able to produce a NO flux of 1.1×10^{-10} mol cm^{-2} min^{-1} under typical physiological conditions (see Figure 5.15).

As mentioned in previous chapters, the catalytic NO generation occurs not only on the LbL surface but also in the polyelectrolyte matrix, which requires the GSNO and GSH reactants to diffuse into the multilayer. If the permeability of the LbL is altered during the heparin immobilization, the efficiency of NO production can be impaired. Therefore, a diffusion experiment was performed in which GSH was allowed to diffuse from a chamber containing 0.5 mM GSH (denoted as G cell) into another chamber containing fresh PBS buffer (denoted as P cell), through a dialysis membrane with $(SePEI/Alg)_{100}$ coated on both sides. As shown in Figure 5.16, the concentration of free thiols in the P cell increased by 12.8 ± 0.8 μM after 12 h diffusion, which confirms that the GSH reducing agent does penetrate the dialysis membrane, as well as the two $(SePEI/Alg)_{100}$ LbLs. However, the concentration increase of GSH in the P cell was increased by only 7.4 ± 0.9 μM after immobilization of heparin. This result clearly suggests a hindered diffusion of GSH through the heparin immobilized multilayer. Such reduced diffusion can be caused by the possible EDC mediated coupling between SePEI and Alg during the heparin immobilization, which forms amide crosslinks that lead to a denser film structure. However, a $(SePEI/Alg)_{100}$ tested after 12 h immersion in PBS

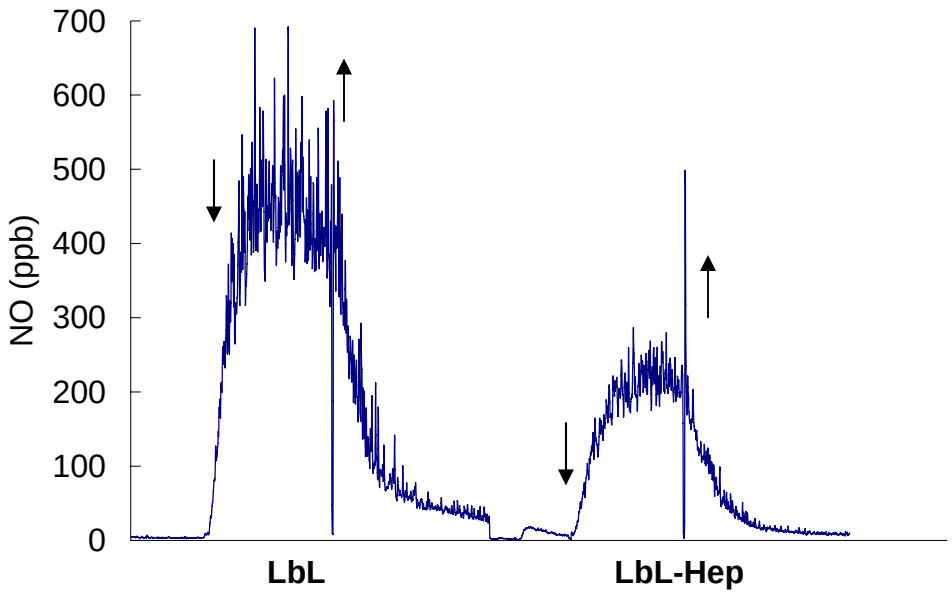

Figure 5.14. Nitric oxide generation from 50 μM GSNO and 50 μM GSH by $(SePEI/Alg)_{100}$ (LbL), and $(SePEI/Alg)_{100}$(SePEI-Hep) (LbL-Hep) which has been reacted with heparin for 12 h. Both coatings are coated on quartz slides with a surface area of 3.3 cm^2. The slide was immersed/removed as indicated by (↓) and (↑) arrows.

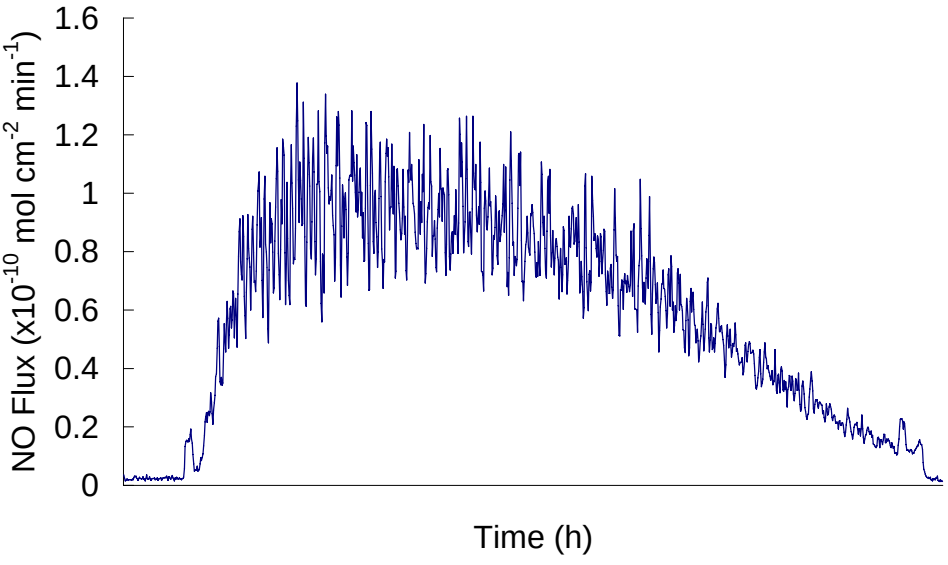

Figure 5.15. Nitric oxide generation from 2.5 μM GSNO and 20 μM GSH at 37°C by an $(SePEI/Alg)_{100}$(SePEI-Hep) coated on quartz slide.

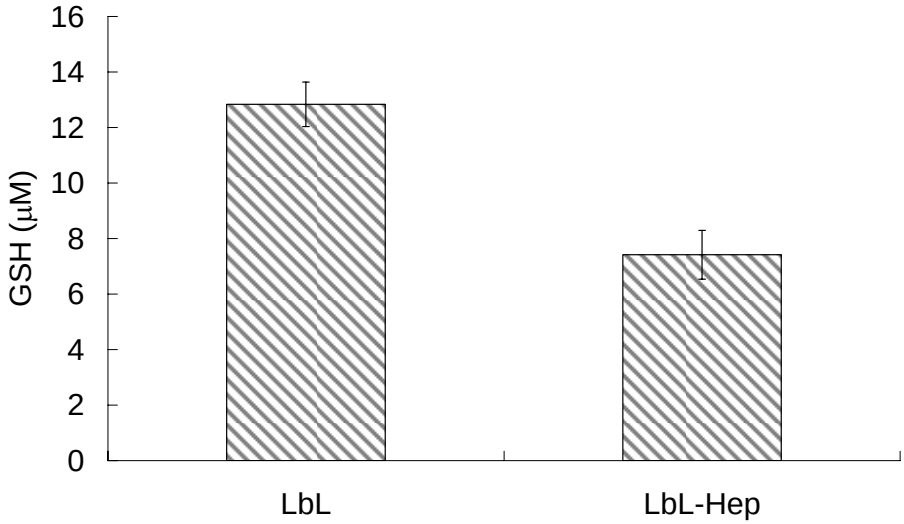

Figure 5.16. Diffusion of GSH reducing agent through $(SePEI/Alg)_{100}$ (LbL) and $(SePEI/Alg)_{100}$(SePEI-Hep) (LbL-Hep). The concentration of free thiol was sampled after 12 h diffusion.

containing 1 mg mL^{-1} EDC did not exhibit any decrease in NO generation activity (see Figure 17), which rules out the crosslinked structure as a possible cause for the slow diffusion. Instead, we speculate that the decreased NO generation is due to the heparin species trapped within the multilayer which occupy the pores and hamper the permeability of the polyelectrolyte matrix. Differing from the electrostatically adsorbed heparin molecules, which usually lay on the surface in a flat conformation, the covalently attached heparin may have loops or tails sticking out from the surface. These free-flowing segments may also act as a negatively charged "fence" to block the GSH from diffusing into the LbL.

5.4. Conclusion

In this chapter, two distinct strategies to immobilize heparin on NO generation

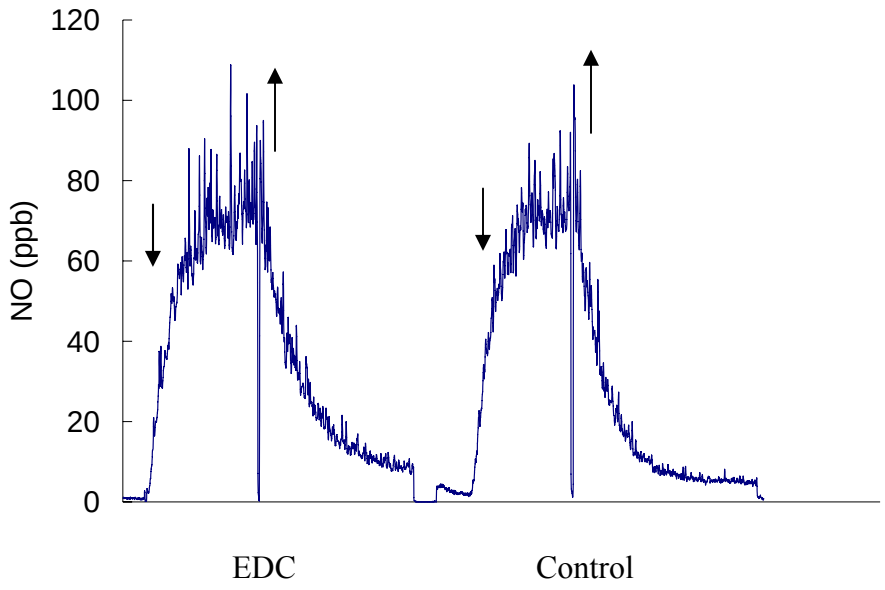

Figure 5.17. Nitric oxide generation from 50 μM GSNO and 50 μM GSH by $(SePEI/Alg)_{100}$ after 12 h immersion in 1 mg mL^{-1} EDC solution, in comparison with the control LbL which was immersed in sole PBS. The slide was immersed/removed as indicated by (↓) and (↑) arrows.

$(SePEI/Alg)_n$ LbL were investigated. First, heparin was electrostatically deposited on the LbL by interacting with SePEI to form a $(SePEI/Hep)_m$ top-layer, which was shown to be stable under typical NO generation conditions, as well as in buffer for extended period of time. Compared with its counterpart without heparin immobilized top-layer, the LbL with $(SePEI/Hep)_m$ did not show a significant difference in overall NO generation activity. However, such a surface with electrostatically adsorbed heparin displays a very limited anti-FXa activity, probably due to the consumption of heparin AT-III binding sites. Alternatively, heparin was also covalently attached to the amine sites on the LbLs with SePEI in the outermost layer. In this case, a higher surface heparin activity was achieved. In the meantime, such LbL-Hep structures show a reduced NO generation activity and impede GSH diffusion through the multilayer, as demonstrated via diffusion tests. These results invoke a very interesting question: which immobilization method

leads to a better anti-thrombotic effect? The thromboresistency of EC layer lining the human vasculature is an overall effect of several anti-coagulant and anti-platelet species, with the contribution from each species poorly understood. Even for surfaces that possess a single anti-thrombotic feature, the threshold dose to achieve the satisfactory prevention of thrombosis has been rarely reported.[19] Furthermore, the performance of an anti-thrombotic coating is also related to the type of device, which makes the question more complicated. The best solution hitherto to this dilemma lies in actually evaluating these two coatings *in vivo*, which is one direction to pursue in the future.

5.5. References

1. Hirsh, J.; Warkentin, T. E.; Raschke, R.; Granger, C.; Ohman, E. M.; Dalen, J. E. *Chest* **1998**, *114*, 489S-510S.

2. Cosmi, B.; Fredenburgh, J. C.; Rischke, J.; Hirsh, J.; Young, E.; Weitz, J. I. *Circulation* **1997**, *95*, 118-124.

3. Young, E.; Prins, M.; Levine, M. N.; Hirsh, J. *Thromb. Haemostasis* **1992**, *67*, 639-643.

4. Petersen, J. L.; Mahaffey, K. W.; Hasselblad, V.; Antman, E. M.; Cohen, M.; Goodman, S. G.; Langer, A.; Blazing, M. A.; Le-Moigne-Amrani, A.; de Lemos, J. A.; Nessel, C. C.; Harrington, R. A.; Ferguson, J. J.; Braunwald, E.; Califf, R. M. *J. Am. Med. Assoc.* **2004**, *292*, 89-96.

5. Lindqvist, P. G.; Dahlback, B. *Thromb. Haemostasis* **2000**, *84*, 140-141.

6. Wu, B.; Gerlitz, B.; Grinnell, B. W.; Meyerhoff, M. E. *Biomaterials* **2007**, *28*, 4047-4055.

7. Zhou, Z. R.; Meyerhoff, M. E. *Biomaterials* **2005**, *26*, 6506-6517.

8. Shively, J. E.; Conrad, H. E. *Biochemistry* **1976**, *15*, 3932-3942.

9. Meng, S.; Liu, Z. J.; Shen, L.; Guo, Z.; Chou, L. S. L.; Zhong, W.; Du, Q. G.; Ge, J. *Biomaterials* **2009**, *30*, 2276-2283.

10. Ruan, Q. C.; Zhu, Y. C.; Li, F.; Xiao, J. W.; Zeng, Y.; Xu, F. F. *J. Colloid Interface Sci.* **2009**, *333*, 725-733.

11. Huang, L. Y.; Yang, M. C. In *International Conference on Nanotechnology in Advanced Drug Delivery* Nagar, INDIA, 2006, p 3163-3170.

12. Sperling, C.; Houska, M.; Brynda, E.; Streller, U.; Werner, C. *J. Biomed. Mater. Res.* **2006**, *76A*, 681-689.

13. Bourin, M. C.; Lindahl, U. *Biochem. J.* **1993**, *289*, 313-330.

14. Zhou, Z. R.; Wu, B. Y.; Meyerhoff, M. E. In *230th National Meeting of the American-Chemical-Society* Washington, DC, 2005, p 166-PMSE.

15. Houska, M.; Brynda, E.; Solovyev, A.; Brouckova, A.; Krizova, P.; Vanickova, M.; Dyr, J. E. *J. Biomed. Mater. Res.* **2008**, *86A*, 769-778.

16. Yang, J.; Welby, J. L.; Meyerhoff, M. E. *Langmuir* **2008**, *24*, 10265-10272.

17. Li, B. Y.; Rozas, J.; Haynie, D. T. In *10th Annual Conference of the*

Institute-of-Biological-Engineering Athens, GA, 2005, p 111-117.

18. Ren, K. F.; Wang, Y. X.; Ji, J.; Lin, Q. K.; Shen, J. C. *Colloid Surf. B.* **2005**, *46*, 63-69.

19. Skrzypchak, A. M.; Lafayette, N. G.; Bartlett, R. H.; Zhou, Z. R.; Frost, M. C.; Meyerhoff, M. E.; Reynolds, M. M.; Annich, G. M. In *Hammersmith Perfusion Workshop* Hammersmith, ENGLAND, 2006, p 193-200.

CHAPTER 6

CONCLUSIONS AND FUTURE DIRECTIONS

6.1. Conclusions

The research in this dissertation has introduced a novel strategy to immobilize organoselenium (RSe) catalysts on diverse biomedical relevant substrates in order to achieve surface nitric oxide (NO) generation from endogenous *S*-nitrosothiols (RSNO). The RSe catalyst was first attached to a cationic polymer, polyethyleneimine (PEI), which was then fabricated into a stable structure via electrostatic interactions with a polyanion, sodium alginate (Alg), using a so-called Layer-by-Layer (LbL) technique. The pure physical driving force of the method is believed to be "universal" across diverse biomedical materials, regardless of their surface functionality and morphology. Provided that the promising *in vivo* anti-thrombotic potency have been observed with the NO release[1-3] and Cu-based NO generation materials,[4,5] such RSe immobilized LbLs have a potential application on various blood-contact biomedical devices to improve their hemocompatibility and reduce incidence of thrombosis.

The concept of such a NO generation LbL was first realized on a quartz surface for characterization convenience (see Chapter 2). Upon manually immersing the substrate into solutions containing organoselenium immobilized PEI (SePEI) and Alg, a successive

deposition of the polyionic species was observed via UV-Vis, contact angles and SEM. The Se content within the polyelectrolyte deposit was confirmed by XPS. A very slow leaching of the RSe species (ca. 3% within 3 d) was discovered by extracting the LbL under exaggerated reaction conditions and determining the Se concentration in the extract with ICP-MS. Nevertheless, the extracts were tested for possible systemic toxicity and irritation response. No obvious symptoms were observed, indicating that such an RSe immobilized LbL is suitable for potential biomedical applications. The NO generation capability of the $(SePEI/Alg)_n$ LbL was thoroughly investigated via chemiluminescence, revealing an enduring catalytic activity and a well-defined correlation between the activity and the number of bilayers deposited in the LbL. Then, the NO generation LbL was successfully translated to biomedical relevant surfaces such as polyurethane and silicone rubber to prove its anticipated "universal" applicability. All the aforementioned experiments strongly suggest that the LbL deposition is an effective approach to immobilize the RSe species to achieve a confined surface NO generation.

The focus was then shifted to whether these RSe immobilized LbLs contain enough bilayers to generate NO at a rate comparable to that of human endothelium, particularly under typical biological conditions in which only low micromolar RSNOs are present (see Chapter 3). For this purpose, one hundred bilayers were deposited on quartz substrates using an automatic coating apparatus. The automatically prepared LbL proved capable of generating a NO flux of 1.5×10^{-10} mol cm^{-2} min^{-1} from typical concentrations of GSNO and GSH. This NO flux is of the same order of magnitude with the natural NO flux from the endothelium monolayer ($0.5 - 4 \times 10^{-10}$ mol cm^{-2} min^{-1}).[6] For the first time, the coating was applied on a polyurethane catheter and

implanted in rabbits. No significant activity loss was detected after 4 h of implantation. This observation, in combination with the biologically relevant amount of NO generated by this RSe immobilized LbL, suggests that this endothelium-mimicking coating may be useful for cardiovascular devices.

Encouraged by the results in Chapters 2 and 3, the LbL was applied on metal substrates which constitute an important class of materials in cardiovascular devices (see Chapter 4). On all three exemplary metals (stainless steel, titanium, and nitinol), the LbL showed significant NO generation capability. Even though the metallic alloys have various elemental compositions; there were no significant deviations in terms of the quantity or the activity of the LbL deposited on their surfaces. Notably, a saturated NO flux was observed which did not scale as more bilayers were added to the LbL, presumably due to the diffusion barrier caused by the highly entangled polyelectrolyte network. Nevertheless, this saturated NO flux is still within the range of the basal NO fluxes from the endothelium monolayer.

In all the abovementioned experiments, the LbLs were fabricated with anionic Alg in the outmost layer. This is because negatively charged surfaces are known to be more hemocompatible by reducing surface protein adsorption. However, the LbL can also be designed to have a SePEI outmost layer. The resulting amine enriched surface is very attractive to immobilize other anti-thrombotic species, such as heparin, for a synergistic multifaceted effect. Two distinct strategies were investigated to immobilize the heparin polysaccharide: 1) electrostatic adsorption, and 2) covalent attachment via amide formation. By monitoring the UV-Vis absorbance from the fluorescently labeled heparin molecules, both methods proved to be effective to immobilize heparin on the

aminated LbL surface. Using a chromogenic assay, it was shown that the surface with covalently attached heparin is more active in terms of inhibition of factor Xa. However, such covalently attached heparin tends to lower the NO generation efficiency of the underlying RSe immobilized multilayer by impeding the diffusion of reactant RSNO and RSH species through the polyelectrolyte matrix.

6.2. Future Directions

6.2.1. In vivo anti-thrombotic evaluation of RSe immobilized LbL

Despite the promising data obtained *in vitro*, the ultimate evidence of an anti-thrombotic effect lies in examining the coating *in vivo*. In the preliminary tests, the LbL was applied to commercial polyurethane catheters which were later implanted in the veins of rabbits (see Chapter 3). After 4 h implantation, the catheters were explanted and tested for surface NO generation activity, which revealed no significant activity loss. This result highlights that the catalyst immobilized in such a polyelectrolyte multilayer can resist the sheer stress of the flowing blood, as well as the large number of reactive species in plasma. However, the LbL is prone to delamination upon insertion of the catheter into the blood vessel, which indicates a poor adhesion of the multilayer on the substrate. In Chapter 2, the LbL has proved applicable on neutral polyurethane surfaces. The growth of the multilayer is believed to be initiated by the non-specific adsorption of branched SePEI onto the polymeric substrates. However, such a non-specific interaction is much weaker than the cooperative electrostatic attractions between two oppositely charged polyelectrolytes, not to mention that the polyions in the highly penetrated structure further stabilize the LbL through chain entanglement. Therefore,

the adhesion of the LbL to the substrate remains the weakest link, although a strong cohesion within the multilayer has been implied by the difficulties encountered in digesting the LbL film. To ensure a successful implantation, catheters with a diameter much smaller than the target blood vessel should be selected in order to mitigate the friction and the shear force upon insertion. Also, an adhesion promoting layer might also be necessary to prevent delamination. For example, the catheters can be top-coated with a thin layer of aminated polyurethane to introduce ionizable free amines, which may enhance the interaction between the polyurethane surface and the first several bilayers.

6.2.2. Aromatic organoselenium species as catalysts for NO generation from RSNO

So far, the RSe species employed in our NO generation chemistry are alkyl diselenides such as 3,3'-diselenidedipropionic acid (SeDPA) and selenocystamine (SeCA). It should be noted that there are other RSe candidates worth exploring in pursuit of a better catalyst. Ebselen (2-phenyl-1,2-benzoisoselenazol-3-(2*H*)-one) is a promising target in particular due to its proven glutathione peroxidase mimicking activity.[7] In the proposed mechanism (see Scheme 6.1), Ebselen reacts with a thiol to afford a selenenylsulfide intermediate, which further disproportionates slowly to the corresponding diselenide with the elimination of disulfide.[8] Given the reported decomposition of RSNOs by the alkyl diselenide species, it is very likely that the Ebselen may display the same catalytic activity. Notably, the compound possesses a Se-C (aromatic) bond that avoids selenium release and maintains the low toxicity of Ebselen. This feature potentially endows the catalyst with long-term activity and reduces the toxicity concern. Indeed, the Ebselen already underwent Phase III clinical trials in Japan as an antioxidant.

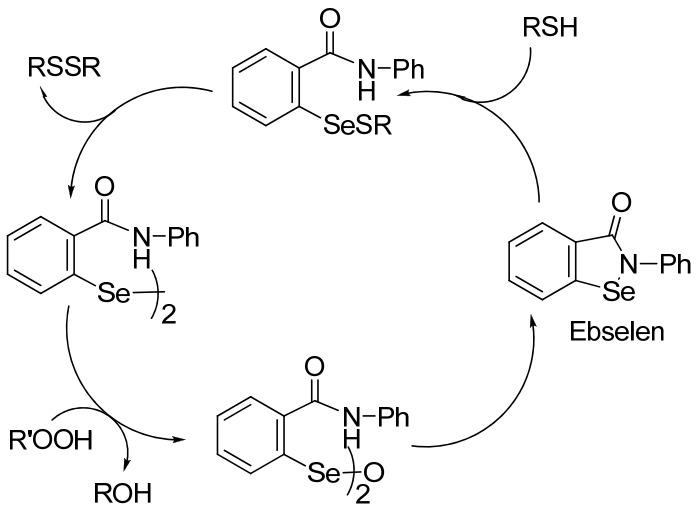

Scheme 6.1. Proposed mechanism of Ebselen catalyzed reduction of peroxide by glutathione. (RSH, glutathione; RSSR, disulfide; R'OOH, peroxide; ROH, alcohol.)

Scheme 6.2 represents a general synthesis pathway of Ebselen derivatives via a diselenosalicylic acid precursor (**1**), which is then converted into a highly reactive 2-(chloroseleno)benzoyl chloride (**2**). Compound **2** can react with derivatized aniline on which the R_1, R_2, and R_3 groups can be systemically tailored to produce the corresponding Ebselen compounds. If the aniline derivative used in the synthesis contains a reactive functionality, such as a carboxylate, amine or hydroxyl group, the resulting Ebselen product can be immobilized into underlying polymer matrices via covalent attachment and herein be utilized as an NO generation material. It is possible that changing the substituent groups R_{1-3} may impact the catalytic activity of the Ebselen species. Therefore, it will be very interesting to examine the activity of different Ebselen derivatives to elucidate the structure-activity correlation with respect to NO

generation from RSNOs.

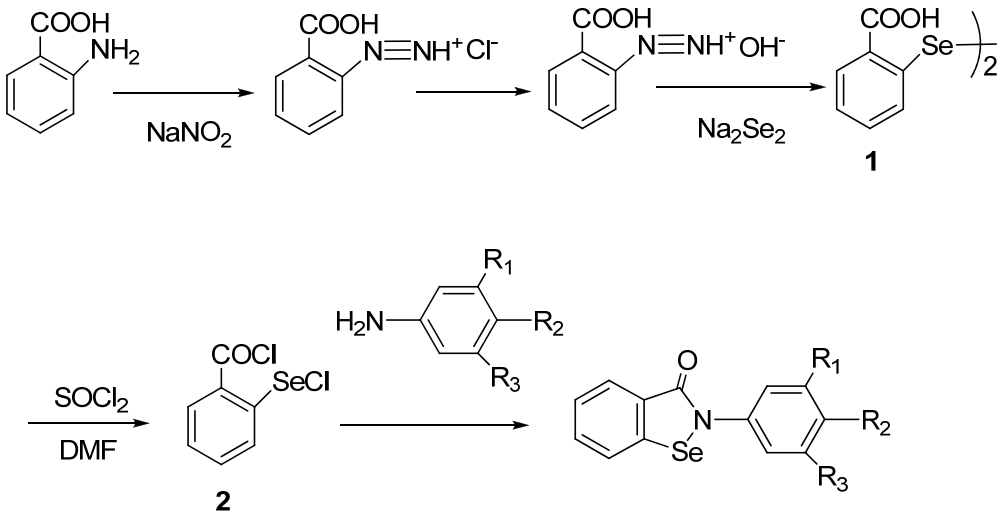

Scheme 6.2. Synthesis pathway of Ebselen through a diselenodisalicylic acid precursor.[9]

6.2.3. NO generation fluorinated surface modifier for polyurethane

All biomedical polymer applications have requirements that can be divided into bulk property and surface property categories. On one hand, the polymer must possess appropriate mechanical features, i.e., robustness, flexibility and processability etc., to perform anticipated functions. On the other hand, the material surface directly contacting the biological environment (i.e., with tissue or blood) has to be "biocompatible" without provoking severe adverse responses. However, the chances are remote that both surface and bulk properties can be optimized in a single polymer. This basic dilemma of biomaterials development has often resulted in a post-fabrication surface treatment or a top-coating, the processing of which must be adapted to the

specific physical form of the device or component.

A strategy to circumvent this post-fabrication surface modification is to blend the base polymer with a small amount of surface modifiers which spontaneously migrate to the surface in high concentration. This approach takes advantage of the propensity of condensed phase material to minimize their interfacial energy. An exemplary surface modifier is a polyethylene oxide (PEO) containing block copolymer, which has been reported capable of migrating to the surface after being blended in a polyurethane base polymer. This enhances surface hydrophilicity and diminishes protein adsorption.[10,11] Recently, tri-block surface modifiers comprising a polyurethane oligomer, a fluoroalkyl end-cap and a bioactive pendant (e.g., a peptide sequence) have also been used to bring the bioactive component to the surface of the polyurethane base polymer.[12-14] It has been found that as little as 0.5 % modifier is enough to saturate the polyurethane surface.[13] More importantly, the bioactive species still exhibit their bio-functionality after migration to the surface. For example, an RGD sequence attached to a fluorinated modifier has been shown to promote the adhesion of human monocytes on polyurethane in which the modifier was blended.[13] The major advantage of using these surface modifiers is that the surface properties can be tailored via a simple blending step before fabrication of the surface without significantly changing the properties of the bulk polymer.

Similarly, the aforementioned chemistry can be used to create a NO generating surface on polyurethane by grafting an RSe catalyst on a fluorinated additive and then blending into the base polymer. By doing so, the catalyst can migrate along the fluoroalkyl chains onto the surface to form a NO generation layer spontaneously after the

blend is molded into the desired shape. The modifier can be prepared via a synthetic route shown in Scheme 6.3.[14,15] First, an excess amount of lysine diisocyanate is reacted with a diol to yield a polyurethane prepolymer with isocyanate groups on both ends. The fluorinated component can be introduced by capping the prepolymer with a small molecule fluoroalcohol. Then, the ester pendant can be hydrolyzed under acidic conditions into carboxylic acid, which reacts with many aminated RSe catalysts via amide bond formation. Alternatively, the carboxylic acid can be converted into an acid chloride, which can react with RSe possessing weaker nucleophiles, such as alcohols.

Obviously, application of these fluorinated PU additives is not limited to the NO generation chemistry discussed above. For example, the additive can also be derivatized with *S*-nitrosothiol species, targeting a new class of NO release materials. Other species capable of enhancing blood compatibility, such as heparin, phospholipids, and plasminogen etc., can also be attached to the fluorinated head group and subsequently blended into the bulk polymer, whereby the polyurethane surface can be modified via the spontaneous migration of the additives.

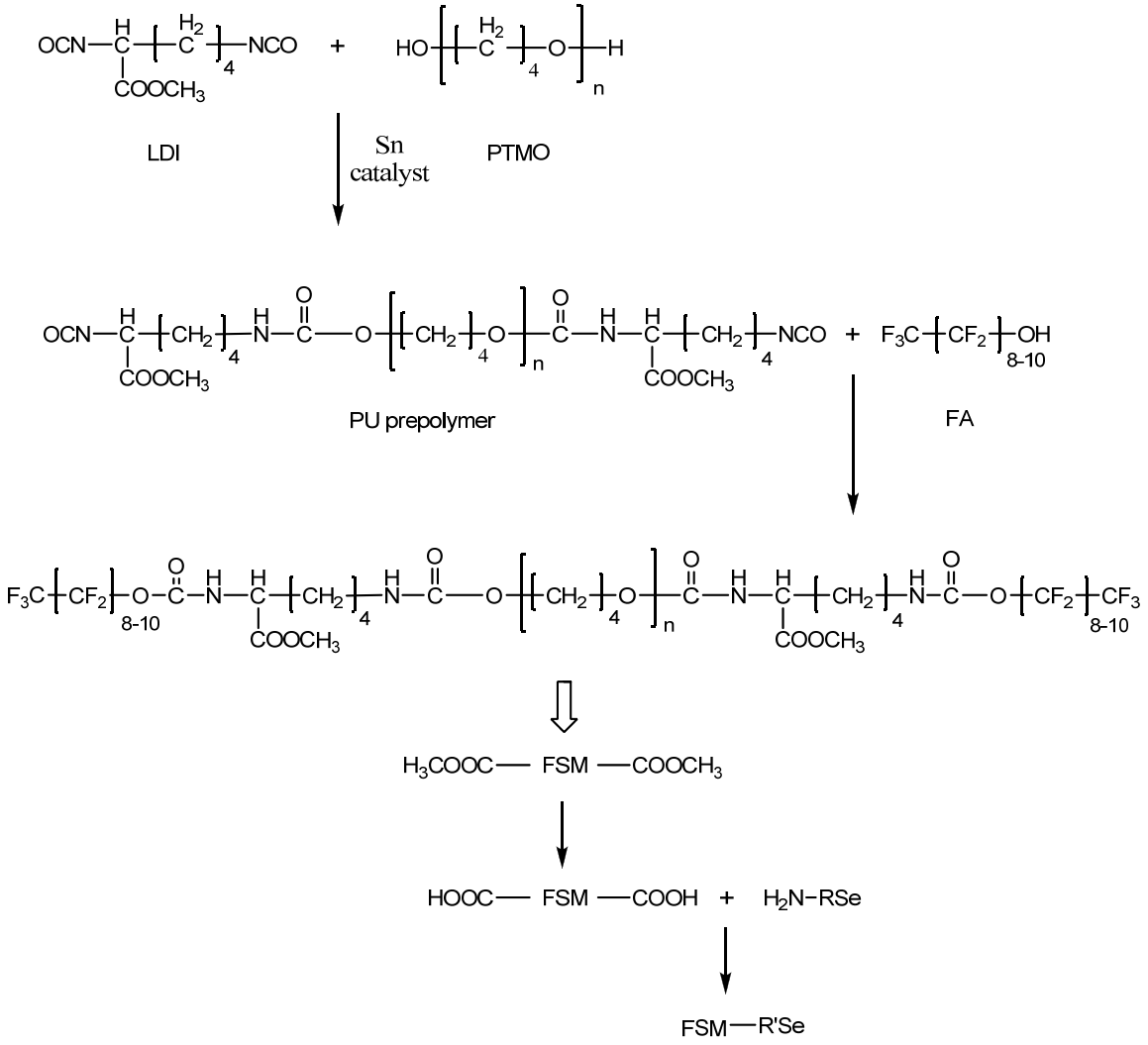

Scheme 6.3. Synthesis of RSe immobilized fluorinated surface modifier. (LDI, lysine diisocyanate; PTMO, polytetramethyl oxide; PU, polyurethane; FA, fluoroalcohol; FSM, fluorinated surface modifier.)

6.3. References

1. Skrzypchak, A. M.; Lafayette, N. G.; Bartlett, R. H.; Zhou, Z. R.; Frost, M. C.; Meyerhoff, M. E.; Reynolds, M. M.; Annich, G. M. *Perfusion-Uk* **2007**, *22*, 193-200.

2. Batchelor, M. M.; Reoma, S. L.; Fleser, P. S.; Nuthakki, V. K.; Callahan, R. E.; Shanley, C. J.; Politis, J. K.; Elmore, J.; Merz, S. I.; Meyerhoff, M. E. *J. Med. Chem.* **2003**, *46*, 5153-5161.

3. Fleser, P. S.; Nuthakki, V. K.; Malinzak, L. E.; Callahan, R. E.; Seymour, M. L.; Reynolds, M. M.; Merz, S. I.; Meyerhoff, M. E.; Bendick, P. J.; Zelenock, G. B.; Shanley, C. J. *J. Vasc. Surg.* **2004**, *40*, 803-811.

4. Wu, Y. D.; Meyerhoff, M. E. *Talanta* **2008**, *75*, 642-650.

5. Wu, Y. D.; Rojas, A. P.; Griffith, G. W.; Skrzypchak, A. M.; Lafayette, N.; Bartlett, R. H.; Meyerhoff, M. E. *Sensor Actuator B Chem.* **2007**, *121*, 36-46.

6. Vaughn, M. W.; Kuo, L.; Liao, J. C. *Am. J. Physiol. Heart Circ. Physiol.* **1998**, *43*, H2163-H2176.

7. Sies, H.; Masumoto, H. *Adv. Pharmacol.* **1997**, *38*, 229-246.

8. Mugesh, G.; Singh, H. B. *Chem. Soc. Rev.* **2000**, *29*, 347-357.

9. Osajda, M.; Mlochowski, J. *Tetrahedron* **2002**, *58*, 7531-7537.

10. Tan, J.; Brash, J. L. *J. Biomed. Mater. Res.* **2009**, *90A*, 196-204.

11. Lee, J. H.; Ju, Y. M.; Lee, W. K.; Park, K. D.; Kim, Y. H. *J. Biomed. Mater. Res.* **1998**, *40*, 314-323.

12. Ernsting, M. J.; Bonin, G. C.; Yang, M. L.; Labow, R. S.; Santerre, J. P. *Biomaterials* **2005**, *26*, 6536-6546.

13. Ernsting, M. J.; Labow, R. S.; Santerre, J. P. *J. Biomed. Mater. Res.* **2007**, *83A*, 759-769.

14. Ernsting, M. J.; Labow, R. S.; Santerre, J. P. *J. Biomater. Sci. Polymer Ed.* **2003**, *14*, 1411-1426.

15. Tang, Y. W.; Santerre, J. P.; Labow, R. S.; Taylor, D. G. *J. Appl. Polym. Sci.* **1996**, *62*, 1133-1145.